

**CHARACTERISATION OF RIGID POLYURETHANE FOAM REINFORCED BALLAST  
THROUGH CYCLIC LOADING BOX TESTS**

by

**Rudolph du Plooy**

Submitted in partial fulfilment of the requirements for the degree

Master of Engineering(Civil Engineering)

in the

Department of Civil Engineering  
Faculty of Engineering, Built Environment and Information Technology  
UNIVERSITY OF PRETORIA

October 2015

## SUMMARY

---

### CHARACTERISATION OF RIGID POLYURETHANE FOAM REINFORCED BALLAST THROUGH CYCLIC LOADING BOX TESTS

by

**Rudolph du Plooy**

Supervisor(s): Prof H. Gräbe  
Department: Civil Engineering  
University: University of Pretoria  
Degree: Master of Engineering(Civil Engineering)

Train speeds and heavy haul axle loads are constantly increasing the forces and stresses experienced by track structures. This is especially true for track transitions that generate high dynamic forces on both the track and vehicles as a result of differing track stiffness values on either side of the track transition. Reducing differential settlement between the two track structures at a track transition is one method of improving the life of the track and increasing maintenance intervals. Ballast attrition and breakdown at these track transition zones is also of major concern as ballast fouling can lead to reduced drainage performance of the ballast as well as a potential loss of strength as the ballast becomes increasingly fouled.

In this study rigid polyurethane foam was used as a means to reinforce ballast. Various tests were conducted using a dynamic load hydraulic load frame in a large ballast box test at heavy haul axle loads. Unreinforced, reinforced and 50 % reinforced ballast layers of 300 mm depth were tested to approximately 5,000,000 load cycles.

The results showed that rigid polyurethane foam reinforced ballast exhibited in the order of 60 % less settlement for a fully reinforced layer and 42 % less settlement for a half reinforced layer. The increase in layer stiffness with increasing load cycles was also observed for the reinforced ballast layers which is contrast with the decrease in layer stiffness for conventional unreinforced ballast. The use of rigid polyurethane foam (RPF) to reinforce ballast has a number of benefits which could result in better track geometry and longer maintenance cycles resulting in lower overall costs.

## ACKNOWLEDGEMENTS

---

This thesis would not have been possible without the guidance and help of several individuals, to only some of whom it is possible to mention here.

Firstly, I would like to express my sincere gratitude to my supervisor **Prof. Hannes Grabe** for the continuous support of my study, for his patience, knowledge and motivation. I could not have imagined having a better supervisor and mentor for my Masters research. The author highly appreciates the 'open door' policy of his supervisor. The author would also like to thank his supervisor for the opportunity to do my Masters.

I would also like to thank the Transnet Freight Rail Chair in Railway Engineering for their financial support over the last two years.

Thanks are also due to **Johan Scholtz**, part of the technical staff in the Civil Engineering laboratory - University of Pretoria, without whom none of the experimental work presented here would have been possible. Thank you for all the assistance, advice and willingness to help during the laboratory testing. I would also like to thank **Derek Mostert** for his help and guidance with the materials testing.

I acknowledge the contribution of various industry members that helped make this research possible. To **Sizwe Mkhize** of Aveng Infraset, for the donation of railway sleepers for use in this research. To **Lynda Araujo** of Afrisam Aggregate for the ballast that was donated. A special mention to **Bruce Elliot** of Resichem for the donation of polyurethane foam and for all the advice given with regard to the preparation and mixing of the foam.

I would like to thank **Paul Vorster** as well as **Paul le Roux** for their help in the laboratory and invaluable contribution during this study, especially with the loading and unloading of each test, despite being extremely busy with their own Masters research.

Thanks are also due to my friend **Justus Immelman** for the help with building of the box and to **Kelsey Yates** for the encouragement and help along the way. A special thanks to the other railway engineering post-graduate students namely: **Rick Vandoorne** and **Afonso Ronda** for the helpful advice and suggestions along the way.

To my family, thank you for your unending love and support during the period of this research.

My most sincere gratitude and heartfelt thanks goes to my girlfriend **Annika Nolte** for all of her love, support, words of encouragement and comfort as well as motivation during the challenging times.

Finally the author would like to acknowledge the financial, academic and technical support provided by the University of Pretoria.

# TABLE OF CONTENTS

<b>List of Tables</b>	<b>9</b>
<b>List of Figures</b>	<b>14</b>
<b>CHAPTER 1 Introduction</b>	<b>1</b>
1.1 Objectives . . . . .	2
1.2 Scope of Study . . . . .	2
1.3 Methodology . . . . .	2
1.4 Organisation of Report . . . . .	3
<b>CHAPTER 2 Literature study</b>	<b>4</b>
2.1 Track Structure Types . . . . .	4
2.1.1 Ballasted Track . . . . .	4
2.1.2 Ballastless Track . . . . .	8
2.2 Track Transitions . . . . .	12
2.2.1 Track Transition Problems . . . . .	13
2.2.2 Track Transition Remedial Measures . . . . .	15
2.3 Ballast . . . . .	19
2.3.1 Ballast Specifications and Testing . . . . .	19
2.3.2 Ballast Fouling . . . . .	22
2.3.3 Shear Strength . . . . .	24
2.3.4 Effect of Particle Size Distribution . . . . .	24
2.3.5 Effect of confining pressure . . . . .	26
2.4 Particle breakage . . . . .	29
2.4.1 Griffith theory . . . . .	29
2.4.2 Ballast Degradation and Particle Breakage . . . . .	30
2.5 Behaviour of aggregate under cyclic loading . . . . .	33



2.5.1	Resilient behaviour . . . . .	33
2.5.2	Permanent deformation of cyclically loaded aggregate . . . . .	36
2.5.3	Effect of Cyclic Loading Frequency . . . . .	41
2.6	Laboratory Tests on Ballast . . . . .	46
2.6.1	Ballast Box Tests . . . . .	46
2.6.2	Ballast Strain . . . . .	53
2.6.3	Ballast Triaxial Test . . . . .	55
2.7	Track Reinforcement Using Polymer Geocomposites . . . . .	56
2.7.1	Rigid Polyurethane Foam (RPF) . . . . .	57
2.8	Rigid Foam Polyurethane Reinforcement of Railway Ballast . . . . .	60
2.9	Summary . . . . .	69
<b>CHAPTER 3 Methodology and Experimental Setup</b>		<b>70</b>
3.1	Introduction . . . . .	70
3.2	Materials . . . . .	70
3.2.1	Ballast Material . . . . .	70
3.2.2	Rigid Polyurethane Foam . . . . .	74
3.3	Ballast Box Test . . . . .	76
3.3.1	Ballast Box Design . . . . .	77
3.4	Hydraulic Load Frame . . . . .	79
3.5	Measuring Instrumentation . . . . .	80
3.5.1	Load Frame Instrumentation . . . . .	80
3.6	Experimental Setup . . . . .	83
3.6.1	Box Test Experimental Setup . . . . .	83
3.7	Materials Testing . . . . .	88
3.7.1	Ballast Grading . . . . .	89
3.7.2	Rigid Polyurethane Foam and Reinforced Ballast Properties . . . . .	89
3.8	Testing Regime . . . . .	92
3.8.1	Initial Phase . . . . .	93
3.8.2	Testing Overview . . . . .	93
3.8.3	Cyclic Testing . . . . .	96
3.9	Data Analysis . . . . .	98
<b>CHAPTER 4 Results and Discussion</b>		<b>101</b>

4.1	Introduction . . . . .	101
4.2	Material Testing . . . . .	101
4.3	Settlement Behaviour . . . . .	107
4.3.1	Initial Phase . . . . .	108
4.3.2	Consolidation Test Phase . . . . .	110
4.3.3	Consolidation Settlement Prediction Functions . . . . .	113
4.3.4	Combined Settlement . . . . .	114
4.3.5	Combined Settlement Prediction Functions . . . . .	119
4.4	Ballast Layer Modulus . . . . .	121
4.5	Load vs Deflection Behaviour . . . . .	126
4.6	Effect of Test Load Frequency . . . . .	128
4.6.1	Frequency Sweep . . . . .	128
4.7	Ballast Breakdown . . . . .	129
4.7.1	Equivalent Tonnage . . . . .	136
4.8	Summary of Results and Discussion . . . . .	136
<b>CHAPTER 5 Conclusion and Recommendations</b>		<b>139</b>
5.1	Conclusion . . . . .	139
5.1.1	Material Testing . . . . .	139
5.1.2	Ballast Breakage . . . . .	140
5.1.3	Settlement Behaviour . . . . .	140
5.1.4	Load vs Deflection Behaviour . . . . .	141
5.1.5	Effect of Test Frequency . . . . .	141
5.2	Recommendations . . . . .	142
5.2.1	The future use of rigid polyurethane foam in ballast reinforcement . . . . .	142
5.2.2	Recommendations for further study . . . . .	142
<b>APPENDIX A Appendix A</b>		<b>149</b>
A.1	Raw Data . . . . .	149
A.2	MATLAB Code . . . . .	149

## LIST OF TABLES

2.1	Total length of various slab track systems constructed worldwide Michas (2012) . . . . .	10
2.2	Ballast properties according to testing as well as different specifications adapted from Al-Saoudi and Hassan (2014) . . . . .	19
2.3	Ballast fouling indices from Selig and Waters (1994) . . . . .	23
2.4	Ballast test setups adapted from Al-Saoudi and Hassan (2014) . . . . .	47
3.1	Summary of Quartzite properties . . . . .	72
3.2	Summary of ballast properties . . . . .	74
3.3	Summary of polyurethane foam physical properties . . . . .	76
3.4	Various ballast box dimensions and properties . . . . .	77
3.5	LVDT Technical Specifications . . . . .	83
3.6	Initial Consolidation Phase - Loading . . . . .	93
3.7	Cyclic ballast box test record summary . . . . .	94
3.8	Settlement Test Summary . . . . .	97
4.1	Polyurethane foam (PF) cylinder densities ( $\text{kg/m}^3$ ) before and after testing . . . . .	105
4.2	Polyurethane reinforced ballast (PRB) composite cylinder densities ( $\text{kg/m}^3$ ) before and after testing . . . . .	105
4.3	Polyurethane foam (PF) and PRB composite cylinder permanent deformation . . . . .	106
4.4	Initial phase settlement values . . . . .	109
4.5	Consolidation test phase settlement values . . . . .	111
4.6	Consolidation phase settlement prediction equation constants and correlation coefficients . . . . .	114
4.7	Total test phase settlement values . . . . .	116
4.8	Combined settlement prediction equation constants and coefficient of correlation ( $R^2$ ) values . . . . .	120

4.9 Comparison of $R^2$ values for different test phases (consolidation phase and combined phase) . . . . .	121
4.10 Ballast Breakage Index (BBI) results in % of total maximum breakage . . . . .	134

## LIST OF FIGURES

2.1	Ballasted track structure components (Adapted from Selig and Waters (1994)) . . . . .	5
2.2	Mud pumping on a heavy haul line . . . . .	12
2.3	AREMA Plan No. 913-52 approach sleeper for open bridge decks . . . . .	16
2.4	South African Heavy Axle Line Ballast Grading . . . . .	21
2.5	Axial and volumetric strain response of different distributions under cyclic loading (Indraratna et al., 2004) . . . . .	25
2.6	Effect of grading on particle breakage (Indraratna et al., 2004) . . . . .	26
2.7	Relationship between axial and volumetric strains for different confining pressures under cyclic loading (Indraratna et al., 2004) . . . . .	27
2.8	Effect of confining pressure on particle breakage, showing degradation zones (Indraratna et al., 2004) . . . . .	28
2.9	Large coordination numbers are less helpful for more angular particles, from McDowell et al. (1996) . . . . .	31
2.10	Definition of ballast breakage Christie et al. (2007) . . . . .	32
2.11	Strain in a granular material during one cycle of load application (Lekarp et al., 2000)	33
2.12	Four stages of shakedown, describing the elastic/plastic response to repeated loading. (Collins and Boulbibane, 2000) . . . . .	35
2.13	Stresses beneath a rolling wheel load (Lekarp et al., 2000) . . . . .	37
2.14	Permanent deformation as a linear function of the logarithm of number of load cycle (Shenton, 1974) . . . . .	37
2.15	Effect of loading sequence on permanent strain (Selig and Waters, 1994) . . . . .	38
2.16	Typical variation in axial strain between ballast samples (Indraratna et al., 1997) . . .	39
2.17	Typical variation in settlement (Indraratna et al., 1997) . . . . .	39
2.18	Influence of drainage on Permanent Deformation Development (Dawson, 1990) . . .	41

2.19	Examples of particle degradation: (a) attrition of asperities and corner breakage in range I; (b) high degree attrition of asperities in range II; (c) particle splitting type 1 in range II; (d) particle splitting type 2 in range III (Sun et al., 2014) . . . . .	42
2.20	Axial strain accumulation with increasing cycle count (Sun et al., 2014) . . . . .	43
2.21	Ballast Breakage Index as a function of frequency $f$ (Sun et al., 2014) . . . . .	43
2.22	Relationship between $\varepsilon_v$ and BBI (Sun et al., 2014) . . . . .	44
2.23	Diagram of a box test (Selig and Waters, 1994) . . . . .	48
2.24	Box test setup (Al-Saoudi and Hassan, 2014) . . . . .	49
2.25	Plan of rail and sleepers showing section represented by the box test (Lim, 2004) . . . . .	49
2.26	Effect of repeated load on horizontal stress in a box test (Selig and Waters, 1994) . . . . .	50
2.27	Settlement as a function of log of cycles (Selig and Waters, 1994) . . . . .	51
2.28	Settlement increase with cycles (Selig and Waters, 1994) . . . . .	52
2.29	Effect of load cycles and axle loads on settlement (Selig and Waters, 1994) . . . . .	53
2.30	Ballast strain plot (Selig and Waters, 1994) . . . . .	54
2.31	Typical large scale triaxial test used for testing railway ballast (Aursudkij, 2007) . . . . .	55
2.32	Compressive strength: two typical force deformation curves for rigid polyurethane foam (Gunter, 1985) . . . . .	58
2.33	Compressive strength with increase in density (Gunter, 1985) . . . . .	59
2.34	A PSB specimen cut in half using a concrete masonry saw showing the complete void filling by the expanding foam(left) and a close up (right) (Keene, Edil, Tinjum and Brown, 2012a) . . . . .	61
2.35	A typical phase diagram of the PSB sample as well as average percentages of PSB compositions (Keene, Edil, Tinjum and Brown, 2012a) . . . . .	62
2.36	Cyclic triaxial compression testing on clean and PSB specimens under a deviator stress $\sigma_d$ of 300 kPa. Fouled ballast results from previous research (Keene, Edil, Tinjum and Brown, 2012a) . . . . .	63
2.37	Comparison of elastic strain measured through cyclic triaxial tests between typical clean ballast and PSB specimens (Keene, Edil, Tinjum and Brown, 2012a) . . . . .	63
2.38	Calculated track modulus for the range of PSB modulus and track components modeled and field validated (Keene et al., 2013) . . . . .	65
2.39	Close-up of geocomposite showing three-dimensional polymer reinforcement while still maintaining full drainage (Woodward, 2007) . . . . .	66

2.40	Comparison of the 3D polymer reinforced ballast test to the measured unreinforced ballast control tests and the predicted unreinforced ballast control test (Kennedy et al., 2013). . . . .	67
2.41	The GRAFT test equipment with XiTrack treated ballast test (Kennedy et al., 2013).	68
3.1	Location of quarry (blue arrow top) in relation to the University of Pretoria (red arrow bottom) (Google and AfriGIS, 2015) . . . . .	71
3.2	Geological map of the Bushveld Complex (Eales and Cawthorn, 1996) . . . . .	71
3.3	The test ballast stone . . . . .	72
3.4	Grading of ballast compared with the S406 ballast grading specification . . . . .	73
3.5	First foam mix test . . . . .	75
3.6	The cylinder of ballast before foaming (left) and after (right) . . . . .	76
3.7	Drawing of ballast box in Solidworks . . . . .	78
3.8	Ballast box dimensions . . . . .	78
3.9	Completed ballast box filled with unwashed ballast . . . . .	79
3.10	Hydraulic load frame with a box test being prepared . . . . .	80
3.11	Hydraulic load frame load cell for force measurement located below actuator . . . . .	81
3.12	LVDT setup to measure sleeper displacement . . . . .	82
3.13	LVDT dimensions (HBM, 2015) . . . . .	83
3.14	Track section simulated in test . . . . .	84
3.15	Main PY sleeper dimensions . . . . .	84
3.16	Ballast box with 300 mm layer ready for sleeper placement . . . . .	85
3.17	Box preparation complete - ready for loading into load frame . . . . .	86
3.18	Ensuring sleeper level and alignment was correct . . . . .	87
3.19	Loading block which was used to transfer the load from the beam to the sleeper at the rail positions . . . . .	87
3.20	Setup ready to commence testing . . . . .	88
3.21	Final setup . . . . .	88
3.22	Preparation of cylindrical samples for testing . . . . .	90
3.23	The foam samples following pouring before being demoulded . . . . .	91
3.24	Top of the sample after being cut with a masonry saw . . . . .	91
3.25	Sample undergoing testing in press . . . . .	92
3.26	Ballast and polyurethane reinforcement configurations tested . . . . .	95

3.27	Loading command and actual force output . . . . .	96
3.28	Controller computer monitoring screen . . . . .	98
3.29	Typical raw data output, actuator displacement vs time . . . . .	99
3.30	Typical raw data output, actuator force vs time . . . . .	99
3.31	Typical raw data output, LVDT output voltage vs time . . . . .	100
3.32	Typical raw data output, actuator displacement output vs cycles for a frequency sweep test . . . . .	100
4.1	Stress vs. strain plot of rigid polyurethane foam sample cylinders . . . . .	102
4.2	Stress vs strain plot of reinforced ballast sample cylinders . . . . .	103
4.3	Reinforced ballast cylinder after testing . . . . .	104
4.4	Rigid polyurethane foam cylinder compressive strength test results (Adapted from (Gunter, 1985)) . . . . .	105
4.5	Foam gluing reinforced ballast layer and sleeper to one another . . . . .	107
4.6	Settlement behaviour breakdown . . . . .	108
4.7	Initial phase settlement . . . . .	109
4.8	Initial phase settlement plotted on a logarithmic scale . . . . .	110
4.9	Consolidation test phase settlement . . . . .	111
4.10	Consolidation test phase settlement results plotted on a logarithmic scale . . . . .	112
4.11	Consolidation phase test settlement results plotted against power and logarithmic settlement prediction functions . . . . .	115
4.12	Total test settlement values . . . . .	116
4.13	Total test settlement values plotted on a logarithmic scale . . . . .	117
4.14	Ballast strain comparison (Vertical (or axial) strain) . . . . .	118
4.15	Compression and settlement of the ballast due to sleeper contact stress . . . . .	119
4.16	Combined test phases settlement results plotted against power and logarithmic settlement prediction functions . . . . .	120
4.17	Resilient sleeper deflection with increasing cycles . . . . .	122
4.18	Ballast layer modulus with increasing cycles . . . . .	123
4.19	Foam filled void between ballast stone (left), foam sufficiently compressed allowing ballast contact to occur (right) . . . . .	125
4.20	Typical load-deflection behaviour of the hydraulic load fram actuator and sleeper during a cycle . . . . .	126

4.21	Ballast layer modulus calculation definition . . . . .	127
4.22	Effect of loading frequency on sleeper deflection . . . . .	128
4.23	Effect of loading frequency on settlement per cycle . . . . .	129
4.24	Positions of ballast removed for grading through the entire ballast layer depth . . . . .	130
4.25	Fines generated during the test as a result of ballast breakdown . . . . .	131
4.26	Breakage of ballast . . . . .	131
4.27	Grading analysis after Test 1 on unreinforced ballast . . . . .	132
4.28	Grading analysis after Test 4 on unreinforced ballast . . . . .	133
4.29	Grading analysis after Test 5 on "semi-reinforced" ballast . . . . .	133
4.30	Reinforced ballast layer after removal from box after testing (upside down) . . . . .	135
4.31	Close-up of a cross section of reinforced foam ballast layer - note full foam penetra- tion and void filling . . . . .	135
4.32	Comparison of initial, consolidation and final total settlement results . . . . .	137
4.33	Comparison of final resilient sleeper deflection and ballast layer modulus results . . . . .	138

# CHAPTER 1

## INTRODUCTION

Train speeds and heavy haul axle loads are constantly increasing the forces and stresses experienced by track structures. This is especially true for track transitions that generate high dynamic forces on both the track and vehicles as a result of differing track stiffness values on either side of the track transition. Limiting differential settlement between the two track structures at a track transition is one means of improving the life of the track and reducing maintenance intervals. Ballast attrition and breakdown at these track transition zones is also of major concern as ballast fouling can lead to reduced drainage performance of the ballast as well as a loss of strength as the ballast becomes increasingly fouled.

By lengthening track maintenance intervals at track transitions and other problem sections, the operating cost of the infrastructure can be reduced. A number of methods have been developed that are aimed at improving the performance at these problem track sections. The use of polyurethane foam for reinforcement of ballast has been conducted before. Very few experimental and empirical methods exist for determining the lifecycle and other material characteristics of track structures stabilised with polyurethane products. Polyurethane stabilisation or reinforcement of ballast has been proven to provide a significant decrease in accumulated plastic strain. Polyurethane stabilised ballast does not require pre-mixing and can be applied without track closure.

This study aims to provide insight into the long-term performance of rigid polyurethane foam reinforced ballast through means of a large scale box test under heavy haul axle loading.

## 1.1 OBJECTIVES

The objective of this study is to study the settlement behaviour and other track parameters through long-term, large scale, cyclic loading box tests subjected to heavy haul axle loads (30 tons). It is hypothesised that the reinforcement of ballast using rigid polyurethane foam will lead to a reduction in ballast layer settlement, an increase in stiffness, reduced ballast breakage and an overall improvement in track performance.

Two main objectives of the study are firstly to characterise the properties of the ballast, polyurethane foam and the ballast polyurethane foam composite material and secondly to characterise the settlement behaviour of the ballast and polyurethane foam reinforced ballast layer.

## 1.2 SCOPE OF STUDY

Only a ballast layer was modelled in the box test with no other foundation layers. Various test configurations were prepared ranging from completely unreinforced ballast to fully reinforced ballast. Each sample was subjected to 5,000,000 load cycles at the specified load.

Settlement prediction models were compared to actual ballast settlement behaviour and the validity of these settlement prediction models for use with polyurethane reinforced ballast samples was examined. Resilient sleeper deflection, ballast layer stiffness, ballast layer strain were all determined and compared. A number of sample material tests were also conducted to compare the material behaviour of rigid polyurethane foam and ballast reinforced with rigid polyurethane foam.

## 1.3 METHODOLOGY

The methodology that was followed is described below:

- A literature review was conducted focussing on track structures, track transitions, ballast and aggregate behaviour under cyclic loading. A review of the current state of knowledge on polyurethane stabilised/reinforced ballast was also conducted.
- The materials and components required for testing were collected/purchased and the box for the testing was designed and built.

- Test preparation and testing for each test configuration as described in Chapter 3.
- Small material samples were prepared and were tested to determine mechanical properties.
- Data was analysed, results were discussed and conclusions were drawn.

#### **1.4 ORGANISATION OF REPORT**

This thesis consists of the following chapters:

- Chapter 1 describes the purpose and importance of the study, the scope and methodology of the research.
- Chapter 2 contains a literature study which explains various track structures, previous research and measuring techniques.
- Chapter 3 describes the laboratory testing that was conducted.
- Chapter 4 presents the results from the data and discusses the results that were obtained.
- Chapter 5 provides the conclusions that were drawn from the research study and includes recommendations for future studies.
- A list of references used while conducting this study is included at the end.

## CHAPTER 2

### LITERATURE STUDY

An overview of different track structure types is presented in this chapter. This is important as track transitions usually occur between different track structure types. Track transitions and various problems and solutions for track transitions are reviewed. Various literature on railway ballast is reviewed with an aim of providing a good understanding of various ballast specifications, properties and the effects of the aforementioned properties on ballast behaviour. Theory on particle breakage and the behaviour of aggregates under cyclic loading is also reviewed. Literature on various laboratory tests is presented followed by an overview of rigid polyurethane foam and its properties.

#### 2.1 TRACK STRUCTURE TYPES

Different types of track structures are presented in this section, as track transitions occur most commonly between different track structure types.

##### 2.1.1 Ballasted Track

Ballasted track can be considered as the "conventional" track structure. Ballasted track is the most widely used track structure worldwide and consists of two main components. The first of which is the track superstructure which is the most visible part. The superstructure consists of sleepers, rails and the fastening system. The second main component is the substructure. The substructure consists of crib, top and bottom ballast, subballast and subgrade, consisting of placed soil (fill) and natural ground. Figure 2.1 depicts a typical ballasted track structure.

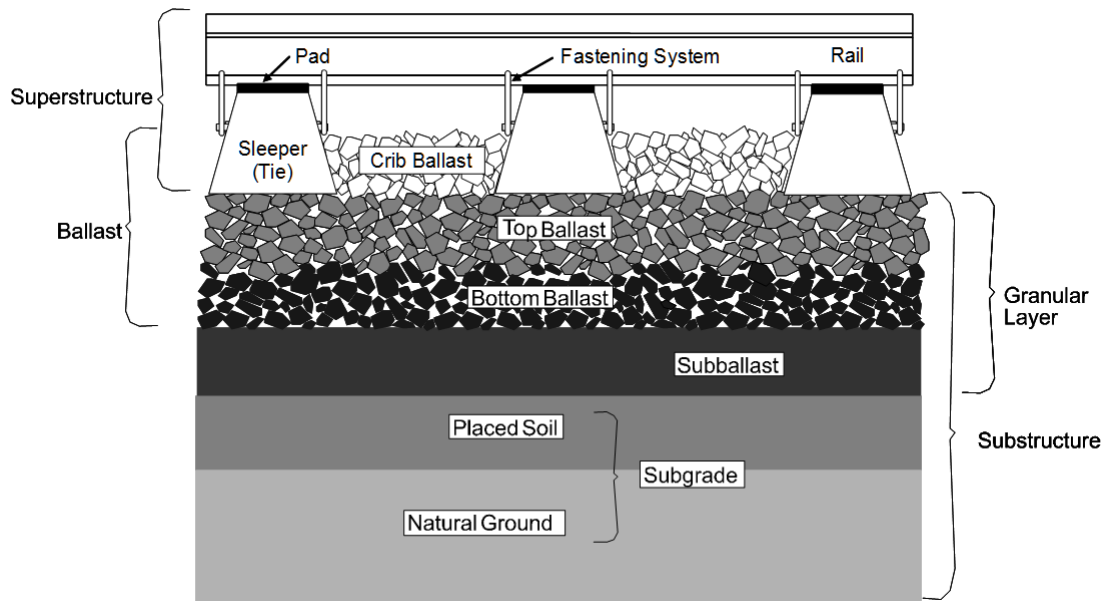


**Figure 2.1** Ballasted track structure components (Adapted from Selig and Waters (1994))

Esveld (2001) stated that the rail can be seen as the most important component of the structure and has the following functions:

- It accommodates the wheel loads and distributes these loads over the sleepers/supports.
- It guides the wheel in a lateral direction, any horizontal transverse forces on the rail head being transferred to and distributed over the sleepers and supports.
- It provides a smooth running surface and distributes accelerating and braking forces by means of adhesion.
- It acts as an electrical conductor on an electrified line.
- It conducts signal currents.

Rails are connected to the sleepers/supports by means of fasteners. The choice of fastener is dependent on the type of rail and sleeper. The purpose of the fastening system is to retain the rails against the sleepers and resist lateral, longitudinal and overturning moments of the rail. In South Africa almost all ballasted track that is built is constructed with concrete sleepers. Concrete sleepers require pads between the rail seat and the concrete sleeper surface to fulfil the following functions:

- Provide resiliency for the rail/sleeper system.

- Provide damping of wheel induced vibrations.
- Prevent or reduce rail/sleeper contact irritation.
- Provide electrical insulation for the track signal circuits.

Selig and Waters (1994) also stated that sleepers have several important functions:

- Receive the load from the rail and distribute it over the supporting ballast at an acceptable ballast pressure level.
- Hold the fastening system to maintain the proper track gauge.
- Restrain the lateral, longitudinal and vertical rail movement by anchorage of the superstructure in the ballast.
- Concrete sleepers provide a cant to the rails to develop proper rail/wheel contact.

Ballast is the select, crushed, granular material placed as the top layer of the substructure in which the sleepers are embedded. According to Selig and Waters (1994) the most important functions of ballast are:

- Resist vertical (including uplift), lateral and longitudinal forces applied to sleepers to retain track geometry.
- Provide some of the resiliency and energy absorption for the track.
- Provide large voids for the storage of fouling material in the ballast, and movement of particles through the ballast.
- Facilitate maintenance surfacing and lining operations (to adjust track geometry) by the ability to rearrange ballast particles with tamping.
- Provide immediate drainage of water falling onto the track.
- Reduce pressures from the sleeper bearing area to acceptable stress for the underlying material.

The thickness of the ballast should be such that the subgrade is loaded as uniformly as possible. The optimum thickness ranges from 250 mm to 350 mm measured from the underside of the sleeper.

The layer separating the ballast and the subgrade is the subballast. The subballast performs two functions that are the same as the ballast:

- Reduce traffic induced stress at the bottom of the ballast layer to a tolerable level for the top of subgrade.
- Extend the subgrade frost protection

However, Selig and Waters (1994) state that the subballast has some functions that cannot be fulfilled by ballast. These are:

- Prevent interpenetration of subgrade and ballast (separation function).
- Prevent upward migration of fine material from the subgrade.
- Prevent subgrade attrition by ballast, which in the presence of water leads to slurry formation (a source of pumping).
- Shed water, intercept water coming from the ballast and direct it away from the subgrade.
- Permit drainage of water that may be flowing upward from the subgrade.

These aforementioned functions are very important for satisfactory track performance. Hence in the absence of a subballast layer, high maintenance effort can be expected (Selig and Waters, 1994).

The superstructure and substructure are separated by a ballast sleeper interface. The track substructure's primary function is to reduce applied stresses so that they do not exceed the strength of the subgrade. The substructure consists of the formation which includes slopes, verges, ditches and any structures in them. The formation must have sufficient bearing strength and stability, must show reasonable settlement behaviour and must provide good drainage. If the existing subgrade is inadequate it can be improved by consolidating the ground with mechanical means or by means of chemical stabilization (Esveld, 2001).

The main advantages of a ballasted track as stated by Esveld (2001) are as follows:

- Low construction costs when compared to other track types.
- Ballasted track has good elasticity.
- Replacement of track components is simple.
- Easy to make small adjustments to track layout.
- Simple to make corrections to track geometry.
- Has good noise damping properties.

- Good drainage of moisture.
- Ballasted track is a proven technology.

### **2.1.2 Ballastless Track**

A general problem that occurs with ballasted track is the slow deterioration and subsequent settlement of the ballast material due to traffic loading. This requires regular maintenance of ballasted track to restore track alignment. However this can be prevented in the case of ballastless track.

Ballastless track can be divided into two further categories, namely track that is supported by discrete beams and track that is supported by a continuous slab.

#### **2.1.2.1 Slab Track**

The term "slab track" is used to describe ballastless track structures that may have combinations of a concrete slab, ties and a road pavement. One of the very first instances of slab track being used occurred in 1899 when the Southern Railroad built a concrete slab under existing track to stabilize a section of track (Bilow and Randitch, 2000). In recent times, factors such as life cycle cost, construction time, durability and availability have begun to play an increasingly important role. In the past, new projects were assessed on the basis of investment costs. As life cycle costing becomes more prominent, ballasted track systems could lose attractiveness in favour of slab track systems (Esveld, 2001).

The structure of a slab track is made of stiff and brittle materials and the required elasticity can be obtained by inserting elastic components below the rail (Michas, 2012). Slab track can be divided into two further categories, namely slab track that provides discrete support and slab track that provides continuous support to the rails (Esveld, 2001).

Slab track costs more to construct than ballasted track but subsequent maintenance costs are substantially reduced (Brown, 1983). Recent slab track construction costs have been found to be 30% to 50% higher than that of standard ballasted track, however in Japan the maintenance costs for slab track are one-quarter of those for ballasted track (Bilow and Randitch, 2000). Esveld (2001) stated that slab track's maintenance costs are approximately 20% to 30% less which agrees with the findings of

Bilow and Randitch (2000).

Research and development of slab track began during the 1960's. The first test section of slab track was built in the Bözberg Tunnel in Switzerland. There has been long term experience with slab track in Germany with a section of slab at the Rheda station that has been in use since 1972. The rails and fastening system have been in place since construction. Since 1972 the track has carried more than 750 million gross tonnes. Slab track has been used extensively in Japan on their high speed lines (Steidl, 2009). Slab track requires the foundation on which it is built to have as little differential settlement as possible in order to provide adequate performance. For this reason slab track is most commonly found in tunnels and on bridges. Due to the fact that there is very little scope to alter the track geometry after construction, special preparation of the subsoil before construction is essential (Esveld, 2001).

There are a number of different slab track systems in use worldwide, each with varying construction methods, performance and cost.

Michas (2012) summarised the total length of various slab track systems that have been constructed worldwide as depicted in Table 2.1.

**Table 2.1** Total length of various slab track systems constructed worldwide Michas (2012)

Slab track design	Country of design	Total Construction (km)
Bögl	Germany	4391
Shinkansen	Japan	3044
RHEDA	Germany	2205
Sonneville-LVT	Switzerland	1031
Züblin	Germany	606
Stedef	France	334
Infundo-Edilon	Netherlands	211
ÖBB-Porr	Austria	122.2
IPA	Italy	100
PACT	United Kingdom	95.4
SATO	Germany	35.8
FFYS	Germany	33.1
BTD	Germany	32
PY SLAB	South Africa	32
ATD	Germany	31.7
Getrac	Germany	15.3
Walter	Germany	9.4

The advantages of ballastless track have been broadly summarised by Michas (2012) as the following:

- Lower maintenance need during its life cycle. No need for tamping and ballast cleaning which results in maintenance costs being 20% to 30% of that of ballasted track.
- Longer life cycle of 50-60 years compared to 30-40 years for ballasted track.
- More cost effective line positioning.
- No ballast or solid particles fouling the track structure.
- Higher safety against lateral forces and accommodation of higher axle loads.

- Cost of vegetation control significantly reduced or excluded.
- Near maximum line availability and minimal disturbance to nearby residents during night time occupations.
- Reduced height and weight of the structure which is particularly important on bridges, where cost savings could be significant with a more economical design (de Wet, 2012).
- Better load distribution resulting in lower dynamic loading of the subsoil.
- Lower wear on vehicle running gear through good retention of track geometry.

The disadvantages have also been broadly summarised by Michas (2012) as the following:

- Limited adaptability to large displacements; large displacements could require significant amounts of work.
- Not really possible to apply any innovations or design improvements once construction has been completed.
- Higher noise emissions which could require extra treatment and hence increased initial cost.
- Cost of reconstruction once the end of its life cycle is reached is not considered.
- Transitions between ballasted and ballastless track require special attention.
- Special care should be given to foundation preparation as homogenous sublayers are required to carry the imposed loads with little settlement.
- Cannot be built in areas where significant consolidation settlement or earthquakes occur.

## 2.2 TRACK TRANSITIONS

To provide a safe and reliable system for high speed lines, the track geometry will have to be consistently good. For heavily used mixed lines, ballast and formation maintenance are a high priority due to the level of stresses induced by the freight. As traffic volumes increase, significantly more track maintenance will be required. In addition, high loading sites such as cross-overs and turnouts generate significant maintenance issues due to high lateral forces that may generate track misalignments. Bridge and other track transitions also require significant maintenance, especially for trains with high axle loads or high speeds.

When maintenance of these transition sections is neglected, accelerated deterioration in track geometry can be expected. This may lead to pumping of ballast, swinging or hanging cross sleepers, permanent rail deformations, worn track components, and deteriorating rail surface and gauge. An example of mud pumping occurring on a heavy haul line is shown in Figure 2.2. This image shows water pumping out from the subballast layer after the ballast layer had been cleared for observation purposes. These track faults may increase the potential for derailment (Lei and Zhang, 2010).



**Figure 2.2** Mud pumping on a heavy haul line

In rail transit systems at grade conventional ballasted track can change to a ballastless track system, or a conventional track system on a structure. The abrupt change in track support that occurs at these locations has often been associated with accelerated rates of track geometry and component

degradation, which in turn can lead to poor ride quality and high maintenance demand. In response to these problems a number of techniques have been proposed to improve track performance by providing a smooth transition between the dissimilar track structures (Read and Li, 2006).

Various track transition problems and their solutions are now discussed.

### 2.2.1 Track Transition Problems

According to Li et al. (2003) and Li and Davis (2005) problems at bridge approaches can be attributed to the following factors:

- The abrupt change in vertical stiffness of the track. This abrupt change causes the wheels to experience an equally abrupt change in elevation due to the uneven track deflection. This abrupt change in elevation causes rapid changes in the vertical acceleration of the wheels. The effect of the load increase depends on the direction of the train. When the train movement is from a section of higher stiffness to one of lower stiffness - such as exiting a tunnel or bridge deck, the dynamic load is applied to the track section with the lower stiffness, increasing the rate of settlement. This condition is characterised by the deterioration of track geometry, ballast migration and sleeper movement on the lower stiffness track. When the train direction is reversed (moving from lower stiffness to a higher stiffness track section) the load increase occurs on the high-stiffness side of the transition over a short distance and is more of an impact load. Typical problems experienced in this case are rail surface fatigue, sleeper deterioration and rail pad deterioration.
- At grade ballasted track may inherently settle more than ballasted track on a structure, which will create a dip in the surface at the transition, even if the dynamic loading effects are minimal. This is especially true when the structure abutment is built on a deep pile foundation where settlement is negligible.
- Geotechnical issues affecting the subgrade performance such as low strength soils, deficient soil placement and compaction as well as poor drainage, can cause the settlement of at-grade track to be variable.
- Environmental factors such as wet/dry and freeze/thaw cycles also affect subgrade settlement behaviour.

Li and Davis (2005) also reported that inadequate ballast and subballast layer performance is the primary cause of track geometry degradation. Using settlement rods installed in a test section they observed no significant subgrade movements. However they did report significant track geometry deterioration for the site that contained a cement-stabilised backfill. On the other hand Li and Selig (1994) identified subgrade stiffness to be the most influential parameter affecting the moduli of ballasted tracks. In track transitions, problems are often related to the stiffness of the approach track bed which would indicate that the subgrade layer plays the most significant role in governing differential movement at track transitions.

Several factors have been identified as most critical affecting the differential movement at track transitions. There is agreement between the literature as to the plausible mechanisms. Sasaoka and Davis (2005) attributed track transition problems to three primary factors:

- Differential settlement
- Differences in settlement characteristics
- Discrepancies in track damping properties between adjacent sections

Similarly Li and Davis (2005) list:

- Track stiffness change
- Ballast settlement
- Geotechnical issues

Following an extensive review of published literature, Nicks (2009) listed ten factors contributing to "bump" development at railway bridge approaches.

- Differential track modulus
- Quality of approach fill
- Impact loads
- Ballast material
- Drainage
- Damping
- Abutment Type

- Bridge Joint
- Traffic considerations
- Quality of construction

### 2.2.2 Track Transition Remedial Measures

Researchers have proposed a number of different remedial measures to mitigate differential movement problems at track transitions. Nicks (2009) categorised remedial measures that aimed at reducing "bump" development at railway bridges into the following categories:

1. Limit approach settlement
2. Decrease modulus on bridge deck
3. Increase modulus on approach track
4. Reduce ballast wear and movement
5. Increase damping on bridge deck

Ame (1993) concluded that the majority of problems that occur at track transitions arise from rapid changes in the vertical acceleration of wheels and cars in the transition zone. Thus all remedial measures should aim to reduce the vertical train deflection. These remedial measures can further be divided into three categories:

1. Smoothing the stiffness ( $k$ ) distribution on the "soft" side of the transition
2. Smoothing the transition by increasing the bending stiffness of the rail-tie structure on the "soft" side, in close vicinity of the transition point, and
3. Reduce the vertical stiffness on the "hard" side of the transition

Various track transition remedial measures are now discussed.

#### Track Stiffness with Longer Sleepers

One of the oldest and most commonly used transition designs is the installation of a series of increasingly longer ties on the ballasted track side of the transition. This approach is demonstrated in Figure 2.3. This method assumes that the track stiffness is increased as a result of the larger bearing area due to the longer sleepers. However, the effectiveness of this approach is dependant on uniform ballast

density of the ballast beneath the tie from the gauge side rail seat to the end of the sleeper (uniform tamping is a requirement) (Ame, 1993). Longer ties may also exceed the embankment width on narrow bridge approaches, allowing the ballast to migrate from sleeper ends. Following a GEOTRACK analysis conducted by Sussman and Selig (1998), it was found that although a longer sleeper may engage a larger bearing area, it does little to increase the track stiffness. In order to increase stiffness it was recommended that longer sleepers be placed at reduced spacing and/or increasing the tie cross section, which in effect creates a stiffer track panel.

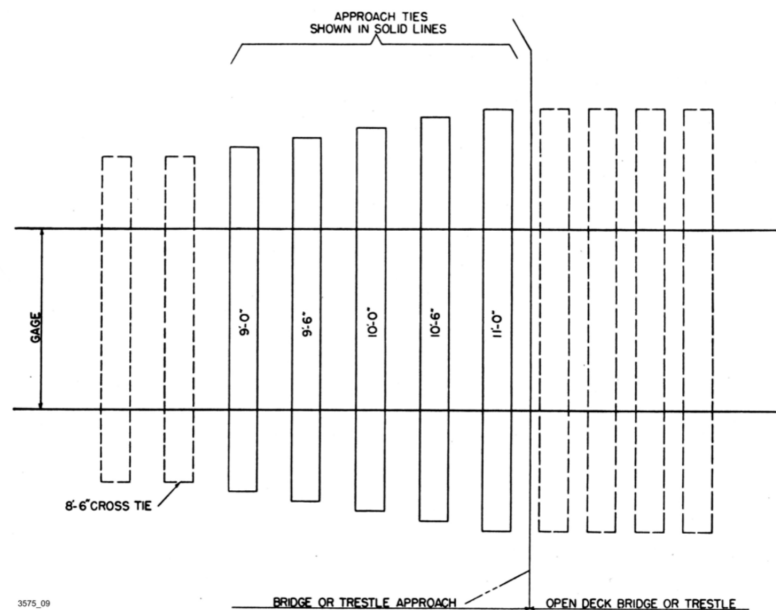


**Figure 2.3** AREMA Plan No. 913-52 approach sleeper for open bridge decks

### Hot Mix Asphalt (HMA) Underlayment

The positive performance of a Hot Mix Asphalt (HMA) underlayment layer placed between the ballast and subgrade layers to reinforce weak subgrades is well documented by Rose (1998) and Rose et al. (2002). These studies show that when properly designed and installed a HMA layer will reduce subgrade stresses and differential settlement and extend track maintenance cycles. Due to HMA being a structural layer it can reduce subgrade stresses to levels that will not exceed the compressive strength of low-strength soils. However, research conducted by Li and Davis (2005) found that HMA placed on the approach to a ballast deck concrete bridge with a well compacted subgrade did not reduce the geometry deterioration of the approach when compared to a similar approach that did not contain HMA underlayment.

Furthermore this reasearch showed that the differential settlement seen on approaches was caused primarily by settlement in the ballast layer rather than the subgrade. Thus the use of HMA, geocell and soil cement will not improve ballast performance on stiff subgrades. For cases where the approach stiffness is already high, it would appear that trying to further increase the approach stiffness is not as effective as reducing the stiffness on the more stiff or "hard" section (Read and Li, 2006).

### **Additional Rails**

The German Federal Railways have a design for high speed lines where lengths of rails are installed between the running rails on the field side of the running track to stiffen the ballasted track panel (Ame, 1993).

### **Approach Slabs**

A reinforced concrete slab that rests on the abutment or slab structure and is tapered toward the at-grade end is often used at transitions to direct-fixation aerial structures and tunnel/subway inverts. General specifications for an approach slab design are provided by Sharpe et al. (2002). In addition to the slab, the design calls for the vertical adjustment of the rail which allows for the ballasted side to be raised higher than the desired final elevation and to settle to the desired final elevation (design tamping) (Read and Li, 2006).

### **Stone Columns and Piles**

The use of stone columns has shown positive results in practice. A stone column consists of a borehole that is filled with aggregate material that is compacted in 150 mm layers. Stone columns are designed to strengthen and enhance drainage of weak subgrades (Read and Li, 2006).

Li et al. (2003) also indicated that other types of piles including concrete, timber and sand are accepted methods of stabilising weak subgrades. The skin friction provides most of the load transfer capability unless the end of the pile is placed in a firm foundation. The effectiveness of the pile is dependant on its length and different length piles can be used to smooth the stiffness of the approach (Read and Li, 2006).

### **Other Geotechnical Considerations**

The use of stone columns, HMA, soil cement, geosynthetic materials and piles are all techniques that can be used to reduce differential settlement at track transitions by reinforcing or stabilising a weak subgrade. Consideration should be given to improving subgrade performance especially during construction, using established geotechnical practices such as the following as described by Read and Li (2006):

- Determination of soil characteristics prior to construction by performing suitable soil tests.
- Using selected non-cohesive soils or the application of admixtures to existing soils if needed to improve subgrade strength.
- Maintenance of the optimum moisture content and correct use of compaction techniques.
- Ensure maximum and uniform soil density by performing adequate soil density testing.
- Removal of ruts, crowning or sloping in the subgrade, and/or the use of end drains.
- Lowering of ground water levels or the installation of cut-off layers if needed.
- Allowing for adequate embankment width to accommodate the ballast/subballast depth.
- Allow for adequate embankment slope angles or the use of benches, retaining walls, or sheet piles for slope stability.

### **Reducing Track Stiffness on Ballast Bridge Decks**

According to Sasaoka and Davis (2005) the use of composite plastic sleepers as replacement for concrete sleepers and the use of concrete sleepers with rubber undersleeper pads were both shown to be successful at reducing track modulus of the stiffer bridge deck sections.

## 2.3 BALLAST

This section discusses the specifications for railway ballast, ballast fouling, shear strength as well the effect of particle size distribution and confining pressure on ballast behaviour.

### 2.3.1 Ballast Specifications and Testing

In order to ensure that ballast used is of good quality, tests exist to determine the ballast quality after it has been quarried as the mechanical and dimensional properties are of importance.

Al-Saoudi and Hassan (2014) tabulated a number of different ballast specifications as shown in Table 2.2. The table compares specifications between the Iraqi Rail specifications (IRR), Railtrack Line specifications in North America (RT/CE), Network Rail in the UK (BS EN) and Australian Rail specifications (AS).

**Table 2.2** Ballast properties according to testing as well as different specifications adapted from Al-Saoudi and Hassan (2014)

Test name	Test Results	IRR limit	RT/CE limit	BS En limit	AS limit
1 Compression Test	850 kg/cm <sup>2</sup>	650 kg/cm <sup>2</sup>	NR	NR	NR
2 Abrasion Test	5.2 %	< 25 %	NR	≤ 20 %	NR
3 Wet Attrition (WAV)	5.3 %	NR	≤ 4 %	NR	≤ 6 %
4 Aggregate Crushing (ACV)	NM	NR	≤ 22 %	NR	≤ 25 %
5 Flakiness index	NM	NR	≤ 40 %	≤ 35 %	≤ 30 %
6 Elongation index	NM	NR	≤ 50 %	≤ 4 %	NR
7 Point load index	NM	NR	NR	NR	No limit
8 Micro-deval	7.36 %	NR	NR	≤ 7 %	NR
9 Misshapen particle	NM	NR	NR	NR	≤ 30 %
10 Crushing strength	NM	NR	NR	NR	No limit

NR not required, NM not measured

The Wet Attrition Value (WAV) is a test where the durability of the ballast is tested by typically placing a specimen mass of 5kg in a cylinder which is then rotated 10 000 times at a rate of between

30 - 33 rpm while at an angle of 30 degrees to the axis of rotation (Selig and Waters, 1994). The amount of material passing the 53.0 mm sieve but retained on the 37.5 mm sieve is referred to as the WAV.

The aggregate crushing value (ACV) test is described in TMH1 Test B1. The ACV of an aggregate is determined by gradually crushing a sample of material (that passes the 13.2 mm sieve and is retained on the 9.50 mm sieve) with a compressive load of 400 kN. The ACV is expressed as a percentage of the test sample material that is crushed finer than a 2.36 mm sieve (CSIR, 1986).

McNally (2002) states that in practice a proportion of misshapen particles - flaky or elongate is always present and this percentage of misshapen particles is severely limited in most standards for the reason (amongst others) that elongated particles are more prone to flexural breakage causing the aggregate mix to become finer than their nominal grading.

Rusnak and Mark (2000) describes the point load test (PLT) as a test that is done to determine the Point Load Strength Index ( $I_{s(50)}$ ) of a rock sample. The PLT involves compressing a rock sample between conical steel platens until failure occurs. The crushing strength of a rock material is often determined by means of an uniaxial compressive strength (UCS) test. The results of the UCS test are widely understood to be a rough index which gives the first approximation of the material strength.

In South Africa the S406 (1998) - Specification for the Supply of Stone is used. Spoornet (1998) states that ballast shall comply with SABS Standard 1083. The standard focuses on the following properties of the ballast:

- Relative density
- Grading
- Flakiness index
- Los Angeles Abrasion (LAA)
- Void ratio
- Plasticity of fines generated from the abrasion test

The Mill abrasion test should also be conducted on ballast samples according to S406. No dolerite stone is to be used. The S406 specification specifies that the ballast specific gravity should not be lower than 2.5. The specification requires the ballast to conform to the particle size distribution as

shown in Figure 2.4.

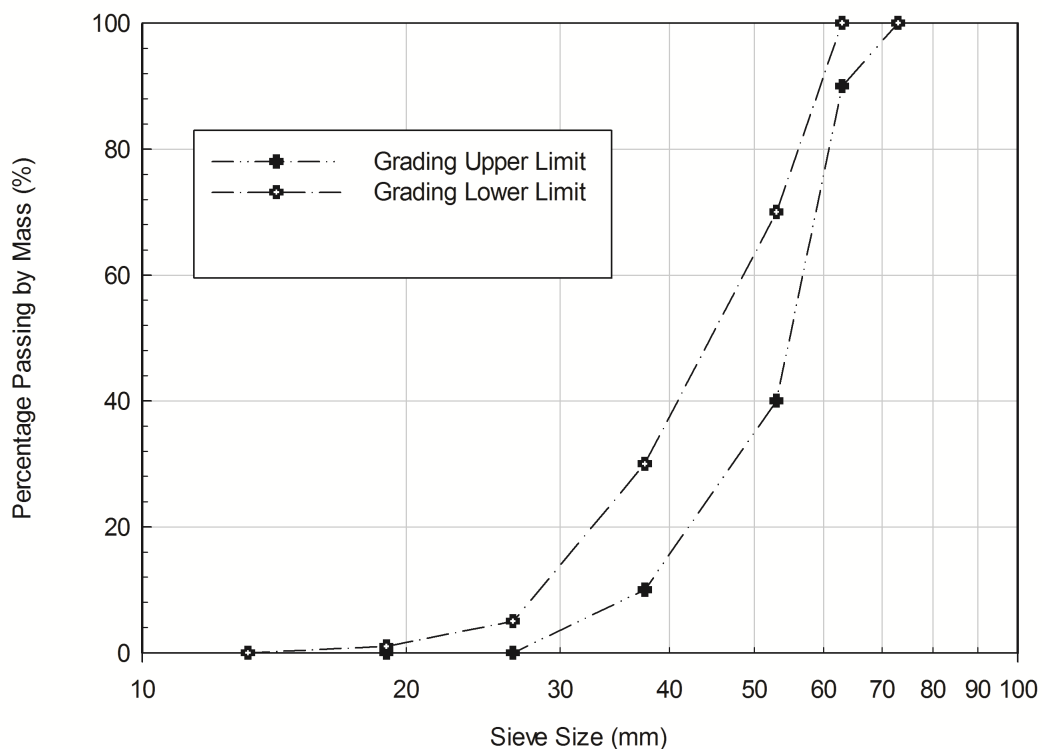


**Figure 2.4** South African Heavy Axle Line Ballast Grading

The South African ballast specification (S406) lists some other requirements as follows:

- The flakiness index should be measured in accordance with SABS 1083 (latest revision) and shall not exceed 30%.
- The Los Angeles Abrasion (LAA) value should be determined in accordance with ASTM C 131 - 89 Grading B, shall not exceed 22%. The fines that are generated while conducting the LAA test should have a plasticity index of less than 6.
- The voids should also be measured in accordance with SABS 1083 (latest revision) and should not be less than 40%.

### 2.3.2 Ballast Fouling

When ballast has been in service for a significant amount of time, it becomes damaged and contaminated. As a result, the grading of the ballast changes which leads to a loss in performance. The process through which this occurs is known as fouling. Selig and Waters (1994) list the five causes of ballast fouling as:

- Ballast breakdown
- Infiltration from ballast surface
- Sleeper wear
- Infiltration from underlying granular layers
- Subgrade infiltration

Ballast fouling prevents the ballast from fulfilling its functions. The impact thereof is dependent on the amount and size of the fouling material. As the mass of sand and fine-gravel-sized fouling particles (0.075 mm to 19 mm) increases, the resiliency to vertical deformation, as well as the void space decreases. Fouled ballast is gap-graded. This results in a reduction in drainage and could make surface lining operations difficult. As the void space is filled, the density of the ballast material increases. Should this material then be tamped, a higher rate of ballast settlement can be expected after tamping. An increase in the mass of clay and silt-sized particles (particle sizes smaller than 0.075 mm) also results in reduced drainage leading to ballast erosion and subgrade attrition. When mixed with water, fine particles may form a slurry that is abrasive to the ballast material. Fouled ballast with high water content leads to higher rates of plastic strain in the fouled ballast.

A ballast fouling index is used to quantify the degree of ballast fouling. The Selig and Waters (1994) fouling index ( $F_I$ ) is used in North America. This fouling index is calculated as the sum of the percentage of particles passing the 4.75 mm (P4) sieve and the percentage of particles passing the 0.075 mm (P200), therefore ( $F_I = P_4 + P_{200}$ ). Using this index, ballast with an index between 20% and 39% is considered highly fouled.

The second parameter to be considered is the rate at which water can flow through the ballast. This is characterised by hydraulic conductivity. Fouled ballast would have a low hydraulic conductivity ( $k$ ). This could be problematic as one of the primary functions of the ballast is to maximise the drainage of water. According to Shukla (2002) the hydraulic conductivity( $k$ ) of fouled ballast can range from

1.5 mm/s to less than 0.005 mm/s.

A number of ballast fouling indices have been established in order to quantify the degree of fouling. This is shown in Table 2.3.

**Table 2.3** Ballast fouling indices from Selig and Waters (1994)

Fouling index			Classification
$F_I = P_{0.075} + P_{4.75}$ (Selig and Waters, 1994)	$F_{IP} = P_{0.075} + P_{13.2}$ (Ionescu, 2004)	$F_{ID} = D_{90}/D_{10}$ (Ionescu, 2004)	
< 1	< 2	< 2.1 & $P_{13.2} \leq 1.5$	Clean
1 to < 10	2 to < 10	2.1 to < 4	Moderately Clean
10 to < 20	10 to < 20	4 to < 9.5	Moderately Fouled
20 to < 40	20 to < 40	9.5 < 40	Fouled
$\geq 40$	$\geq 45$	$\geq 40$ , $P_{13.2} \geq 40\%$ , $P_{0.075} > 5\%$	Highly Fouled

South Africa uses a method proposed by Pretorius (1993), based on the percentage fine material passing the 19.0 mm, 6.7 mm, 1.18 mm and 0.15 mm sieves. The degree of fouling is calculated through the following formula:

$$F_e = (K_1 \times F_{19}) + (K_2 \times F_{6.7}) + (K_3 \times F_{1.18}) + (K_4 \times F_{0.15}) \quad (2.1)$$

Where:

$F_e$  = Effective degree of fouling

$$F_{19} = \frac{[\text{percentage passing (19 mm) sieve}] \times 100}{27}$$

$$F_{6.7} = \frac{[\text{percentage passing (6.7 mm) sieve}] \times 100}{18}$$

$$F_{1.18} = \frac{[\text{percentage passing (1.18 mm) sieve}] \times 100}{11.5}$$

$$F_{0,15} = \frac{[\text{percentage passing } (0.15 \text{ mm}) \text{ sieve}] \times 100}{5.5}$$

With  $K_1 = 0.4$  ;  $K_2 = 0.3$  ;  $K_3 = 0.2$  ;  $K_4 = 0.1$

The effective degree of fouling  $F_e = 0$  corresponds to clean ballast, while  $F_e = 100$  corresponds to fouled ballast where all voids are filled with fine material. It is possible to obtain a degree of effective fouling  $F_e > 100$ , where separation of the ballast structure has taken place as a result of mud pumping.

### 2.3.3 Shear Strength

The shear strength of granular materials is assumed to vary linearly with the applied stress, and Mohr-Coulomb failure is used to describe the shear behaviour. However, research by Indraratna et al. (1993) and Ramamurthy (2001), among others, has shown that when soils at high stresses and rocks at low normal stresses are tested, a non-linear shear strength response is found. For this reason the cohesion intercept value  $c$  and the shear resistance angle ( $\phi$ ) cannot be used to describe the failure envelopes for the entire range of stresses (Shahin et al., 2007).

For this reason Indraratna et al. (1993) proposed a non-linear strength envelope which is represented by Equation 2.2 :

$$\frac{\tau_f}{\sigma_c} = m \left( \frac{\sigma'_n}{\sigma_c} \right)^n \quad (2.2)$$

Where  $\sigma_c$  is the uniaxial compressive stress of the parent rock determined from the point load test,  $m$  and  $n$  are dimensionless constants,  $\tau_f$  is the shear stress at failure and  $\sigma'_n$  is the effective normal stress.

### 2.3.4 Effect of Particle Size Distribution

Currently the ballast size distributions used in railway lines are very uniform and contain only a small percentage of fines. Several studies have found well-graded distributions to have several benefits such as superior strength and reduced settlement, but they are rarely employed due to reduced drainage capacity and increased fouling risk (Shahin et al., 2007). Indraratna and Salim (2003) conducted large-scale cyclic triaxial tests on four different distributions of ballast in order to study how slight

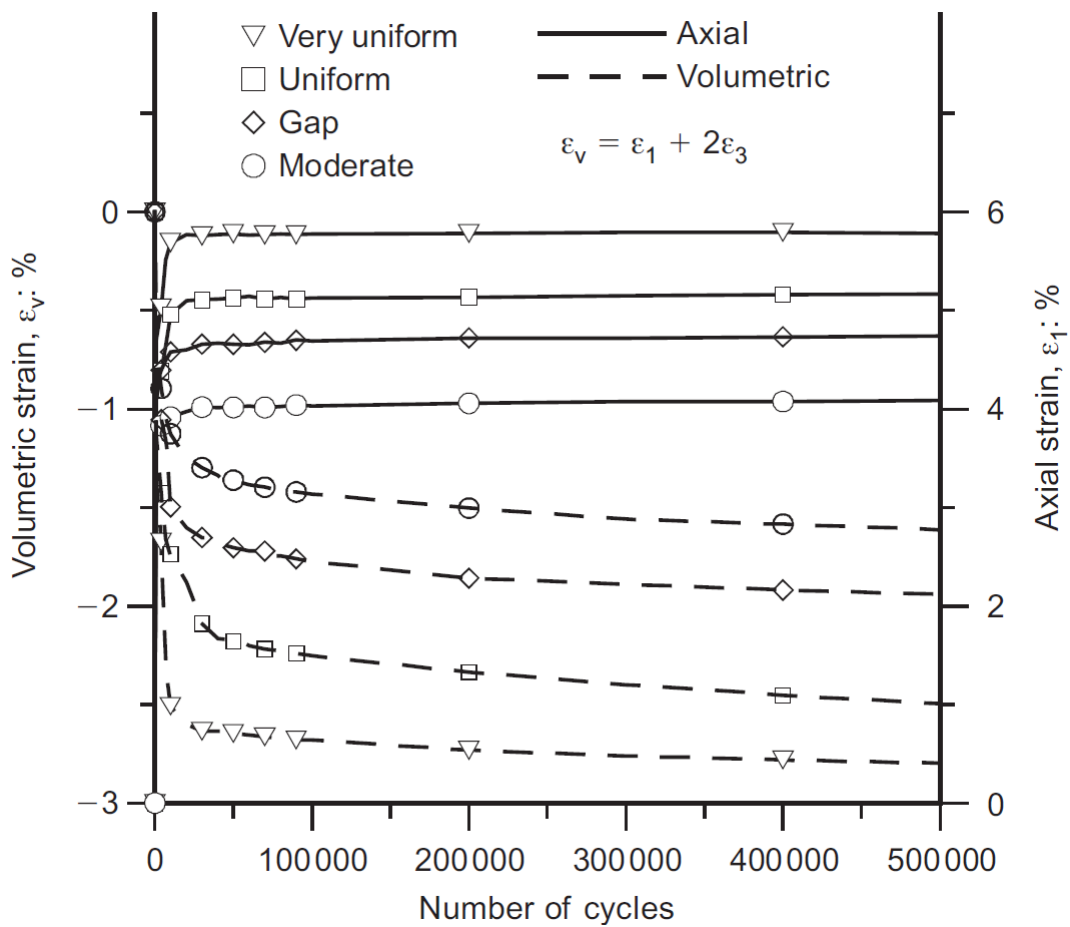


**Figure 2.5** Axial and volumetric strain response of different distributions under cyclic loading (In-draratna et al., 2004)

changes in particle size distribution can affect the deformation and degradation behaviour of the ballast. It is well known that well-graded specimens can be compacted to higher densities than uniform specimens. Samples were compacted to equivalent heights using a fixed compaction time; thus the specimens initial and void ratio varied. A confining pressure of 45 kPa was applied to mimic the low in situ pressures experienced on site. Loading was applied cyclically at a frequency of 20 Hz up to a maximum deviator stress  $q_{max}$  of 300 kPa. Figure 2.5 shows the effect of particle size distribution on axial and volumetric strain behaviour. The very uniform and uniform samples exhibit higher axial and volumetric strains, which is due largely to their looser states before cyclic shear. The gap-graded and moderately graded samples have a higher coordination number (number of contact points between particles) and form more dense particle arrangements which would result in a track structure that would experience reduced settlement and greater shear strength.

Figure 2.6 shows the relationship between the coefficient of uniformity ( $Cu_u$ ) and particle breakage.

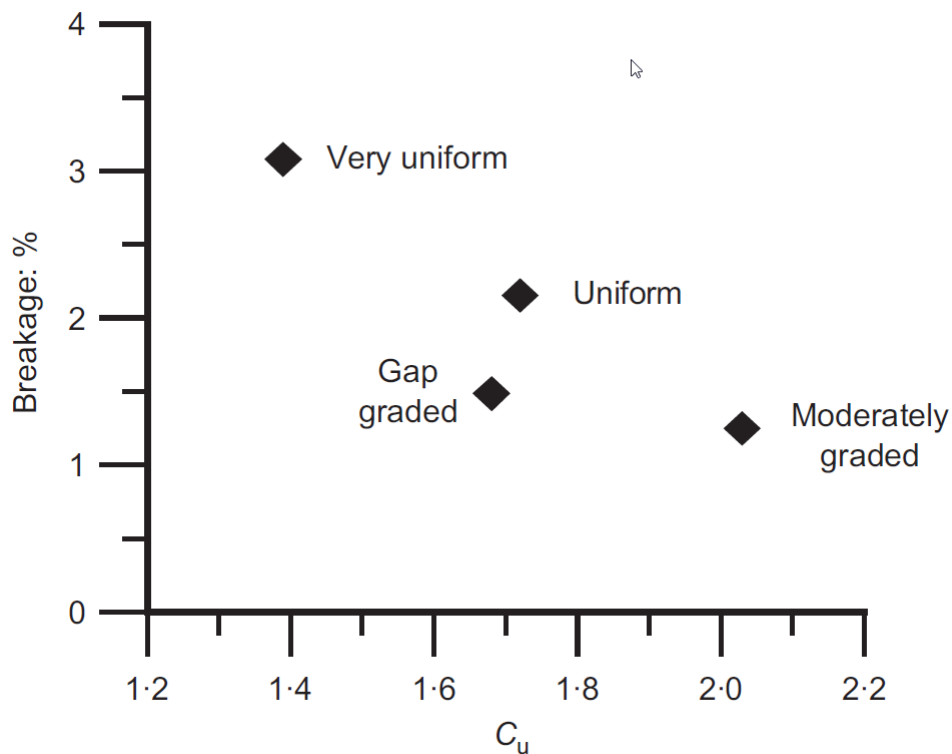


**Figure 2.6** Effect of grading on particle breakage (Indraratna et al., 2004)

All the samples apart from the gap-graded sample experience a decrease in the amount of particle breakage as the value of  $C_u$  decreases. Test results with a variable grading indicate that even modest changes in  $C_u$  can have a substantial effect on strain and breakage behaviour.

### 2.3.5 Effect of confining pressure

The effective confining pressure is considered to be one of the key criteria in various design procedures in geotechnical engineering, however in rail track design it is not considered as a significant factor. Rail track is essentially self supporting with minimal lateral restraint, meaning that during the passage of trains ballast and capping materials are free to spread laterally contributing to increased track settlement and decreased shear strength. Shahin et al. (2007) and Indraratna et al. (2004) conducted research into the effect of confining pressure on ballast behaviour using cyclic triaxial tests. Figure 2.7 shows the relationship between axial strain ( $\epsilon_1$ ) and volumetric strain ( $\epsilon_v$ ) as a function of confining pressure ( $\sigma'_3$ ). As expected increasing  $\sigma'_3$  leads to a decrease in  $\epsilon_1$ . Volumetric strain behaviour changes from dilation towards compression with an increase in  $\sigma'_3$ . Coarse materials will first compress and then dilate under static loading at low  $\sigma'_3$  values. Samples that dilate significantly

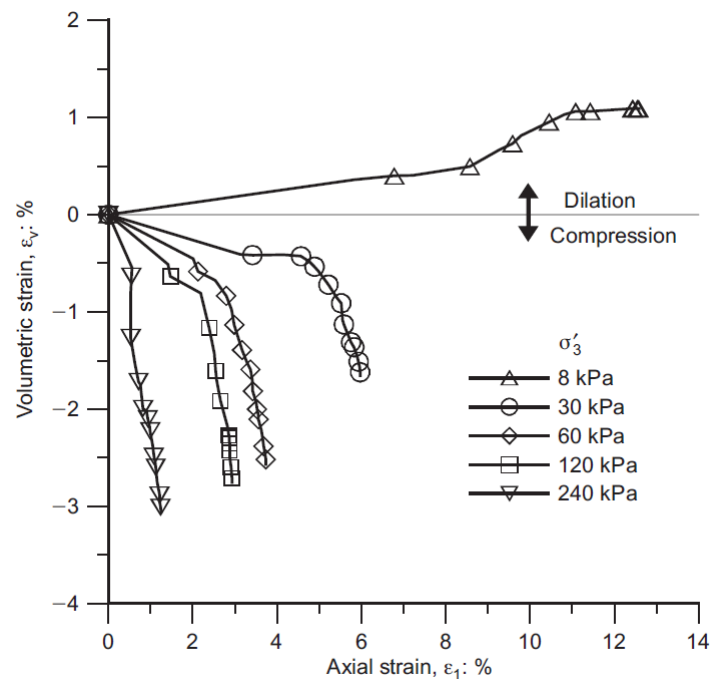


**Figure 2.7** Relationship between axial and volumetric strains for different confining pressures under cyclic loading (Indraratna et al., 2004)

do not usually show an initial period of compression under cyclic loading.

The effect of confining pressure ( $\sigma'_3$ ) on particle breakage is shown in Figure 2.8 where the sample breakage can be divided into three regions: (I) dilatant unstable, (II) optimum and (III) compressive stable degradation zones. At low confining pressures ( $\sigma'_3 \leq 30$  kPa), ballast specimens are subjected to rapid and large axial and expansive radial strains, resulting in an overall volumetric increase (dilation). Due to the small confining pressure in this zone specimens in this degradation zone are characterised by a limited coordination number (number of contact points between particles) and small particle-to-particle contact areas.

Increasing the confining pressure ( $\sigma'_3$ ) to a value of between 30 kPa to 75 kPa, the axial strain rate is greatly reduced owing to increased apparent stiffness and the overall volumetric behaviour is slightly compressive. Particles have sufficient lateral confinement to provide an optimum contact stress distribution and increased interparticle contact areas. Further increasing  $\sigma'_3$  to the compressive stable region with a  $\sigma'_3$  value of  $> 75$  kPa, the particles are forced against each other with limited ability to slide and roll and therefore breakage is not significantly increased.

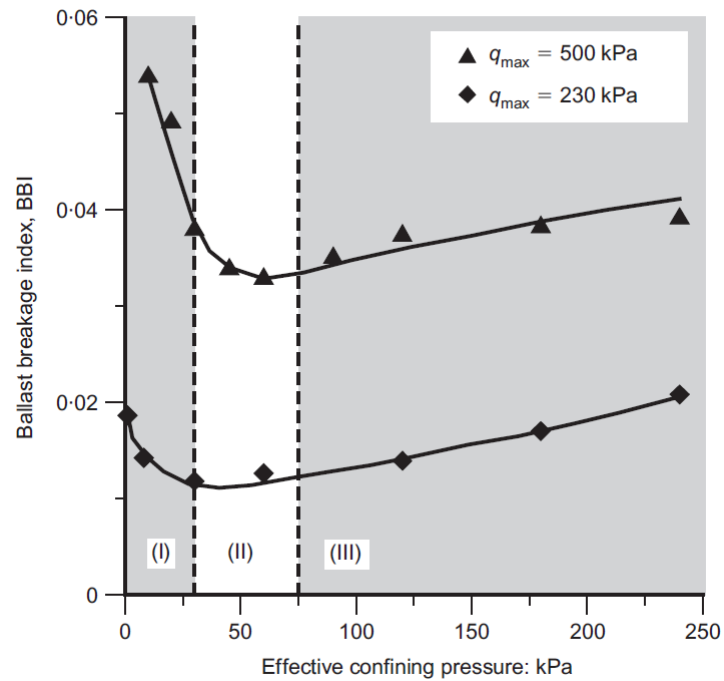


**Figure 2.8** Effect of confining pressure on particle breakage, showing degradation zones (Indraratna et al., 2004)

Although there is no direct measure of the in-situ confining pressure, it is expected that the effective confining pressures are estimated to be less than 20 kPa, meaning that the ballast is in the dilatant unstable region. Furthermore it is recommended that if ballast breakage is a problem on a particular track an increase in track confinement pressure may result in decreased breakage and superior track performance. Measures for increasing confinement include:

- reduction of sleeper spacing
- increase height of shoulder ballast
- use of intermittent lateral restraints at various track sections
- use of winged precast concrete sleepers.

## 2.4 PARTICLE BREAKAGE

This section deals with the fracture behavior of solids under loading.

### 2.4.1 Griffith theory

The Griffith theory is a widely used theory used by engineers and materials scientists to explain and determine the fracture behaviour of solids. Solids such as ceramics, glasses and rock may have flaws or cracks. Following an increase in stress at a crack, the material will have little plasticity to resist crack propagation and the failure mechanism will be a fast fracture. The fast fracture criterion according to Griffith theory is given by Equation 2.3:

$$\sigma\sqrt{\pi a} = \sqrt{EG_c} \quad (2.3)$$

where:

$\sigma$  = applied stress

$a$  = crack length

$E$  = Young's Modulus

$G_c$  = toughness

Toughness ( $G_c$ ) is the energy required to generate a unit area of crack. The unit is energy per unit area i.e. ( $J/m^2$ ) and is a property of the material. There are two cases when fast fracture can occur:

- When a material is under stress ( $\sigma$ ) and a crack grows and reaches critical size ( $a$ ), or
- A material with a crack length of  $a$  is under stress which increases to the critical stress  $\sigma$

The right hand side of the equation is dependent on material properties only. The constant on the right hand side of the equation is known as the fracture toughness or  $K_{IC}$  ( $K_{IC} = \sqrt{EG_c}$ ). The term on the left hand side of the equation is generally referred to as the "stress intensity factor" or  $K$  ( $K = \sigma\sqrt{\pi a}$ ). In order for fast fracture to occur, a critical combination of the stress and crack length must reach a

certain value. Fast fracture will occur when  $K = K_{IC}$ .

#### 2.4.2 Ballast Degradation and Particle Breakage

Shahin et al. (2007) summarised the main causes of ballast degradation as:

- Excessive cyclic loading and vibration
- Temperature
- Moisture changes
- Impact loads due to severe train braking.

The ballast degradation can occur in three ways: (1) the grinding-off of small-scale particles (abrasion), the resulting fines cause fouling and reduce drainage, (2) the breaking of fragments which influences the initial settlement and (3) the fracturing and splitting of individual particles.

Research by Hardin (1985) and Lade et al. (1996) found that the size effect, i.e. the larger a particle is, the lower its strength. Thus, as particle size increases the probability of it breaking also increases. This is because larger particles contain more flaws. Smaller particles are generally formed by larger particles fracturing along their defects, as a result, smaller particles are less likely to fracture as they contain fewer defects. Angular particles break more easily because stresses can concentrate along their narrow dimension.

McDowell et al. (1996) stated that the probability of breakage occurring in an aggregate increases with an increase in applied macroscopic stress, an increase in particle size and a reduction in coordination number. The coordination number refers to the number of contacts a particle has with neighbouring particles. Increasing the number of contacts a particle has could therefore reduce the probability of breakage. This is as a result of the loads being distributed between a larger number of contact points on the surface of the particle. This reduces the induced tensile stress. However, this effect is also dependent on the shape of the particle as shown in Figure 2.9. Cyclic tests conducted by Salim et al. (2006) and Indraratna (2000) indicated that well-graded ballast does not break as easily as uniformly graded ballast. Higher relative densities of ballast also reduce the amount of particle breakage.

Indraratna and Salim (2003) observed ballast degradation under both wet and dry conditions and upon saturation ballast experiences significant particle breakage. The main factors influencing ballast

breakage have been summarised by Shahin et al. (2007) as follows:

- ballast properties related to the characteristics of the parent rock (e.g. hardness, toughness, specific gravity, weathering resistance, grain texture, internal bonding and mineral composition)
- physical properties associated with individual particles (e.g. durability, particle shape, size, angularity, and surface roughness)
- factors relating to the assembly of particles and loading conditions (e.g. confining pressure, initial density, porosity, thickness of ballast layer, ballast grading, presence of water, or ballast moisture content, cyclic loading amplitude and frequency).

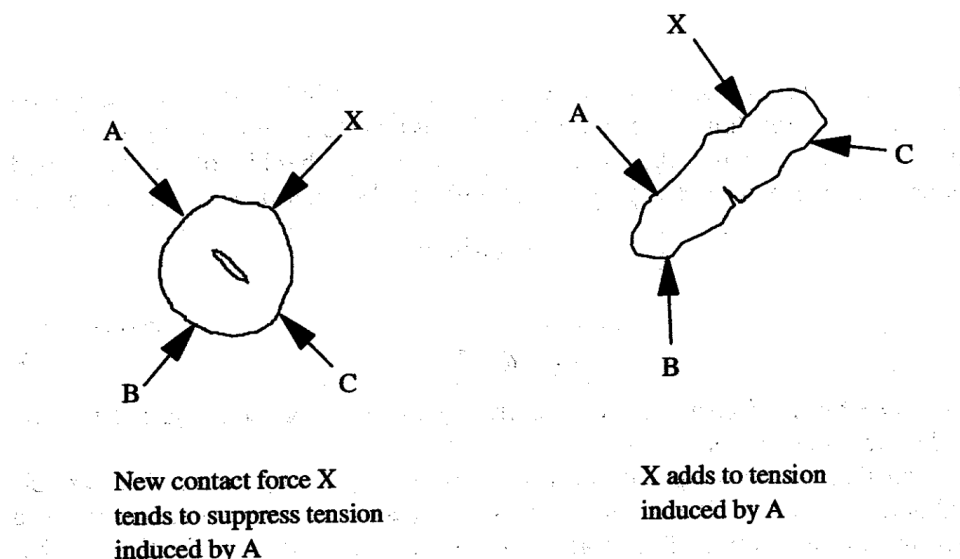


**Figure 2.9** Large coordination numbers are less helpful for more angular particles, from McDowell et al. (1996)

In order to quantify the amount of particle breakage a number of particle breakage indices have been proposed. These indices are primarily based on the changes in particle size before and after testing. The various techniques can be divided into two main categories:

- breakage factor based on increase in percentage passing a single sieve size (Lee and Farhoomand (1967), Leslie (1975), Lade et al. (1996) , Nakata et al. (1999))
- breakage factor based on change in the entire particle size distribution (Hardin (1985), Marsal (1967))

Hardin (1985) defined three measures based on changes in the entire particle size distribution: the breakage potential, total breakage and relative breakage. The breakage potential is defined as the area between the original grain size distribution curve and the 0.074 mm sieve size. Total breakage was defined as the area between the original and final particle size distribution curves. The relative breakage (a number between 0 and 1) was defined as the ratio between the total breakage and the potential breakage.

The breakage index could be quantified by comparing the plots of the particle size distributions. As the amount of breakage increases the particle size distribution shifts to the left and the area between this new line and the original particle size distribution is considered as the breakage zone (Christie et al., 2007). Christie et al. (2007) states that the breakage potential is considered to be the area between the original particle size distribution and an arbitrary reference line connecting point between the intersection of  $d_{95}$  of the largest sieve size and the minimum particle size of 2.36 mm. This is shown in Figure 2.10.

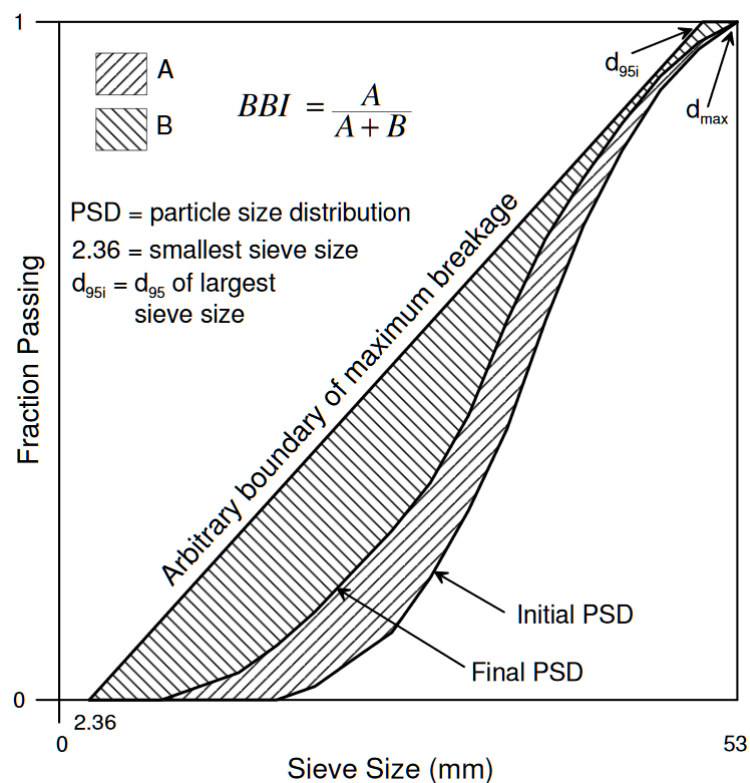


**Figure 2.10** Definition of ballast breakage Christie et al. (2007)

## 2.5 BEHAVIOUR OF AGGREGATE UNDER CYCLIC LOADING

The permanent deformation in railway track granular materials is usually in the form of settlement. The track structure undergoes cyclic loading with passing of railway traffic. This section discusses the behaviour of aggregate under cyclic loading.

### 2.5.1 Resilient behaviour

A granular material that experiences cyclic loading undergoes deformation and this deformation can be divided into resilient deformation and permanent deformation.

The strains experienced in a granular material during one cycle of loading are shown in Figure 2.11.

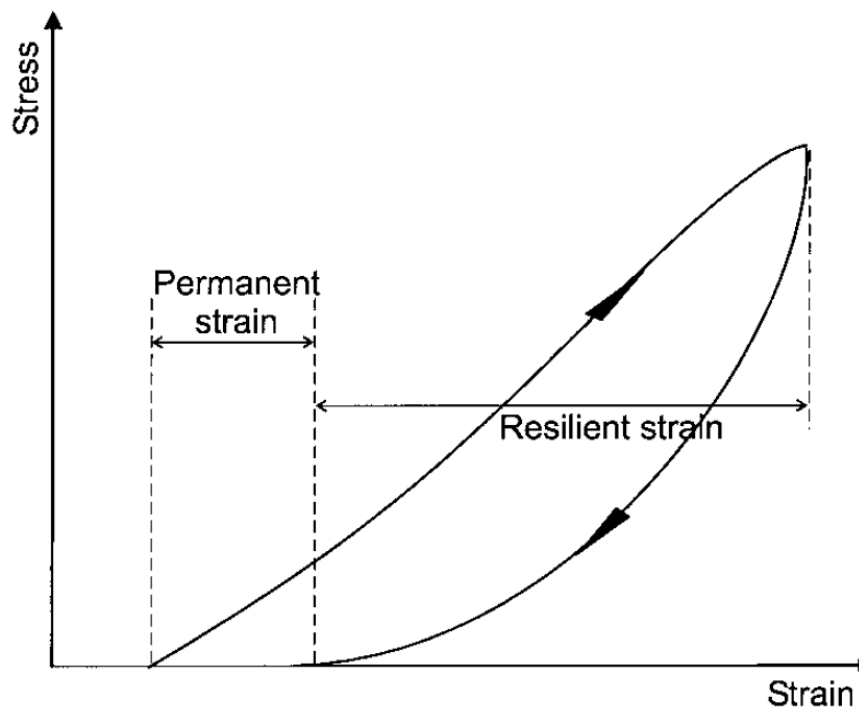


**Figure 2.11** Strain in a granular material during one cycle of load application (Lekarp et al., 2000)

For repeated loading in a triaxial test the resilient behaviour of granular material is characterised by the resilient modulus ( $M_r$ ) and Poisson's ratio ( $\nu$ ) defined in the Equations 2.4 and 2.5:

$$M_r = \frac{\Delta(\sigma_1 - \sigma_3)}{\epsilon_{1,r}} \quad (2.4)$$

$$\nu = -\frac{\epsilon_{3,r}}{\epsilon_{1,r}} \quad (2.5)$$

Where:

$\sigma_1$  = Major principal stress (axial stress)

$\sigma_3$  = Minor principal stress (horizontal stress)

$\epsilon_{1,r}$  = Resilient axial strain

$\epsilon_{3,r}$  = Resilient horizontal strain

The stiffness,  $K$ , at any one cycle is calculated as shown in Equation 2.6:

$$K = \frac{\sigma_{max} - \sigma_{min}}{\delta_r} \quad (2.6)$$

Where  $\sigma_{max}$  and  $\sigma_{min}$  are the maximum and minimum applied stresses respectively, and  $\delta_r$  is the resilient sleeper displacement.

Compaction, rearrangement and particle breakage are the main effects of stress history. The resilient modulus of the granular particles is also affected by the previous number of load cycles. In order to negate the effects of stress history while conducting repeated load resiliency tests, Hicks and Monismith (1971) suggested that test samples be loaded for 1000 cycles in order to ensure they were at the same level of compaction. Research conducted by Brown and Hyde (1975) concluded that provided the stress applied to granular materials did not cause failure, the resilient properties of the material would be unaffected.

As the number of load applications to a granular material increases, the material becomes stiffer resulting in an increase in the resilient modulus. After a number of load cycles, the resilient modulus reaches a constant value. Shenton (1974) conducted triaxial tests on railway ballast and found that when the maximum deviatoric stress were close to the material's failure level, the resilient modulus

increased rapidly during the first 10 cycles and became approximately constant after 100 cycles. Hicks and Monismith (1971) also found that in the case of partially crushed gravel and crushed rock the resilient modulus becomes constant after 50 to 100 load cycles provided that the ratio between maximum axial stress and confining stress does not exceed 6 or 7.

Collins and Boulbibane (2000) explained the concept of shakedown. Shakedown is shown in four stages as demonstrated in Figure 2.12. When the cyclic loading begins, there are no permanent strains. If the load then exceeds the elastic load, permanent strains will be induced. Eventually, after a finite number of applied load cycles, the behaviour becomes purely elastic. Once this point has been reached, the material is said to have reached "shakedown" and the resilient strain becomes constant resulting in a resilient modulus that remains constant, shown by Stage 2 in Figure 2.12.

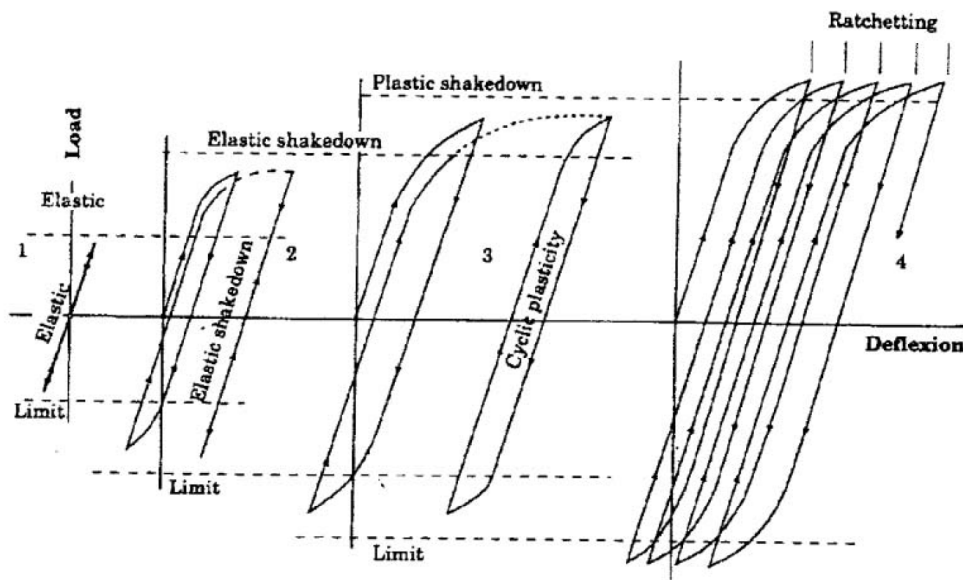


**Figure 2.12** Four stages of shakedown, describing the elastic/plastic response to repeated loading. (Collins and Boulbibane, 2000)

Should the material experience higher loads, shakedown does not occur and the behaviour will be either "cyclic plasticity" shown in Stage 3 in Figure 2.12 or "ratchetting" shown in Stage 4 in Figure 2.12, where permanent strain increases indefinitely. Should either of Stage 3 or Stage 4 occur, the material/structure will fail. The shakedown load is the critical load that separates shakedown and loads that cause failure.

During cyclic loading there is an accumulation of plastic strains and a reduction in void ratio which

is then followed by an increase in the stiffness of the specimen regardless of the initial bulk density. In uniaxial compression tests conducted by Indraratna et al. (1997) the resilient modulus ( $E_r$ ) varied from 105 MPa to 464 MPa for uncompacted ballast specimens, and from 313 MPa to 510 MPa for the compacted ballast.

### **2.5.2 Permanent deformation of cyclically loaded aggregate**

Granular materials in a railway track usually experience permanent deformation in the form of settlement. The settlement of ballast can be both elastic (such as initial settlement due to ballast compaction) and plastic (due to breakage of ballast particles). Selig and Waters (1994) identified that ballast settlement may not be a problem if it occurs uniformly along the length of the track. Differential settlement that may occur is of more concern than total track settlement.

Various sources do agree that permanent deformation of granular materials under cyclic loading is affected by many factors, such as:

- Stress Level
- Principle stress rotation
- Load cycle
- Moisture content
- Stress history
- Density
- Loading sequence
- Grading
- Frequency of loading

Brown and Hyde (1975) found that the permanent strain in a sample was directly proportional to the ratio of deviatoric stress to confining pressure. As a result permanent deformation increases with increased deviatoric stress or confining pressure.

Research conducted by Lim (2004) noted that near sleepers, no principle stress rotation occurred. The traffic load is transferred through the sleeper onto the ballast with the load being more concentrated near the sleeper. As a result of this the major principle stress of the ballast near the sleeper increases

suddenly as the wheels pass above it. However deeper ballast and subgrade material will be subject to principle stress rotation depending on the load spreading capability of the ballast. The stresses beneath a rolling wheel load are shown in Figure 2.13.

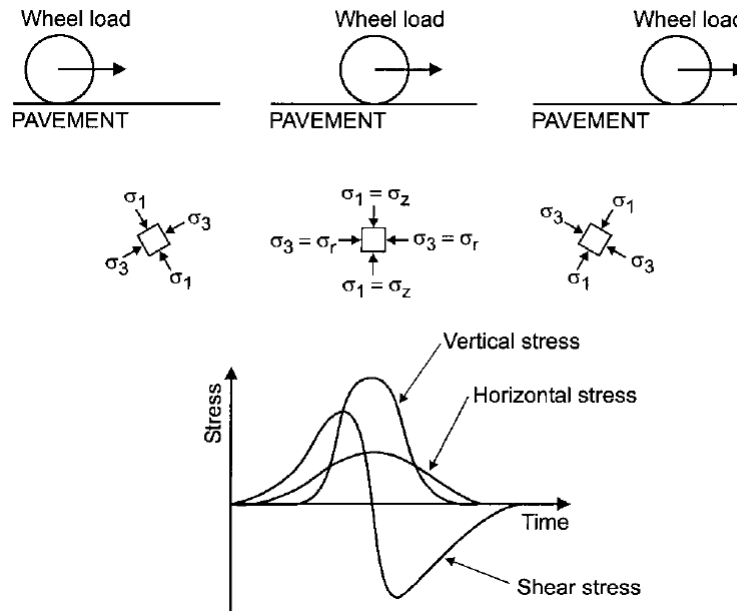


**Figure 2.13** Stresses beneath a rolling wheel load (Lekarp et al., 2000)

The number of load cycles also has an effect on the permanent deformation. Shenton (1974) found that permanent deformation is a linear function of the logarithm of the number of cycles as shown in Figure 2.14.

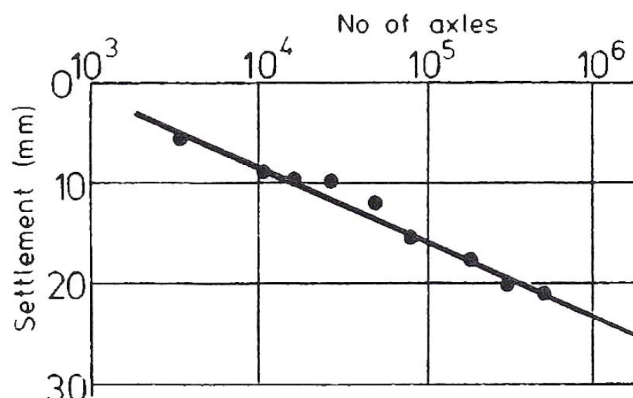


**Figure 2.14** Permanent deformation as a linear function of the logarithm of number of load cycle (Shenton, 1974)

According to Selig and Waters (1994) the loading sequence has no effect on permanent strain accumulation. The permanent strain of different samples under different loading sequences where the deviator stress was altered every 1000 cycles was shown to be approximately equal. This is shown in Figure 2.15.

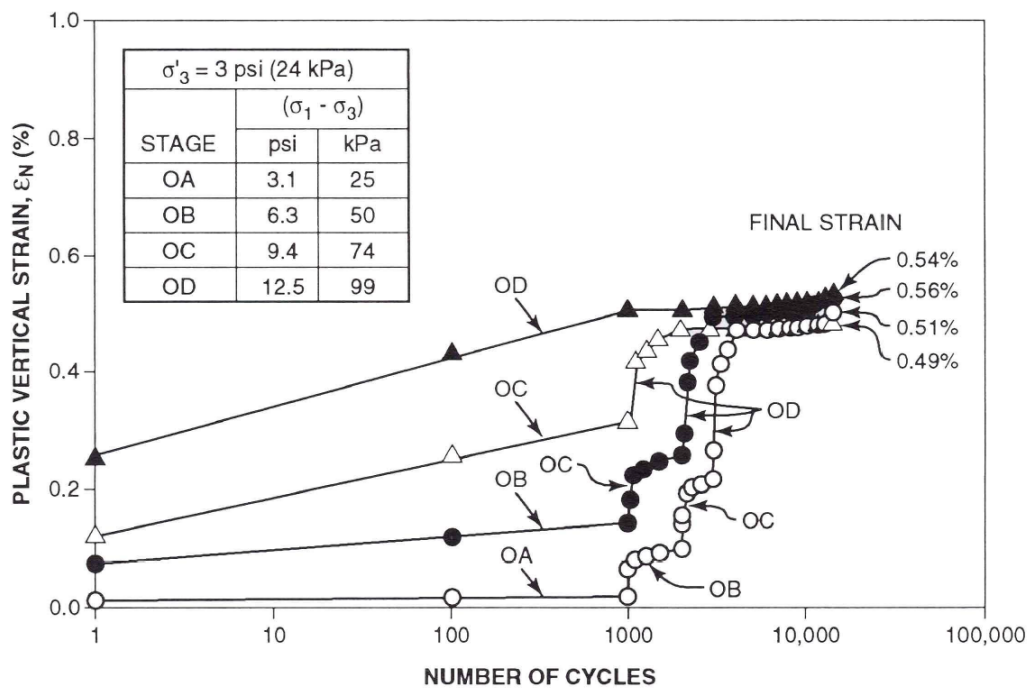


**Figure 2.15** Effect of loading sequence on permanent strain (Selig and Waters, 1994)

Ballast specimens under repeated loading behaved in a non-linear and stress-state dependant manner. The behaviour was also significantly different from the behaviour of the same material under static loading. In research conducted by Indraratna et al. (1997) it was found that during the first loading cycle of uncompacted specimens the axial strain developed rapidly (2.8% strain), and this was only partially recovered upon unloading (0.4%) as shown in Figure 2.16. Each additional cycle of loading caused an increment of plastic strain, but at a diminishing rate, varying from 0.24 % after the first cycle to 0.001% after approximately 50 cycles. Compacted ballast indicated much smaller permanent axial strain, i.e. 0.58% after the first cycle.

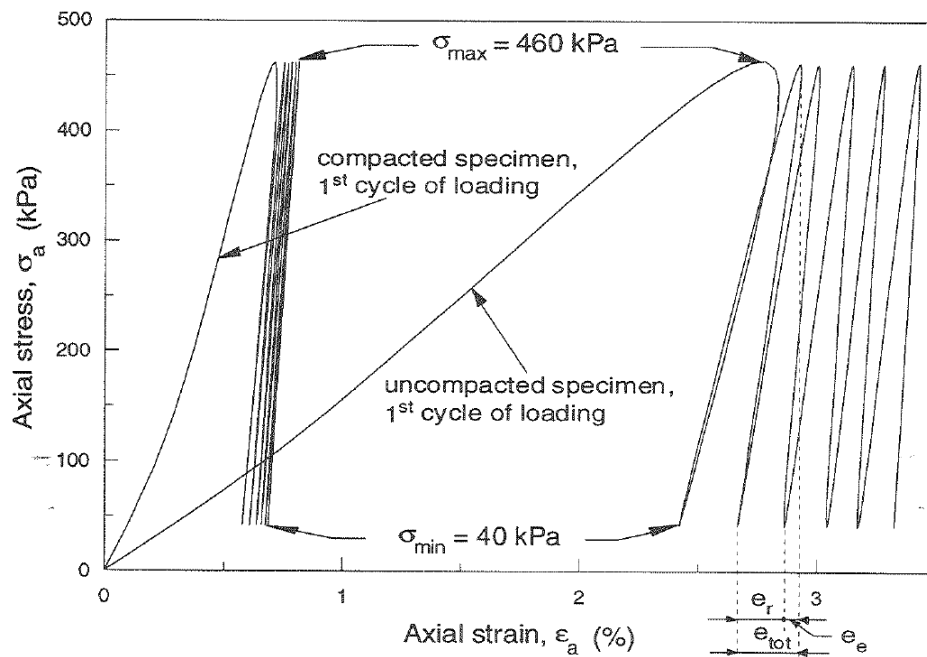


**Figure 2.16** Typical variation in axial strain between ballast samples (Indraratna et al., 1997)

The typical variation between compacted and uncompact ballast specimens is shown in Figure 2.17.

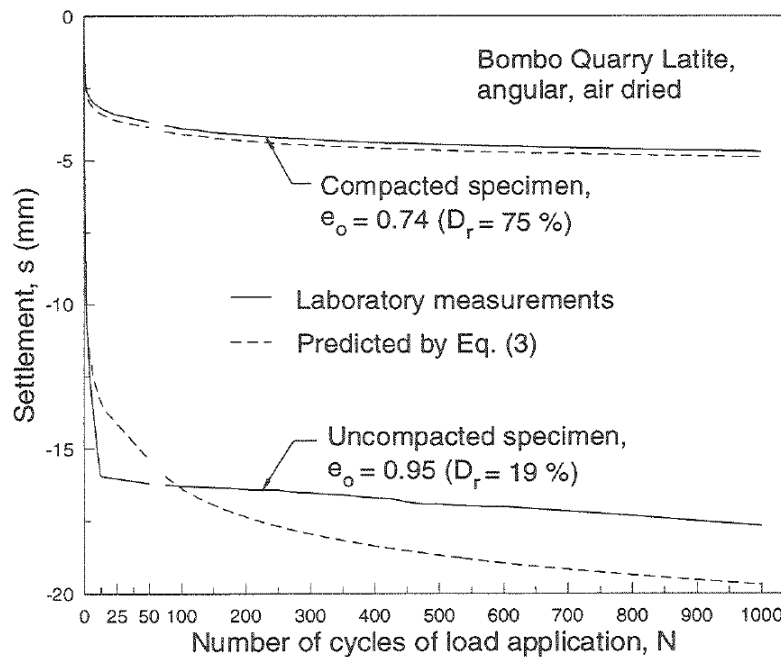


**Figure 2.17** Typical variation in settlement (Indraratna et al., 1997)

The settlement behaviour of compacted ballast specimens can be described by Equation 2.7.

$$s_N = s_1(a \log N + 1) \quad (2.7)$$

Where:

$s_N$  = settlement at N number of cycles

$s_1$  = settlement after the first cycle

$N$  = number of loading cycles

$a$  = empirical coefficient obtained by non-linear regression

Uncompacted ballast settles rapidly in the initial stages of loading as a result of immediate particle packing. Subsequent gradual settlements are related to the degradation of sharp edges and coarser grains at increased compaction rates. Initial particle packing is not as significant in compacted ballast as its settlement is only a function of particle degradation. Indraratna et al. (1997) concluded that rapid loading at a higher amplitude caused larger initial settlements. Long term settlements were not affected by the the loading pattern which agrees with the research conducted by Selig and Waters (1994). Furthermore, it was concluded that an increase in the degree of initial compaction would considerably reduce the final settlement, irrespective of the loading pattern.

The amount of permanent strain in granular materials is also greatly influenced by the presence of water. At high levels of saturation, resistance to deformation by the material decreases rapidly. Proper drainage in granular pavement layers and railway track structures is thus of the greatest importance. The influence of drainage is shown in Figure 2.18

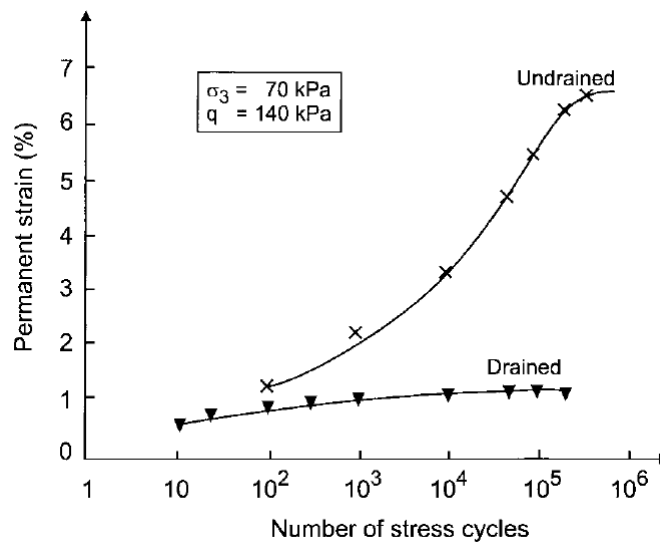


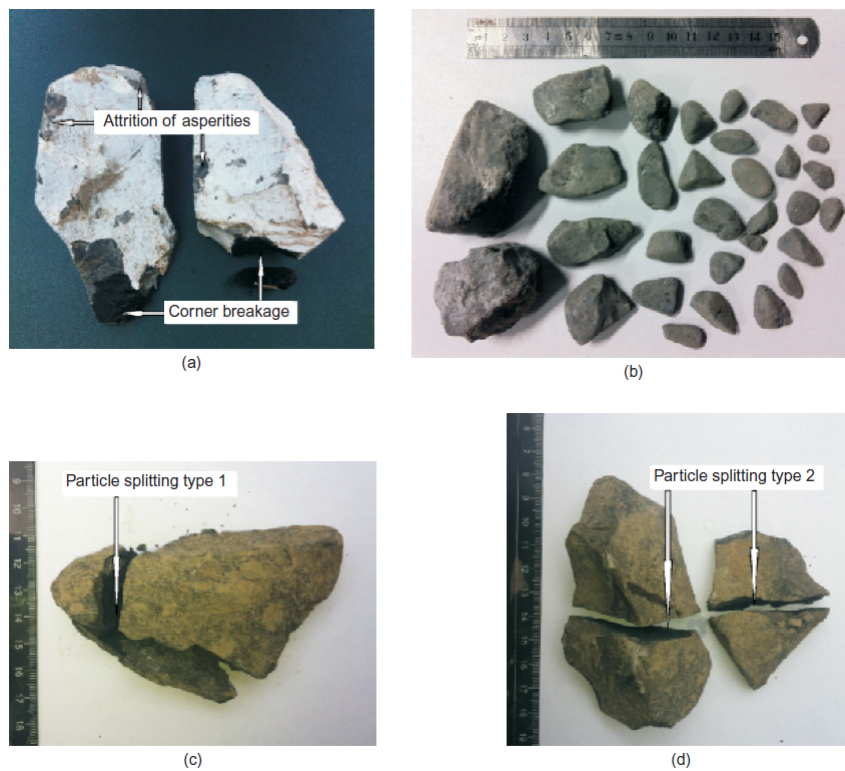
**Figure 2.18** Influence of drainage on Permanent Deformation Development (Dawson, 1990)

### 2.5.3 Effect of Cyclic Loading Frequency

Sun et al. (2014) conducted a series of large-scale triaxial tests on railway ballast to determine how the frequency  $f$  (or train speed,  $V$ ) affects the permanent deformation and degradation of railway ballast. Test frequencies were varied between values of 5 Hz and 60 Hz. Three categories of permanent deformation mechanisms were observed in response to the applied cyclic loads:

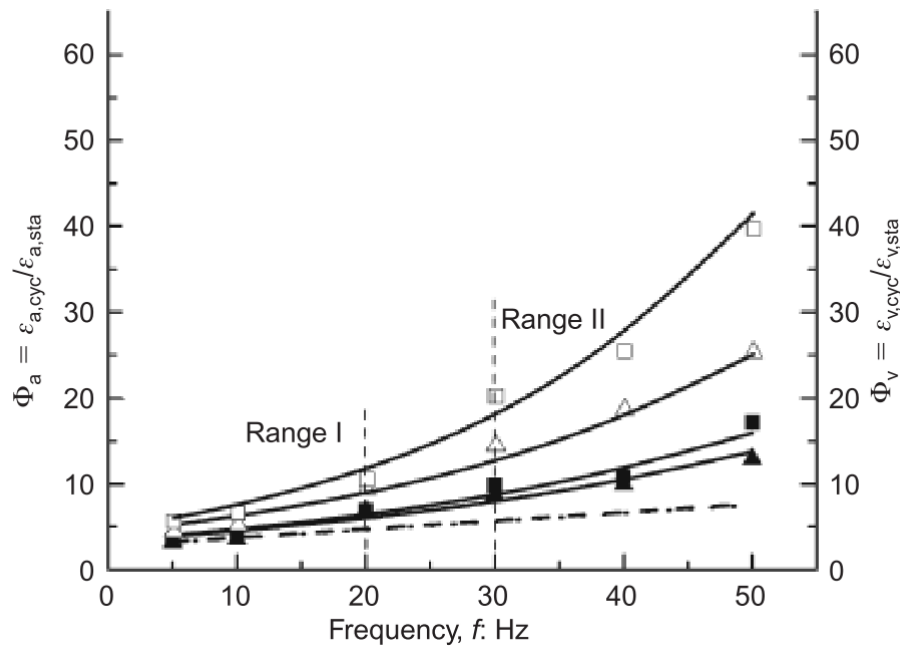
- the inception of plastic shakedown ( $f \leq 20$  Hz (or  $V \leq 145$  km/h))
- plastic shakedown and ratcheting ( $30$  Hz  $\leq f \leq 50$  Hz (or  $220$  km/h  $\leq V \leq 360$  km/h))
- plastic collapse at higher frequencies ( $f \geq 60$  Hz (or  $V \geq 400$  km/h)).

Figure 2.19 shows the various types of particle degradation that occur in each frequency region. Figure 2.20 shows these three categories of permanent deformation mechanisms.



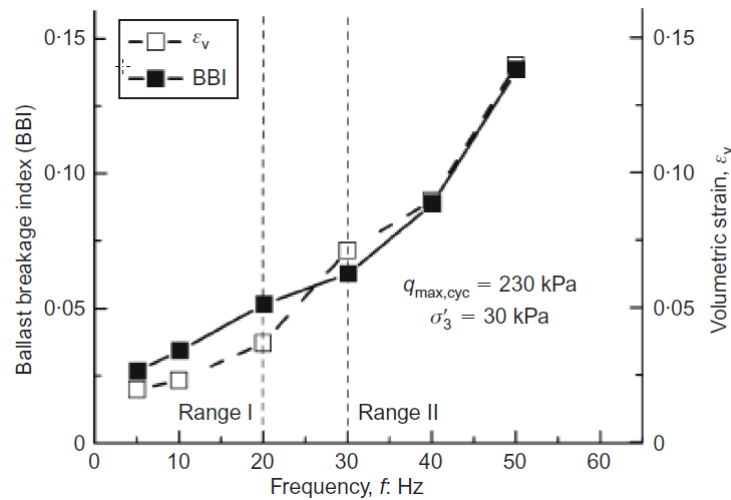
**Figure 2.19** Examples of particle degradation: (a) attrition of asperities and corner breakage in range I; (b) high degree attrition of asperities in range II; (c) particle splitting type 1 in range II; (d) particle splitting type 2 in range III (Sun et al., 2014)

Ballast permanent strain and particle breakage increased with the frequency and number of load cycles.



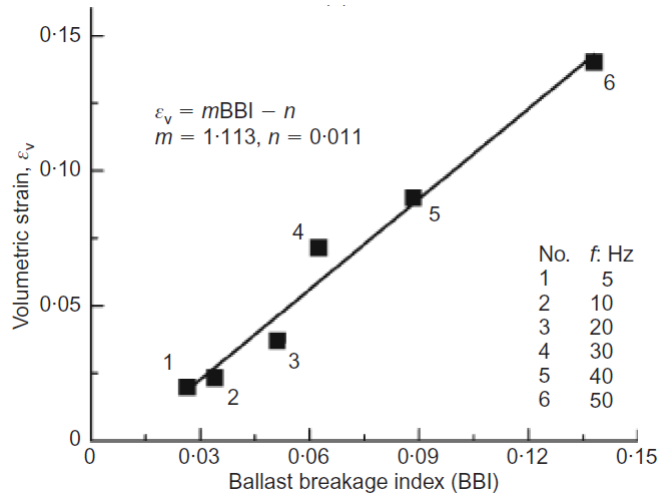
**Figure 2.20** Axial strain accumulation with increasing cycle count (Sun et al., 2014)

Figure 2.21 shows breakage and volumetric strain behaviour as a function of frequency  $f$ . As expected the load frequency had profound influence on the magnitude of BBI which increased with  $f$ . For Range I (i.e.  $f \leq 20$ Hz), particle degradation was in the form of attrition of asperities and corner breakage. For Range II with the higher frequency ( $f \geq 30$  Hz) particle splitting caused by fatigue and a high degree of attrition became predominant, which contributed to a continual increase of volumetric deformation at a constant rate.



**Figure 2.21** Ballast Breakage Index as a function of frequency  $f$  (Sun et al., 2014)

Figure 2.22 shows relationship between volumetric strain  $\epsilon_v$  and Ballast Breakage Index (BBI).



**Figure 2.22** Relationship between  $\epsilon_v$  and BBI (Sun et al., 2014)

Sun et al. (2014) defined the cyclic axial strain ratio as (CASR)  $\Phi_a = \epsilon_{a,cyc} / \epsilon_{a,sta}$  in order to study how frequency affected the axial strain. A simple relationship for latite basalt relating  $\Phi_a$  and  $f$  can be given as:  $\Phi_a = ae^{bf}$ .

A similar relationship exists between the cyclic volumetric strain ratio ( $\Phi_v$ ) and  $f$  shown in Equation 2.8.

$$\Phi_v = ce^{df} \tag{2.8}$$

An empirical equation to calculate  $\epsilon_a$  was proposed using Equation 2.9.

$$\epsilon_a = ae^{(0.138bf)} \epsilon_{a,sta} \tag{2.9}$$

Sun et al. (2014) also concluded that the volumetric strain ( $\epsilon_v$ ) reached at the end of the test can be related to the Ballast Breakage Index (BBI) by a linear relationship that is given by Equation 2.10.

$$\epsilon_v = 1.113BBI - 0.011 \tag{2.10}$$

Based on these tests it appears there exists a critical train speed between 145 km/h and 220 km/h above which track failure may occur in the form of ratcheting or plastic collapse. This train speed should be avoided in ballasted track or further lateral confinement may be required in order to reduce settlement.

## 2.6 LABORATORY TESTS ON BALLAST

Laboratory testing allows experimental variables to be controlled as opposed to testing in the field. Different laboratory testing techniques are discussed in this section, primarily the difference between box tests and triaxial tests which are the two most common test types on railway ballast.

Laboratory repeated load triaxial tests on ballast as well as box tests on ballast have shown that vertical plastic strain and corresponding specimen compression can be related to the number of cycles (Selig and Waters, 1994). A number of laboratory tests have been conducted on ballast as summarised by Al-Saoudi and Hassan (2014) in Table 2.4.

### 2.6.1 Ballast Box Tests

In order to test ballast behaviour under field conditions, a box test can be conducted. Ballast is placed in a box with some form of sleeper arrangement. The test can simulate traffic loading on the rail section. It is a very versatile test as parameters such as sleeper settlement, horizontal ballast stress and ballast stiffness and density can be measured (see Figure 2.23 for a typical box test). A box test as conducted by Al-Saoudi and Hassan (2014) is also shown in Figure 2.24.

**Table 2.4** Ballast test setups adapted from Al-Saoudi and Hassan (2014)

Reference	Model Size (mm)	Material Size and Type (mm)	Setup
Panucio (1979)	482 diam and 305 high	Crushed limestone ranges (20 38)	127 mm diameter surface plate
Morgan and Markland (1981)	1200 x1200 x 700 deep	Crushed limestone, 19 single size grading	Vibrating table equipment
Harry et al. (1985)	300 x 600 x 475 deep	Angular traprock, Conform to AREA No.4 gradation	Laboratory box testing device
Dave (1998)	900 x 200x 330 deep	Rounded denstone ceramic particle, 3 single size grading	193.5 cm <sup>2</sup> air pressure loading piston
Indraratna et al(1998)	300 diam and 600 high	Latite basalt, Conform to (AS1996)	Large-scale triaxial equipment
William et al. (2000)	1000 x 800 x 600 deep	Angular medium gravel, 50 single size	Sine wave loading unloading cycle between (2.1 18.2) kN
Suiker (2002)	153 diameter and 357 high	Traprock, conform to ASTM D2487, 1997.	Static and cyclic triaxial tests
Salim (2004)	600 x 600 x 800 deep	Crushed volcanic basalt, conform to NSW gradationc	Large prismatic triaxial apparatus
Wee Loon (2004)	700 9 300 9 450 deep	Granodiorite and granite, conform to (RC/CE)	Sleeper sin wave load of 40 kN on box-test
Khawla (2007)	600 x 300 x 450 deep	Limestone, conform to IRR (IRR 2000)	Repeated loading

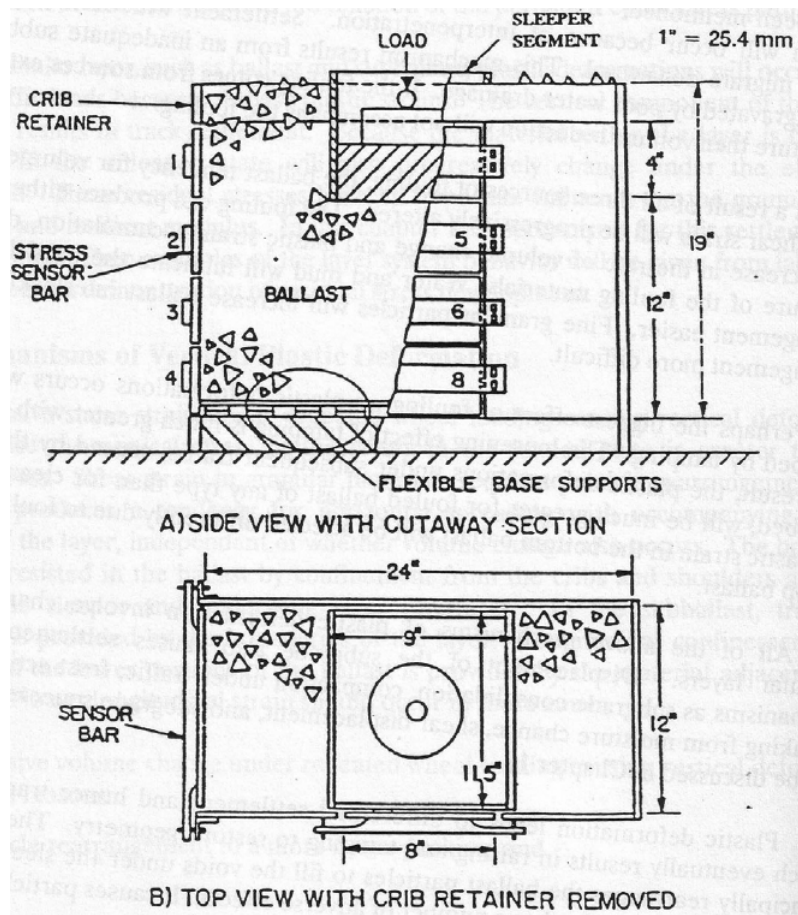


Figure 2.23 Diagram of a box test (Selig and Waters, 1994)



Figure 2.24 Box test setup (Al-Saoudi and Hassan, 2014)

The part of the track structure that is simulated by a typical box test is shown in Figure 2.25.

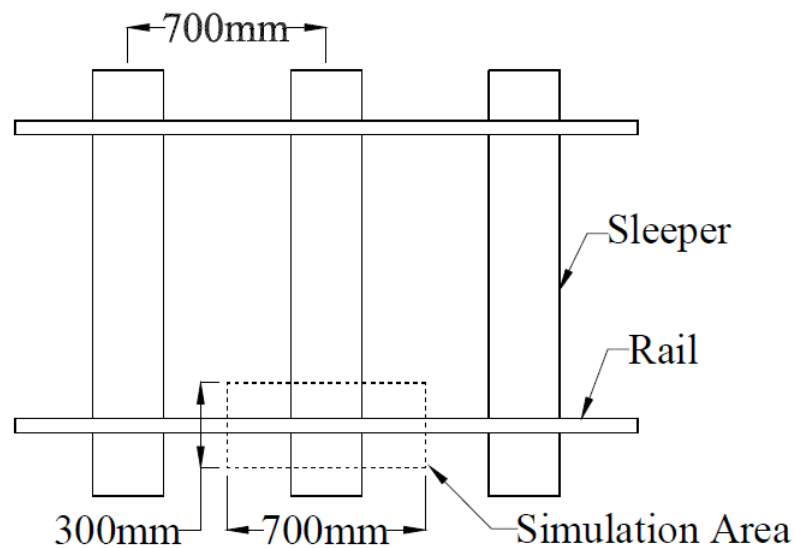
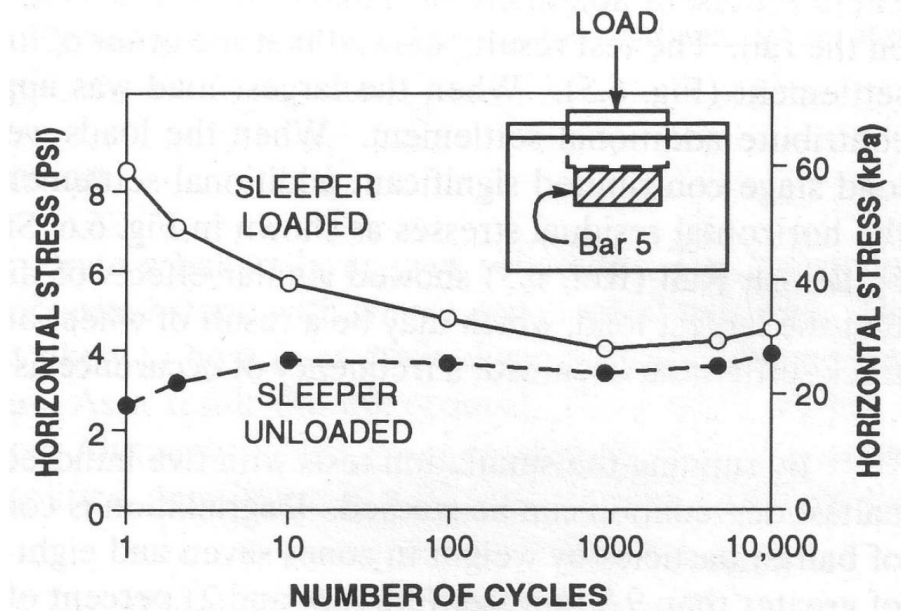


Figure 2.25 Plan of rail and sleepers showing section represented by the box test (Lim, 2004)

Sleeper settlement can be measured through the use of an Linear Variable Differential Transducer (LVDT). Selig and Waters (1994) installed stress sensors in the wall of the box test in order to measure the horizontal ballast stress. The results of the horizontal stresses from one of their tests is shown in Figure 2.26.



**Figure 2.26** Effect of repeated load on horizontal stress in a box test (Selig and Waters, 1994)

From this test it can be seen that the horizontal stresses in the ballast at both the loaded and unloaded states (maximum and minimum load of the cyclic loading cycle, respectively) eventually reached 30 kPa. The ballast stiffness obtained from the box test is very similar to the resilient modulus. The stiffness can be calculated by dividing the applied deviatoric stress by the resilient displacement of ballast ( $\delta_r$ ) in a cycle as shown in Equation 2.11.

$$K = \frac{\sigma_{max} - \sigma_{min}}{\delta_r} \quad (2.11)$$

In a box test the breakage of the ballast usually occurs directly under the sleeper segment as this area is vertically loaded. Lim (2004) observed that the ballast degradation in other areas was negligible. In tests conducted by Selig and Waters (1994) the ballast was coloured with a dye in the area under the sleeper to better observe the breakage.

Ballast vertical plastic strain and corresponding specimen compression can be related to the number of cycles by a semilog relationship in the form of the following equation presented by Selig and Waters (1994). The permanent strain after  $N$  cycles,  $\epsilon_N$ , can be approximately related to the permanent strain after one cycle,  $\epsilon_1$ , by Equation 2.12

$$\epsilon_N = \epsilon_1(1 + C \log N) \tag{2.12}$$

Where  $C$  is a material constant with typical values ranging from 0.2 to 0.4.

According to Selig and Waters (1994) an evaluation of settlement trends in track as well as results from box tests carried out to large numbers of cycles suggests that the semilog relationship increasingly underestimates the cumulative plastic strain as the number of cycles increases. Figure 2.27 shows the settlement trends of a box test. The plot shows that up until the reset point the settlement trend is not semilog, but that the settlement rate increases at a greater rate than the semilog relationship.

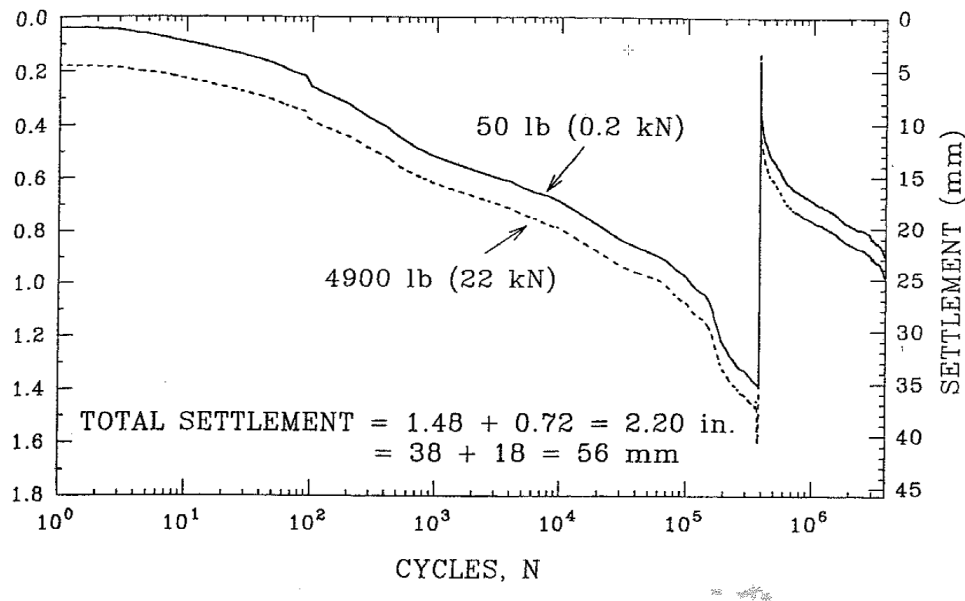


**Figure 2.27** Settlement as a function of log of cycles (Selig and Waters, 1994)

The same test plotted against a linear axis shows the the settlement increases at a diminishing rate as shown in Figure 2.28.

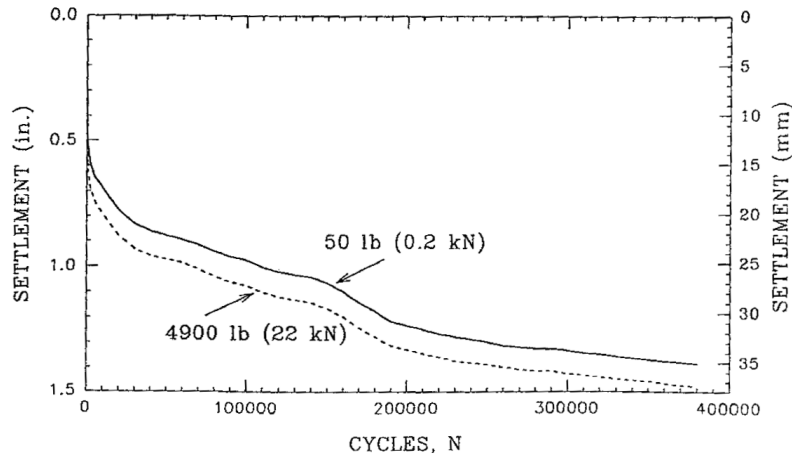


**Figure 2.28** Settlement increase with cycles (Selig and Waters, 1994)

Recent settlement results (Neidhart, 2005) suggest that settlement prediction is approximated by Equation 2.13.

$$S_N = S_1 + \frac{c \log N}{1 + d \log N} \quad (2.13)$$

Where  $c$  and  $d$  are shape parameters. This formula implies that for very high cycle counts (e.g.  $N > 10^6$ ) the rate of change of ballast settlement is small. The box test trends were compared to semilog, hyperbolic, parabolic and power relationships. The best overall trend was represented by the power relationship of the form shown in Equation 2.14.

$$S_N = S_1 N^b \quad (2.14)$$

Where:

$S_N$  = settlement (layer compression after  $N$  load cycles)

$S_1$  = settlement from the first load cycle, and

$b$  = exponent.

Figure 2.29 shows the results of research conducted by Indraratna (2000) showing the effect of load cycles and axle loads on settlement. It should be noted that the variation of the applied load only affects the coefficient  $S_1$ ; the coefficient  $b$  remains relatively unchanged.

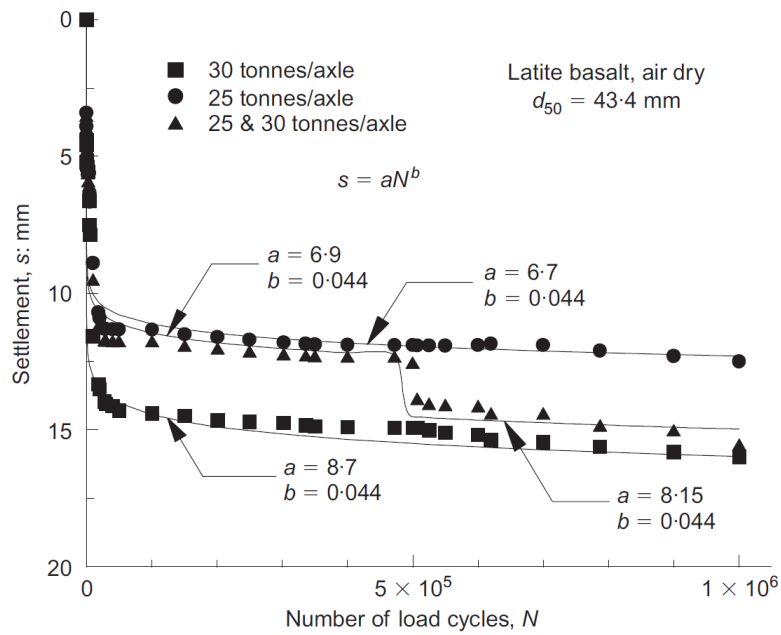


**Figure 2.29** Effect of load cycles and axle loads on settlement (Selig and Waters, 1994)

## 2.6.2 Ballast Strain

Ballast strain is defined as the ballast layer compression divided by the ballast layer thickness Selig and Waters (1994). The settlement equation can be expressed in terms of strain by dividing both sides of the equation by the appropriate layer thickness as shown in Equation 2.15.

$$\epsilon_N = \epsilon_1 N^b \quad (2.15)$$

Ballast strain for a field test section is shown in Figure 4.14.

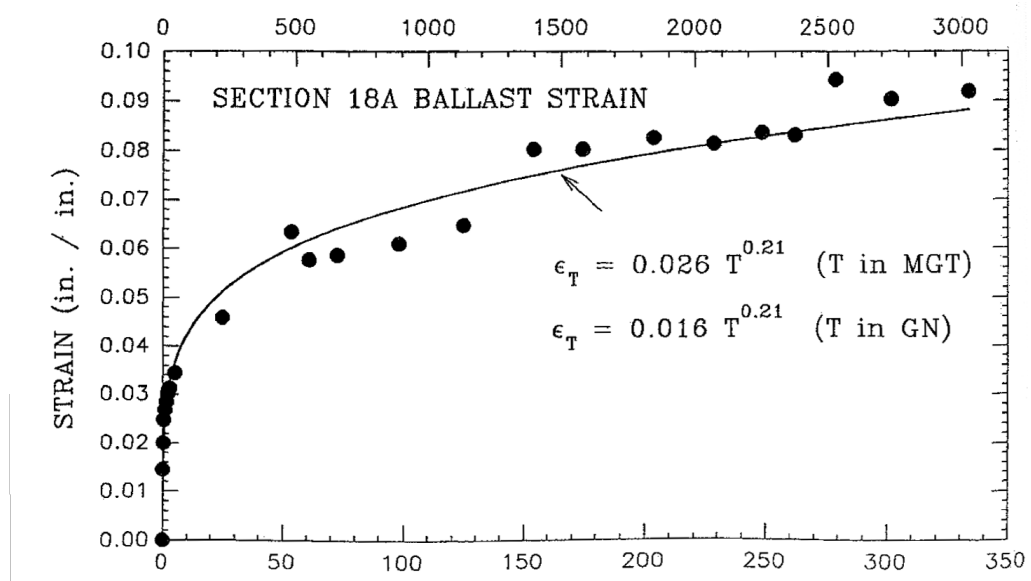


Figure 2.30 Ballast strain plot (Selig and Waters, 1994)

Thus the rate of settlement, and strain development decreases as the number of load cycles is increased.

### 2.6.3 Ballast Triaxial Test

Testing large coarse aggregates in a conventional triaxial apparatus can lead to misleading results because of the disparity between equipment size and the particles being tested. As a result, triaxial testing that is conducted on ballast is done in a large-scale triaxial apparatus. The large scale triaxial test is one of the most important laboratory tests for the investigation of the mechanical behaviour of railway ballast. It provides an efficient way of studying the stress-strain behaviour, strength and degradation characteristics.

The triaxial test has the advantages that the drainage conditions can be controlled. A cylindrical specimen usually with a length/diameter ratio of 2 is used in this test. This sample is placed within a chamber of pressurised water or air. The sample is stressed axially by a loading ram and radially by the confining fluid pressure (Craig and Knappett, 2012). A large-scale triaxial test apparatus used for testing railway ballast is shown in Figure 2.31.



**Figure 2.31** Typical large scale triaxial test used for testing railway ballast (Aursudkij, 2007)

## 2.7 TRACK REINFORCEMENT USING POLYMER GEOCOMPOSITES

Granular materials such as railway ballast experience problems over poor formations due to the development of tensile strains at the formation interfaces. The continued rotation of the principle stresses causes ballast densification and hence settlement. This increases over soft formations as a result of low track stiffness and hence higher induced ballast plastic strains (Woodward et al., 2009a). One method of improving the strength of the ballast layer and reducing the amount of plastic strain and settlement is to reinforce the ballast layer. This section discusses the work done on reinforcing ballast with polyurethanes.

The first research effort into polymer reinforcement of railroad ballast was made by Rostler et al. (1966) to stabilise a ballast layer that was trafficked by high speed trains. The general term "polyurethanes" (PUR) has become known for a wide variety of polymers that are prepared according to the diisocyanate-polyaddition principle. Polyurethanes are a wide variety of polymers with numerous different compositions and properties (Gunter, 1985). Polymer specimens of different polymer mixtures were prepared and tested in a triaxial apparatus. The samples were tested under dynamic loading and the specimens were rated from good to poor. Following these results a polymer mixture was developed and static triaxial testing was performed to measure the strength improvements provided by polymer bonding. Results showed that the polyurethane reinforcement increased the strength properties of the aggregate samples.

Keene, Edil, Tinjum and Brown (2012a) conducted a study into the characterisation of polyurethane ballast. The aim was to study the two targets of polyurethane reinforced ballast. The first of which is reduced particle breakage and rearrangement; therefore, mitigating the generation of fines which would cause the ballast to become fouled. The second aim of polyurethane reinforced ballast is the increase in overall strength and load carrying capacity of the track structure.

Following the injection of rigid polyurethane foam (RPF) which is a type of expanding polyurethane, the capacity for in-situ drainage of the track structure is removed. For this reason, the application of this remedial measure would have to be placed with care, and only in areas where the ballast experiences high-intensity repeated loading. Filling the void space with the RPF would prevent the infiltration of water and other contaminants from reaching the substructure, which would further protect the track structure from rearrangement and settlement, while relying on areas of the track that were un-injected to still maintain drainage.

According to Keene, Edil, Tinjum and Brown (2012a) there are no standards for conducting of engineering tests on polyurethane-fortified materials, such as stabilised soils and aggregates. The mechanical properties of geomaterials stabilised with polyurethane are not well documented.

### 2.7.1 Rigid Polyurethane Foam (RPF)

Due to the high strength and lightweight properties of rigid-compact polyurethanes, the unique expansive and quick setting properties of RPF and improvements in technology and affordability of manufacturing polyurethane, the applications in structural engineering and geotechnical engineering are increasing (Keene, Tuncer and Tinjum, 2012).

Keene, Tuncer and Tinjum (2012) provided a summary of the five predominant industries where polyurethanes are used. Soft-foams and semi-rigid foams have been used for seating and padding while rigid-foams have been used in door panels. The furniture industry make use of soft-foams for cushioning. Semi-rigid polyurethane foams have been used for their insulation properties in the construction industry as a result of their lightweight and low thermal conductivity properties. A number of applications for rigid foams have been found in the consumer appliance industry such as in geysers and fridges.

Gunter (1985) describes rigid polyurethane foam as a highly crosslinked closed celled thermoset material of low density. The thermoset character is evident in the fact that the foam is not fusible, has a high softening point and exhibits good resistance to chemicals and solvents. The material can be used in the temperature range of  $-200^{\circ}\text{C}$  to  $+150^{\circ}\text{C}$ . Despite this thermoset character, the foam is ductile rather than brittle. The properties of the foam are dependent on the foam density. As the density of the foam increases so do the strength values and moduli.

Most rigid polyurethane foams are predominately closed celled. Closed cells result when the cell walls remain intact during the foaming process, and are not burst by the expanding gas pressure. Pressure formation during the reaction is dictated by the temperature increase in the reaction mixture. This reaction can be "cooled" through the use of physical blowing agents (Gunter, 1985).

Two typical force deformation curves are shown in Figure 2.32. Graph (a) shows the foam collapsing suddenly under increasing stress and on graph (b) there is no definitive point of failure. The value at the maximum point on the curve is the compressive strength  $\sigma_{dB}$ . In the case where there is no

definitive point of failure, the value at 10% strain ( $\sigma_{dB,10\%}$ ) is used as the compressive strength. Experience shows these two values do not differ greatly when measured on the same foam.

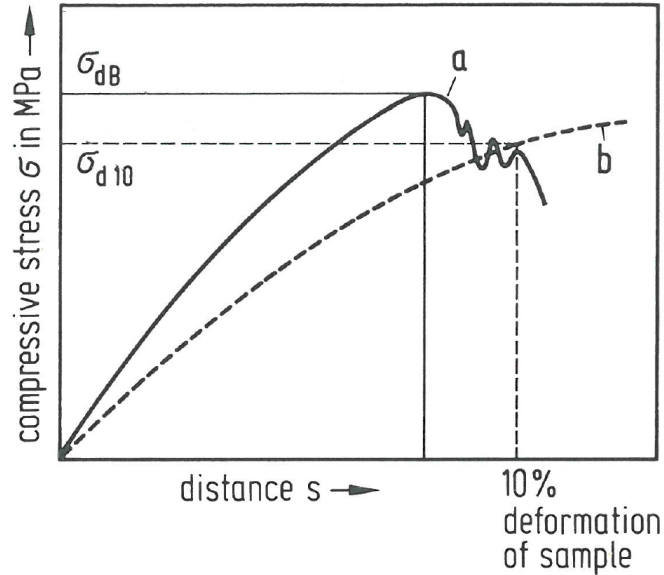


**Figure 2.32** Compressive strength: two typical force deformation curves for rigid polyurethane foam (Gunter, 1985)

Typical values for compressive strength as a function of density are shown in Figure 2.33. It is recommended that a minimum compressive strength of 0.1 MPa for closed celled foams is used. Since it is often more difficult to measure the compressive strength than the density, it is recommended that a minimum density be specified.

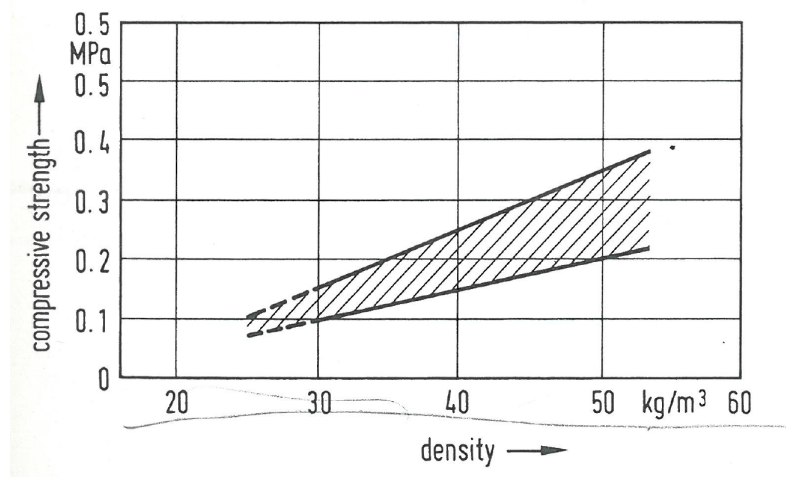


**Figure 2.33** Compressive strength with increase in density (Gunter, 1985)

RPF generally comes in two components prior to mixing and application. The two components are generally referred to as the "A" component and the "B" component. For the synthesis of thermoset polyurethane-resin forms, the two components (polyester or polyether polyol and organic polyisocyanate) are mixed proportionally in the presence of a catalyst (Szycher, 1999). The closed cell properties of RPF may be used to better understand the overall bonding properties and mechanical response of RPF (Keene, Edil, Tinjum and Brown, 2012a).

## 2.8 RIGID FOAM POLYURETHANE REINFORCEMENT OF RAILWAY BALLAST

After RPF injection and solidification into a granular material the strength is improved by occupying the voids and cementing the particles together. The expansive properties of the foam, current applications include the re-leveling of foundation footings and slabs. The application of PSB is an *in-situ* stabilisation method and does not require premixing with aggregate, soil or water. It does not require track shutdown and reaches 90 % of full strength in 15 minutes after injection (Keene et al., 2013).

Keene, Tuncer and Tinjum (2012) reports that while rigid-compact polyurethane in rail infrastructure has been used, very few experimental and empirical methods have been developed for ascertaining the mechanical properties and lifestyle characteristics of rail substructures that have been stabilized with polyurethane. The investigation into the injection of RPF into rail substructure is an uncharted area. Standard laboratory tests for the the fabrication and characterisation of Polyurethane Stabilised Ballast (PSB) is aimed at contributing to research infrastructure. The overall objective is to reduce maintenance life cycle costs, increase rail freight load capacity and provide maintenance techniques that are undistruptive to railroad traffic.

Keene, Edil, Tinjum and Brown (2012a) conducted tests by injecting RFP into the voids of railway ballast. Following injection, the RFP would flow and expand into the ballast pore space which resulted in expansive forces and dynamic interactions. While the RFP polymerises and expands into the void space, bonds were established with the ballast material. The resulting material was termed polyurethane-stabilised ballast (PSB), shown in Figure 2.34.



**Figure 2.34** A PSB specimen cut in half using a concrete masonry saw showing the complete void filling by the expanding foam(left) and a close up (right) (Keene, Edil, Tinjum and Brown, 2012a)

The bonding of the rigid polyurethane foam with the ballast was reported as being substantial and an important process during the polyurethane foaming reaction. Other materials such as PVC, vinyl plastic, oil-coated materials and water-based lubricants did not bond with RFP during the polyurethane reaction. The bonding of the polyurethane with the aggregate was unique. This is most likely as a result of the rough surfaces of the aggregate particles and intermolecular bonds formed during the polyurethane reaction due to aggregate mineralogy (Keene, Edil, Tinjum and Brown, 2012a).

The phase relationship of the PSB is shown in Figure 2.35 as conducted by Keene, Edil, Tinjum and Brown (2012a). On average the ballast accounted for 95% of the sample by weight and 58% by volume. Polyurethane (PU) - the airless phase of RFP was 5% by weight and 7% by volume. RFP was 42% by volume, while Air + CO<sub>2</sub> made up 35% of the volume. The overall PSB density is controlled by the density of the ballast. The influence by weight of RFP is comparable to that of binding properties of asphalt (Keene, Edil, Tinjum and Brown, 2012a).

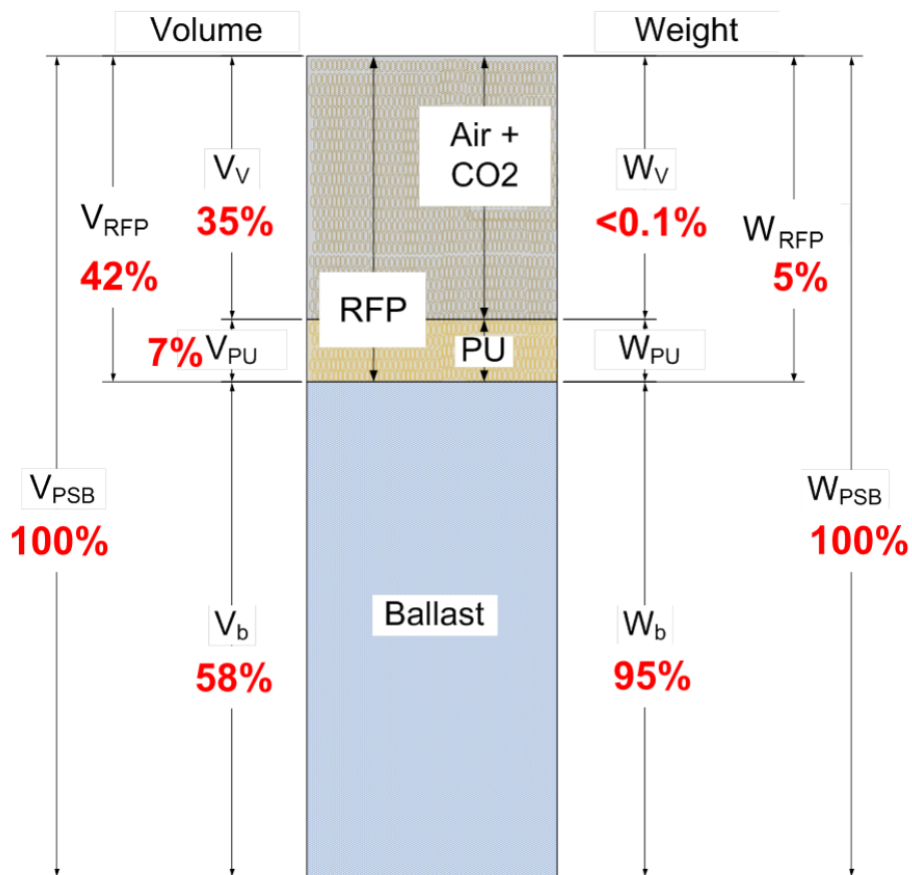


**Figure 2.35** A typical phase diagram of the PSB sample as well as average percentages of PSB compositions (Keene, Edil, Tinjum and Brown, 2012a)

A further advantage of using RFP is that no premixing with aggregates is required before using RFP which is a distinguishing feature between RFP and other forms of aggregate stabilisation such as cement and asphalt.

The samples were tested using cyclic triaxial compression tests. It was found that after 200 000 loading cycles the PSB specimen accumulated 74% less plastic strain than that of clean ballast and 97% less than that of fouled ballast with 15% moisture content and a fouling index of 5%. Elastic modulus of PSB was also found to be 64 % less than that of clean ballast (Keene, Edil, Tinjum and Brown, 2012a). This is shown in Figure 2.36.

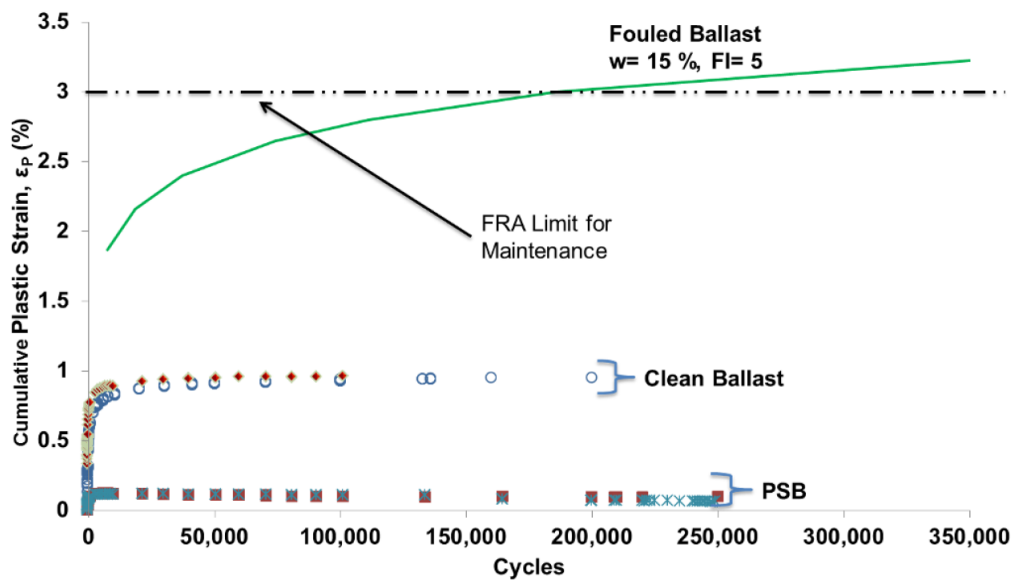


**Figure 2.36** Cyclic triaxial compression testing on clean and PSB specimens under a deviator stress  $\sigma_d$  of 300 kPa. Fouled ballast results from previous research (Keene, Edil, Tinjum and Brown, 2012a)

Futhermore, under the same load conditions it was found that in clean ballast the elastic strain decreased 26% over 200 000 cycles and in the PSB samples it only decreased 5%-9% which shows significantly better performance. These elastic strain results are shown in Figure 2.37.

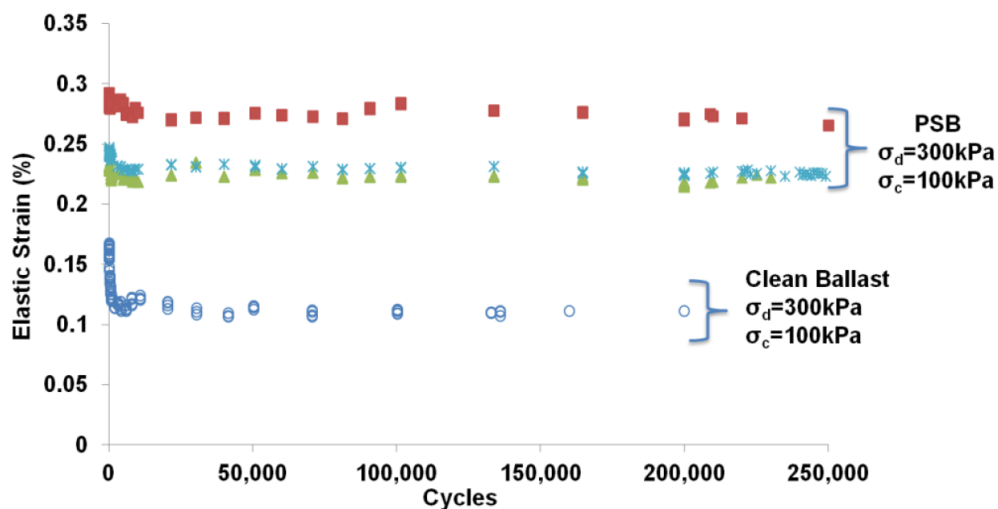


**Figure 2.37** Comparison of elastic strain measured through cyclic triaxial tests between typical clean ballast and PSB specimens (Keene, Edil, Tinjum and Brown, 2012a)

PSB maintains its elastic response while resisting the accumulation of plastic strain and thus would be beneficial for use in areas where the preservation of track geometry is crucial. Several track elements could benefit from this stabilisation where maintenance access is difficult and where construction methods are disruptive to railway operations, such as bridge approaches, turnouts, tunnel entrances and crossings. The polyurethane stabilisation method could provide a maintenance approach for enhancing railway capacity and reduction of maintenance intervals for problematic track sections (Keene, Edil, Tinjum and Brown, 2012a).

Keene, Edil, Tinjum and Brown (2012b) summarised the mechanical property result of the work as follows:

- PSB outperforms other track-substructure materials.
- PSB had typically higher elastic deformational behaviour.

Futhermore Keene, Edil, Tinjum and Brown (2012b) concluded that with regard to the feasibility of using polyurethanes to stabilize track substructure that:

- Stabilisation does not have have a negative impact on elastic response.
- Injection methods that are currently employed are feasible for track stabilisation.
- PSB can greatly increase track mechanistic lifecycle.

Following Keene, Edil, Tinjum and Brown (2012a), Keene et al. (2013) conducted numerical modelling into the effect of polyurethane stabilisation on rail track response. The numerical model was used to determine the effects of various parameters such as location, thickness and polyurethane properties on the ballast layer and how resilient behaviour is influenced. A larger range of PSB modulus, than observed in the laboratory, was also incorporated into the numerical model. The results of the numerical modelling work that was carried out is shown in Figure 2.38.

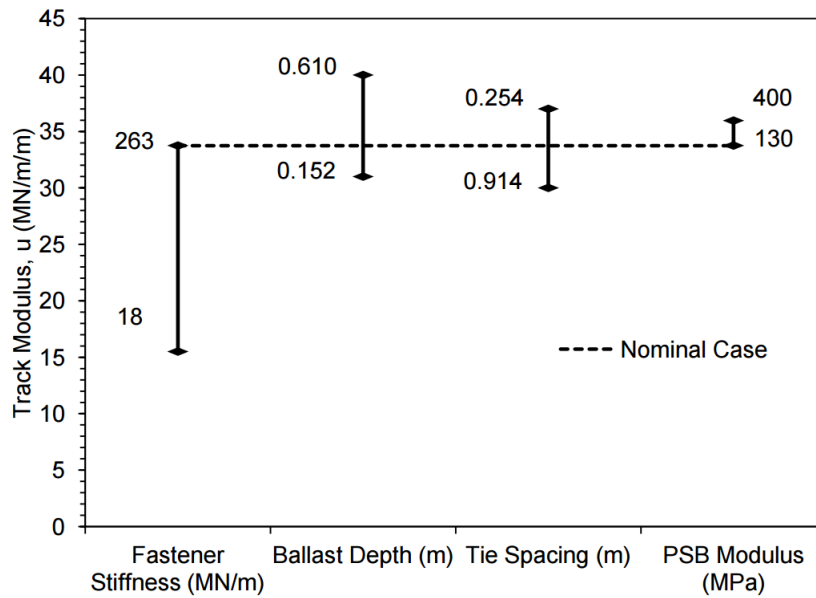


**Figure 2.38** Calculated track modulus for the range of PSB modulus and track components modeled and field validated (Keene et al., 2013)

These simulations by Keene et al. (2013) showed that there are minimal changes in the strain of each substructure layer (i.e., ballast, subballast and subgrade) and no negative effect on the overall elastic response under loading due to the change in stiffness of the polyurethane reinforced areas - an important consideration due to the fact that PSB generally has a lower elastic modulus than ballast. Specific material properties and structural components of the track system appear to have far greater influence on substructure elastic strain and track modulus.

Warren (2015) conducted research into the field application of expanding rigid polyurethane stabilization of railway track substructure, a bridge approach was selected, a geotechnical investigation was conducted and the site instrumented for monitoring following the injection of the polyurethane at a later date. In a Life Cycle Cost Analysis conducted by Warren (2015) found that polyurethane injection consumes 72 % less water, 10 % less CO<sub>2</sub> and 25 % more oil than traditional maintenance techniques, this increased oil usage is as a result of the increased energy requirements to create the foam.

There has been use of non-expanding polyurethane (no complete filling of ballast voids) in rail infrastructure and some of this work is discussed below:

### XiTrack ®

The XiTrack polymer is a urethane-cross linked type (polyurethane) and it is applied to the surface of the ballast and consists of two components (isocyanate and polypol) (Kennedy et al., 2013).

XiTrack has been studied extensively by Woodward et al. (2004, 2005, 2007, 2009, 2010, 2012). XiTrack consists of two components that are mixed in a delivery hose and then applied to the ballast layer. Once XiTrack has been applied it starts to cure after approximately 10 seconds. After one hour, the XiTrack mixture gains 90% of its optimum strength. After curing the XiTrack ® forms a 3-dimensional polyurethane net that holds the aggregate intact. The main goal of the XiTrack product is to create the 3-dimensional polyurethane net that surrounds the ballast aggregate rather than bonding them together. The use of XiTrack still allows the ballast to be free draining as it does not fill a significant amount of voids. A typical application fills approximately 26% of the void structure (Kennedy et al., 2013). An example of this can be seen in Figure 2.39.

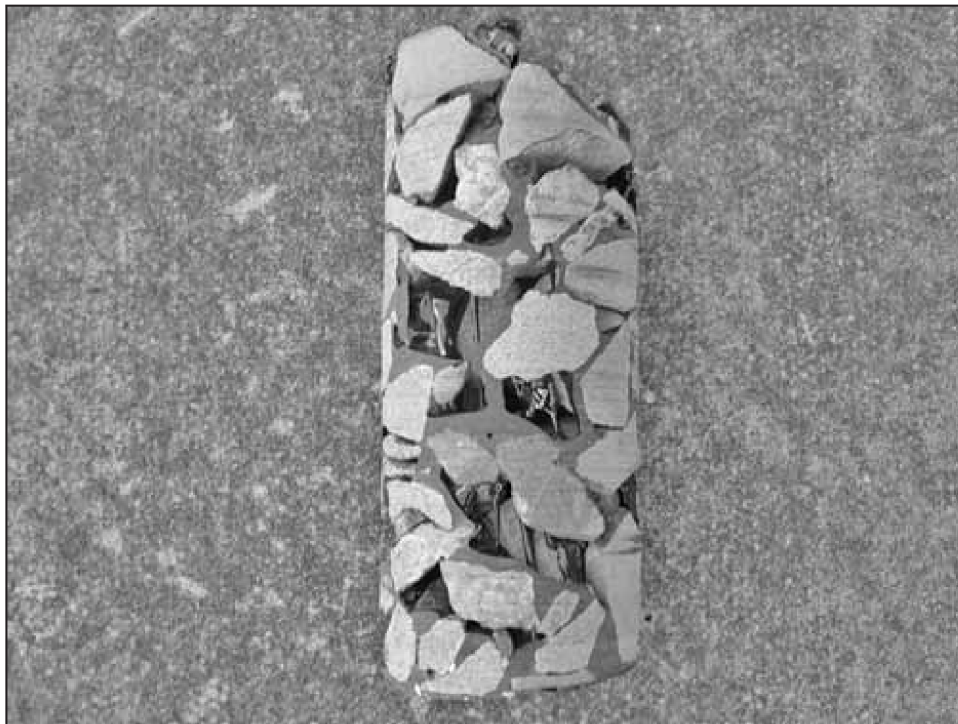


**Figure 2.39** Close-up of geocomposite showing three-dimensional polymer reinforcement while still maintaining full drainage (Woodward, 2007)

The XiTrack technique improves the load-distributing properties of the ballast by forming a resilient

geocomposite across the formation, significantly reducing long term settlements at high loading locations. The polymer is viscoelastic and thus exhibits very desirable hysteretic damping properties. Good granular interlock between treated and non-treated sections occurs, resulting in high degrees of ballast integrity and stability (Woodward, 2007).

Research conducted by Kennedy et al. (2013) showed that ballast that had been reinforced using XiTrack had significantly lower settlement than the same track structure that had not been treated. This is shown in Figure 2.40. The testing was conducted using the Geopavement & Railway Accelerated Fatigue Testing (GRAFT) test facility at Heriot-Watt University, Edinburgh, UK as shown in Figure 2.41.

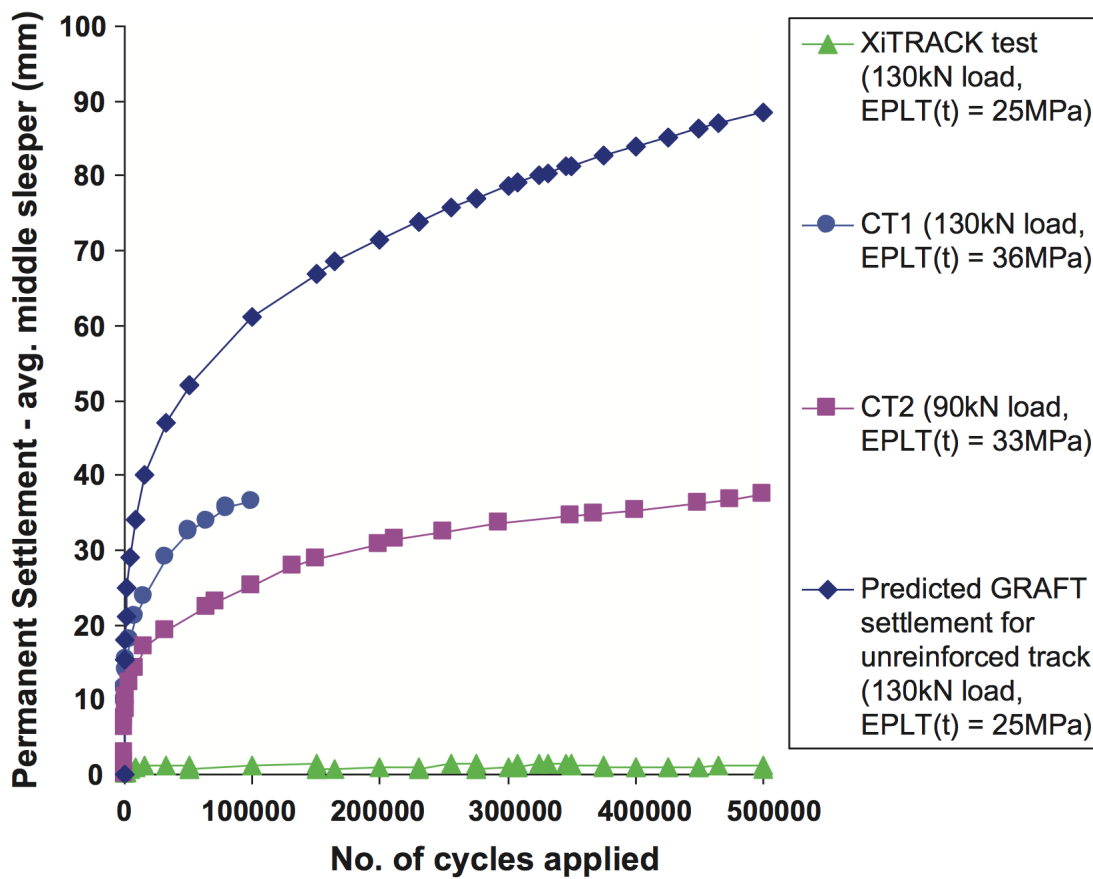


**Figure 2.40** Comparison of the 3D polymer reinforced ballast test to the measured unreinforced ballast control tests and the predicted unreinforced ballast control test (Kennedy et al., 2013).



**Figure 2.41** The GRAFT test equipment with XiTrack treated ballast test (Kennedy et al., 2013).

Woodward (2007) stated that following the monitoring of treated sites using track recording vehicles showed that the technique will significantly improve the ability of the track to maintain its geometry. In many cases before the polymer was installed the sites were considered to be unmaintainable (i.e. previous renewals had failed to maintain the track geometry). XiTrack has also been successfully used over the last 12 years on a variety of different sites in the UK and outside the UK. Sites include bridge transitions, cross-overs, turnouts, clearance issues, tunnel formations, track over poor ground, concrete-slab track transitions and lateral stability issues (Kennedy et al., 2013).

## 2.9 SUMMARY

The literature review gives a brief review of various different track structures, the problems experienced at the transition between various different track structures and possible remedial solutions.

Various properties of railway ballast were reviewed, along with the behavior of aggregate under cyclic loading conditions and the various factors that may influence the permanent deformation of the aggregate.

Geopolymer ballast reinforcement was then discussed as a means of improving and maintaining track geometry. The stabilisation of ballast with a rigid-foam polyurethane could generate a more isotropic material due to the void filling properties it exhibits.

No large scale box tests have yet been conducted on ballast using rigid-foam polyurethane, leaving scope for investigation into the behaviour of this material. Most tests that have been conducted on reinforced ballast samples have been to cycles of  $\leq 1$  million cycles. The very long term behaviour of this reinforced ballast material under cyclic loading is uncertain.

Large differences in mechanical properties between conventional clean ballast and PSB were observed with the PSB generally being superior. This has led to the development of ballast reinforcement/maintenance methods that could be used at specific problem track sections.

## **CHAPTER 3**

# **METHODOLOGY AND EXPERIMENTAL SETUP**

### **3.1 INTRODUCTION**

This section deals with the test setup and testing methodology that was employed during the course of this study. The testing was conducted during the period of July 2015 to October 2015 at the University of Pretoria in the Department of Civil Engineering's Laboratory.

Basic tests were performed to characterise the ballast and the rigid polyurethane foam. Following this, a series of cyclic loading tests were carried out to establish the behaviour of of rigid polyurethane foam reinforced ballast.

### **3.2 MATERIALS**

#### **3.2.1 Ballast Material**

The ballast material used in this study was obtained from a quarry north of Pretoria. The location of the quarry in relation to the University of Pretoria is shown in Figure 3.1. The quarry is located approximately 10 km North-East of the University of Pretoria. The stone is part of the Bushveld Complex as shown in Figure 3.2



**Figure 3.1** Location of quarry (blue arrow top) in relation to the University of Pretoria (red arrow bottom) (Google and AfriGIS, 2015)

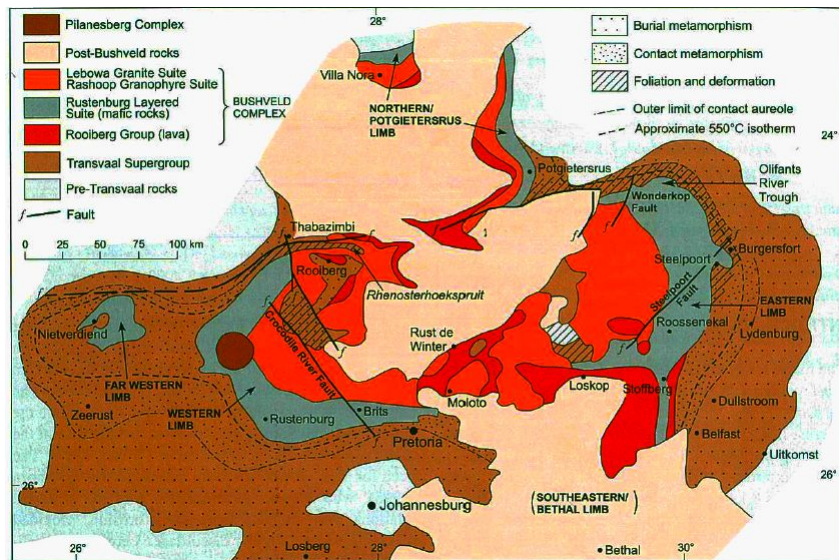


**Figure 3.2** Geological map of the Bushveld Complex (Eales and Cawthorn, 1996)

The ballast material is quartzite, a metamorphic rock. Quartzite is a very tough, durable rock with properties shown in Table 3.1. The test ballast used is shown in Figure 3.3.

**Table 3.1** Summary of Quartzite properties

Property	Value
Ballast Material	Quartzite
Hardness (Moh's Scale)	6.5-7
Compressive Strength (MPa)	90-140
Tensile Strength (MPa)	10-12
Porosity	Low
Friction Angle (deg)	55
Poisson Ratio ( $\nu$ )	0.25



**Figure 3.3** The test ballast stone

Commercial laboratory tests conducted on the ballast stone found that the ballast stone had an Aggregate Crushing Value (ACV) of 14.5 % dry and a water absorption value of 0.3 %. The ballast stone was supplied according to the S406 Ballast Specification and this was verified by conducting a grading analysis the results of which are shown in Figure 3.4. The ballast grading was conducted by selecting three random sample batches from the available ballast. The ballast was then sieved through the following sieve sizes and the results were recorded: 73 mm, 63.5 mm, 50.8 mm, 38 mm, 22.5 mm and 19 mm.

The ballast material fell within the specified grading envelope and thus met the S406 ballast grading specifications.

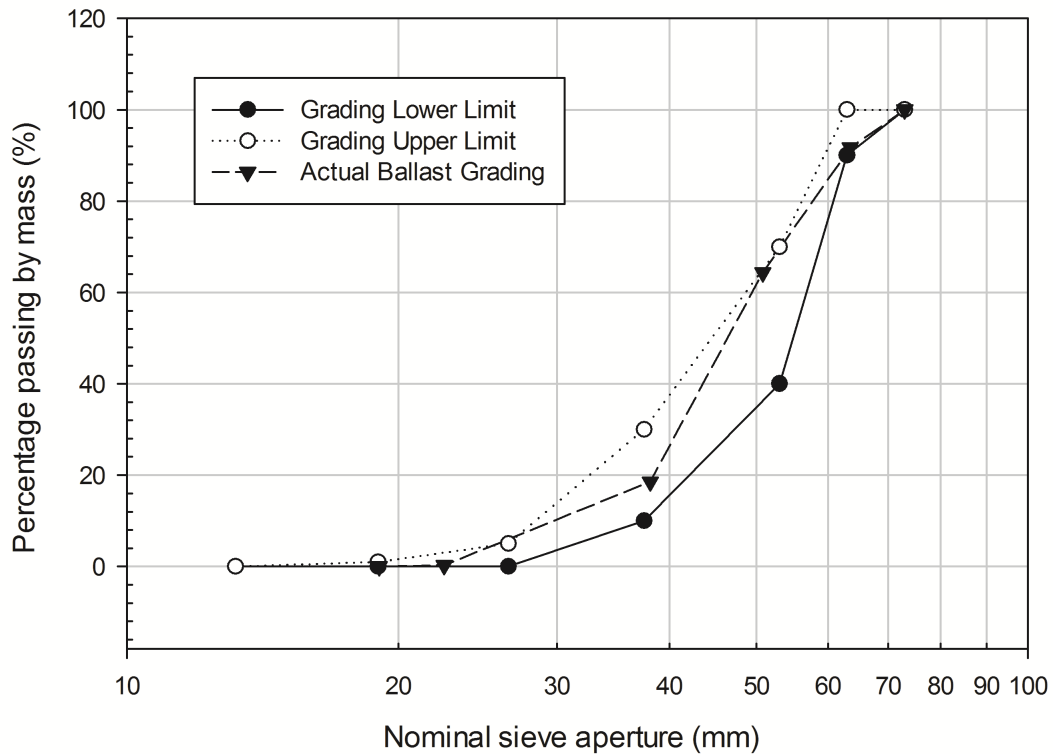


**Figure 3.4** Grading of ballast compared with the S406 ballast grading specification

Tests were conducted in the laboratory to determine the following other properties of the ballast, i.e. the bulk density ( $\rho$ ), specific gravity ( $G_s$ ), void ratio ( $e$ ) and porosity ( $n$ ) of the ballast was calculated.

The aforementioned parameters were calculated. These values are for loose samples and the density would be higher while the void ratio would be lower during actual testing. A summary of the ballast properties is given in Table 3.2. The ballast was washed to ensure that there were no fines present.

**Table 3.2** Summary of ballast properties

Property	Value
Ballast Material	Quartzite
Loose Bulk density ( $\rho$ )(kg/m <sup>3</sup> )	1511
Void ratio ( $e$ ) - Loose	0.857
Porosity( $n$ ) - Loose	0.461
ACV	14.5%
Water absorption (%)	0.3

### 3.2.2 Rigid Polyurethane Foam

The Rigid Polyurethane Foam that was used to reinforce the ballast is Elastopor ®H 1311/1. The foam is supplied in two separate components namely a Polyol-component (A-component) and an Iso-component (B-component). The polyol component is a mixture of polyetherpolyols, stabiliser, catalyst, flame retardant and water. The iso-component is Polymeric Diphenylmethane Diisocyanate (IsoPMDI 92140). The two components are then mixed together at room temperature in a ratio of A:B = 100:107. The stirring time is 10 seconds, followed by a cream time of 32 seconds, a string time of 155 seconds and shortly after that the foam is relatively set. The cream time is the time it takes for the polyol and isocyanate mixture to change from a liquid state to a creamy texture and subsequent expansion begins. String time is the time taken for the foam to begin to stiffen. Figure 3.5 shows the first test mixture of the two components.



**Figure 3.5** First foam mix test

A cylindrical ballast sample was prepared and foam was poured in order to test the void filling capability and ensure that the foam would work as intended for the full scale test. A small quantity of the foam was mixed in separate container and then poured into/over the ballast specimen. As the foam has not yet begun to expand rapidly, the mixture is able to run between the ballast stone and reach the bottom. The result of the test shows that the foam is able to expand to fill all voids within a ballast sample. This is shown in Figure 3.6. The ballast was lifted by the expansive forces generated by the expansion of the foam into the voids.



**Figure 3.6** The cylinder of ballast before foaming (left) and after (right)

The typical physical properties of the foam are as shown in Table 3.3.

**Table 3.3** Summary of polyurethane foam physical properties

Property (Unit)	Value
Density (kg/m <sup>3</sup> )	40
Compressive Strength (MPa)	0.2
Percentage closed cells (%)	90

### 3.3 BALLAST BOX TEST

Ballast and reinforced ballast testing was done by means of a box test. The following section discusses the design and building of the box, the hydraulic test frame that was used for testing and the

instrumentation used.

### 3.3.1 Ballast Box Design

The size constraint of the hydraulic load frame was the main factor determining the size of the box test that could be conducted. The load frame test bed has dimensions of 1065 mm x 2030 mm. However as a result of the frame supporting the hydraulic actuator, the usable width is 700 mm. In order to be able to load and unload each test safely and easily, a box width of 600 mm was chosen. In order to accommodate a PY sleeper (2200 mm length) a box length of 2400 mm was selected. Testing was planned to be conducted on 300 mm ballast layers, thus a box height of 400 mm was chosen.

The final internal box dimensions were 2400 mm long x 600 mm wide x 400 mm high. A design of steel plate with a hollow square tubing external support frame was used. The thickness of the steel plate that was used for the sides and base was 2 mm. The hollow square tubing which formed the support frame had dimensions of 38 mm x 38 mm x 2 mm. The whole box was welded together. The box was designed using hand calculations and also drawn in Solidworks CAD software. M12 lifting eyes were also installed to enable the box to be moved around the laboratory test floor. Design drawings are shown in Figure 3.7 and Figure 3.8 . The various box properties are summarised in Table 3.4. The box sides were lined with a 2 mm thick layer of neropene material in order to provide a small degree of damping.

**Table 3.4** Various ballast box dimensions and properties

Property (Unit)	Value
Width - Internal (mm)	600
Width - External (mm)	676
Length - Internal (mm)	2408
Length - External (mm)	2488
Height (mm)	400
Internal Volume (m <sup>3</sup> )	0.597
Mass (kg)	96.5

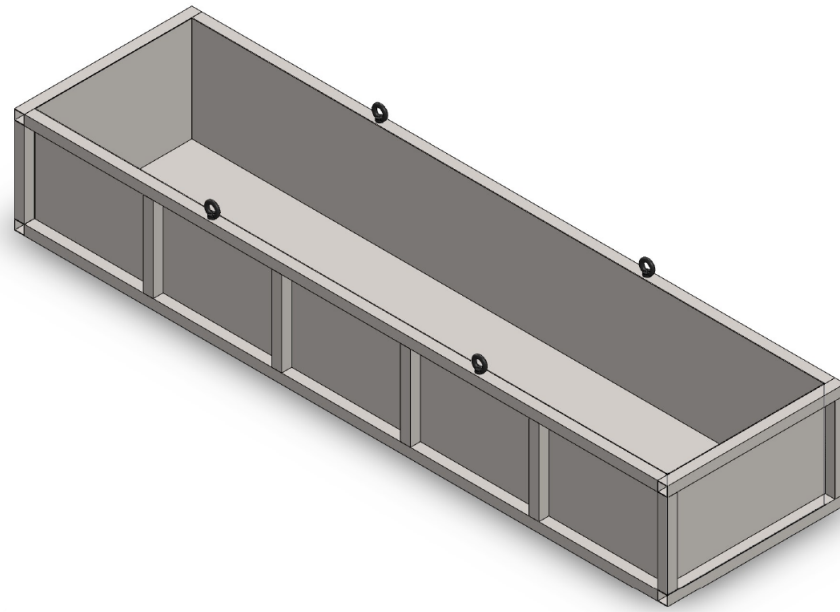


**Figure 3.7** Drawing of ballast box in Solidworks

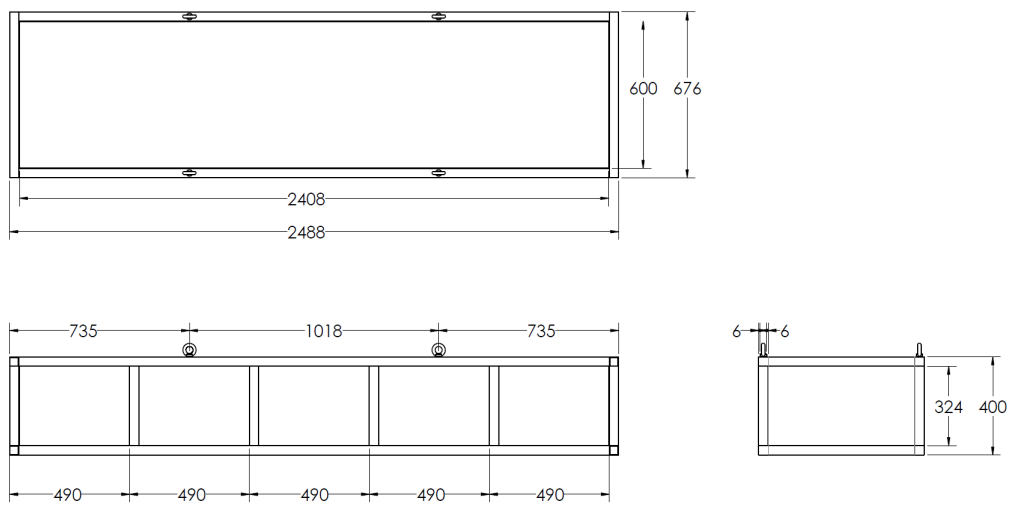


**Figure 3.8** Ballast box dimensions

Figure 3.9 shows the box after completion and before testing commenced.



**Figure 3.9** Completed ballast box filled with unwashed ballast

### 3.4 HYDRAULIC LOAD FRAME

A large hydraulic MTS load frame was used to apply the cyclic loading to the ballast samples. The machine is an integrated table load frame with a crosshead mounted actuator. The hydraulic load frame has a dynamic load rating of 500 kN. The hydraulic actuator is driven by three hydraulic pumps with flow being controlled by a servo-valve. The hydraulic fluid is cooled by a chiller that is situated on the roof of the laboratory. The machine is theoretically capable of testing specimens at frequencies of 30 Hz at full load provided the piston rod displacement is small enough. The load frame is shown in Figure 3.10. The load frame has an overall system stiffness of  $7.4 \times 10^8$  N/m.



**Figure 3.10** Hydraulic load frame with a box test being prepared

### 3.5 MEASURING INSTRUMENTATION

This section discusses the measurement instrumentation that was used during this study.

#### 3.5.1 Load Frame Instrumentation

The hydraulic load frame actuator has an internal LVDT (Linear Variable Differential Transducer) to measure the vertical displacement of the actuator. The LVDT converts a position or linear displacement from a mechanical reference (zero, or null position) into an electrical signal. There is no physical electrical coupling between the moving part (probe) and the coil assembly as it uses an electromagnetic connection instead.

Attached below the actuator is a load cell which is used to measure the force that is being applied. The load cell is a single bridge load cell and is rated for loading of 500 kN (tension and compression). Non-linearity of the load cell is 0.15% of the full scale. Hysteresis is given as 0.20% of full scale. The load cell is shown in Figure 3.11. The actuator LVDT was calibrated and the largest error was found to be 1.06 % at almost the full scale range.



**Figure 3.11** Hydraulic load frame load cell for force measurement located below actuator

The load frame controller has the ability to accept analog signal inputs from other measuring instrumentation as well. An external LVDT was placed on each end of the sleeper in order to measure the sleeper displacement during testing. By placing an LVDT on each end of the sleeper, differential settlement (if any) could be monitored and accounted for. An additional advantage of using additional, external LVDTs to measure the sleeper displacement is that the bending of the beam that was used to apply the load to the sleeper is neglected. This bending should be taken into account when using the displacement measurements of the actuator LVDT. This LVDT setup is shown for one side of the sleeper in Figure 3.12.



**Figure 3.12** LVDT setup to measure sleeper displacement

The properties of the LVDTs that were used to measure the sleeper displacement are given in Table 3.5. The dimensions of the LVDT are shown in Figure 3.13. The dimensions are given as A: 20 mm, E: 24 mm and F: 170 mm (HBM, 2015). The LVDTs were calibrated before use using an LVDT calibration apparatus in the laboratory. The LVDT was calibrated with a full scale of 20 mm corresponding to +10 V to - 10 V (1 mm / V).

**Table 3.5** LVDT Technical Specifications

Property (Unit)	Value
Nominal Displacement (mm)	0 - 20
Sensitivity (mV/V)	80
Excitation Voltage (V)	2.5
Operating Voltage Frequency (V)	0.5 - 10
Linearity (%)	0.1 - 0.2

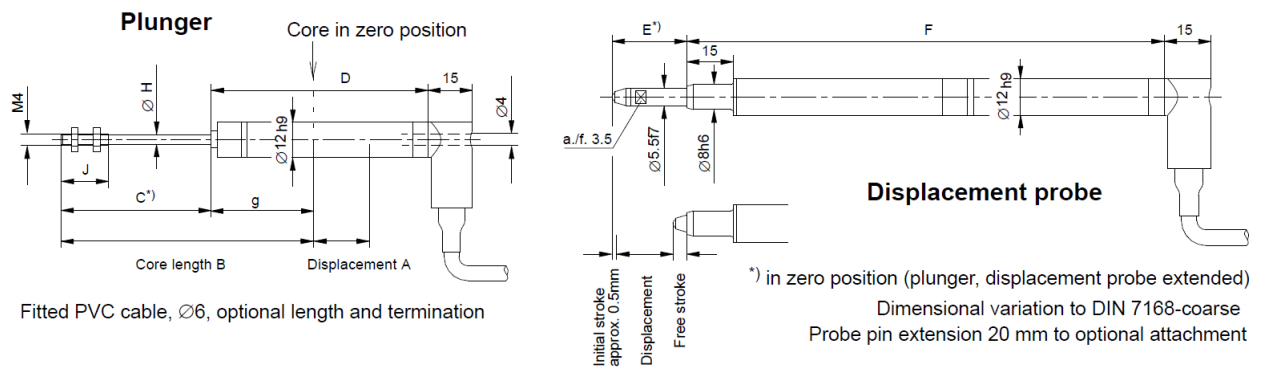


**Figure 3.13** LVDT dimensions (HBM, 2015)

### 3.6 EXPERIMENTAL SETUP

This section describes the experimental setup and testing procedure that was followed.

#### 3.6.1 Box Test Experimental Setup

For each test that was conducted, an initial ballast layer depth of 300 mm was used. The ballast was shovelled into the box by hand. This ballast was uncompacted and very high initial settlement and particle reorientation was expected at the start of each test. Following the filling of the box with ballast material, a PY sleeper was placed on the ballast ensuring that it was aligned correctly and level. The section of track simulated by the test is shown in Figure 3.14. A significant limitation of ballast box testing such as this is the fact that the sides of the box offer a significant amount of lateral resistance that is not experienced by unrestricted ballast in the field. The steel box bottom as well as the hydraulic test frame bed also offer significantly more underlying rigidity than in the field.

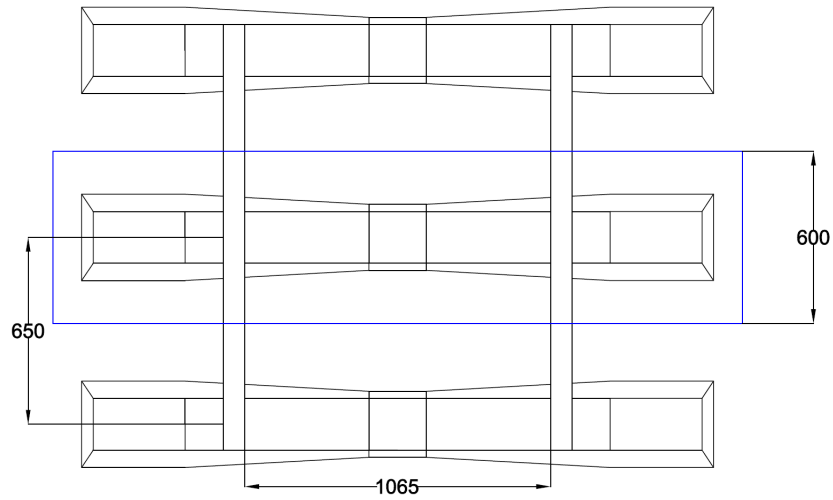


**Figure 3.14** Track section simulated in test

A drawing showing the typical dimensions of the PY sleeper used in the testing is shown in Figure 3.15. Each sleeper typically weighs in the region of 280 kg - 300 kg. The box filled with ballast ready for sleeper placement is shown in Figure 3.16. The completed box preparation is shown in Figure 3.17. The unreinforced ballast test setups had an approximate mass of 1210 kg. The reinforced ballast test setups weighed slightly more due to the mass of the ballast reinforcement.

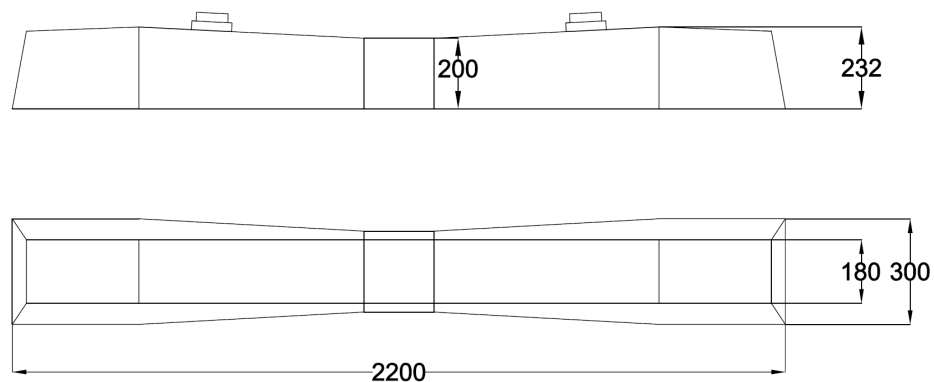


**Figure 3.15** Main PY sleeper dimensions

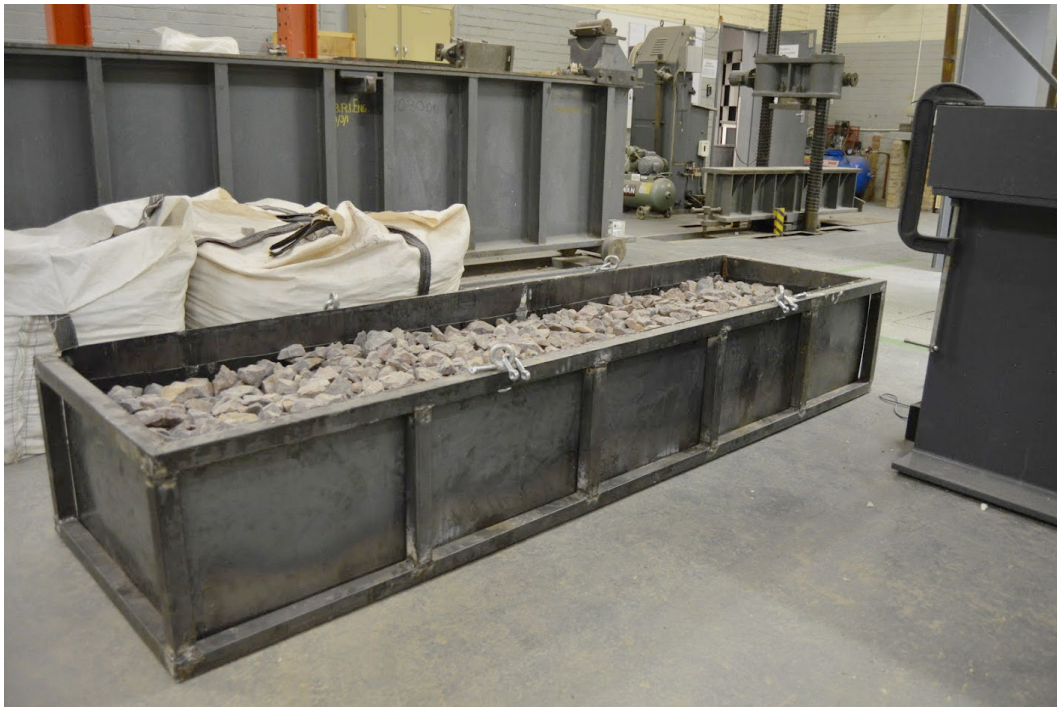


**Figure 3.16** Ballast box with 300 mm layer ready for sleeper placement

For the reinforced ballast tests the ballast layer was placed to the correct 300 mm depth. The foam was then mixed and poured over the ballast. The foam expansion did not occur immediately so the foam was able to penetrate to the bottom of the ballast layer which ensured that all the voids were filled by the reinforcing foam. It was not immediately possible to verify the full void filling of the foam. The full void penetration of the foam was verified after the completion of the test when the sample was removed, broken apart and observed. The final test consisted of a 300 mm ballast layer, but only the first 150 mm of the layer was reinforced. Care was taken to ensure that the correct volume of foam was calculated so as to ensure that all the voids were filled without generating extra foam which would influence the upper 150 mm of the ballast layer.



**Figure 3.17** Box preparation complete - ready for loading into load frame

The box was then loaded carefully into the load frame with the help of a crane and metal rubber coated rollers. The sleeper and loading beam alignment was then checked as shown in Figure 3.18. This was done to ensure that eccentricities are kept to a minimum. The loading blocks were then placed onto the sleeper. The loading block that was used is shown in Figure 3.19. No pads were used during this test to ensure that the system was as stiff as possible. For this reason a subgrade layer was also not used. This was done to ensure that it was only ballast properties and behaviour that was tested and measured.



**Figure 3.18** Ensuring sleeper level and alignment was correct

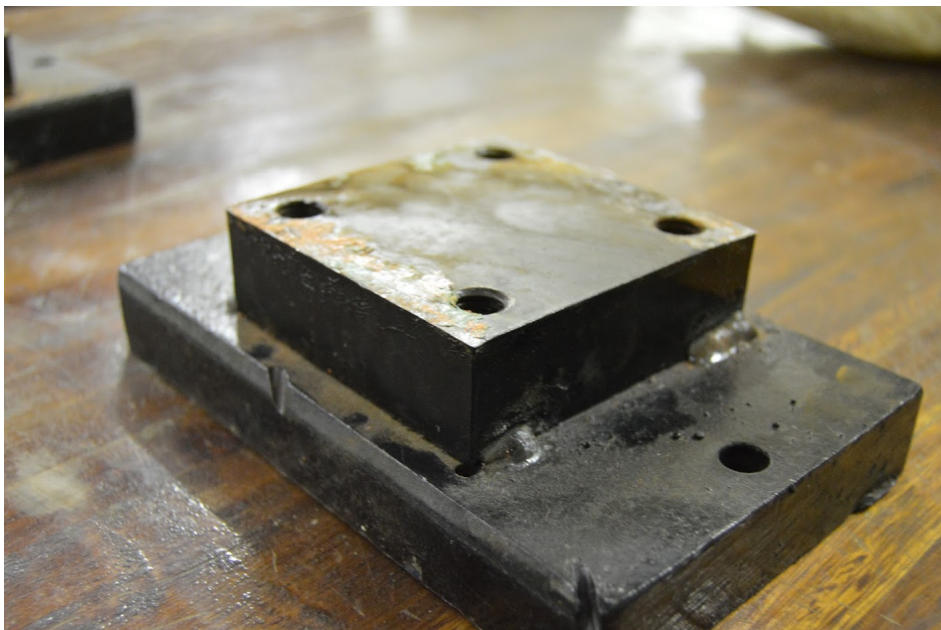


**Figure 3.19** Loading block which was used to transfer the load from the beam to the sleeper at the rail positions

Once the box was in position, the external LVDTs were positioned and clamped into place. The final setup, ready for testing is shown in Figure 3.20 and a labelled diagram of the final test setup is shown in Figure 3.21.



**Figure 3.20** Setup ready to commence testing

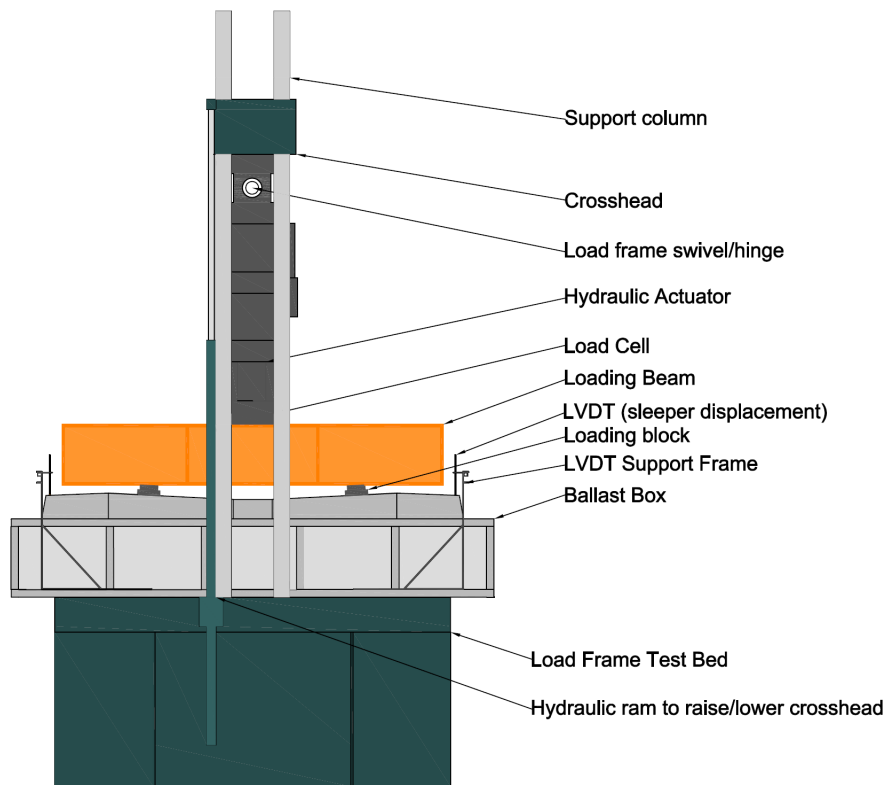


**Figure 3.21** Final setup

### 3.7 MATERIALS TESTING

This section discusses the methodology and tests that were conducted in order to quantify the material properties.

### **3.7.1 Ballast Grading**

After the completion of the unreinforced ballast tests a grading analysis was conducted on the ballast samples.

As before, grading analyses were conducted with sieves of the following sizes: 73 mm, 63.5 mm, 50.8 mm, 38.1 mm, 22.5 mm and 19.05 mm.

It was not possible to grade the samples of the completely reinforced ballast samples.

### **3.7.2 Rigid Polyurethane Foam and Reinforced Ballast Properties**

A number of foam and polyurethane foam reinforced ballast cylinders were cast to test the material properties. The dimensions of the test samples were 300 mm high and 150 mm in diameter. Before casting the cylinders, the inside of the cylinders were coated with a mixture of petroleum jelly and graphite to prevent the foam from bonding to the sides of the cylinder moulds and to ensure that demoulding would occur without disturbing the sample significantly. Figure 3.22 shows the cylinders after being coated and Figure 3.23 shows the foam samples following pouring.



**Figure 3.22** Preparation of cylindrical samples for testing



**Figure 3.23** The foam samples following pouring before being demoulded

Three samples of each type were cast, i.e. three foam and three reinforced ballast samples. The dimensions of the samples were measured and each sample was prepared for testing by cutting the top with a masonry saw to provide a smooth level surface for the loading plate. The result of this process is shown in Figure 3.24.



**Figure 3.24** Top of the sample after being cut with a masonry saw

Samples were placed into a servo hydraulic universal testing machine and tested as shown in Figure 3.25. Samples were loaded at a rate of 1.5 mm/minute. The force and displacement of the sample were recorded during the duration of the test. Samples were all tested to a minimum of 5% axial strain ( $\epsilon_a$ ). This value corresponds to an approximate deformation of 15 mm. In some cases the reinforced ballast samples were compressed axially by 60 mm which corresponds to an approximate axial strain( $\epsilon_a$ ) of 20%. The load vs deflection data was then analysed.



**Figure 3.25** Sample undergoing testing in press

### 3.8 TESTING REGIME

This section deals with the cyclic ballast box testing that was conducted.

### 3.8.1 Initial Phase

During the initial ballast consolidation phase of the testing the settlement experienced by the ballast was very high which meant the test had to be paused in order to reset the LVDTs before they reached the end of their measuring range. This initial consolidation phase was divided into a number of steps which allowed for the test to be monitored closely at each stage when the frequency or magnitude of the loading was altered. The loading regime that was followed during this initial consolidation phase is given in Table 3.6. Due to the rapid settlement that occurred during this initial phase of testing, data was logged every minute for the first 7700 cycles and then every 5 minutes for the next 50 000 cycles.

**Table 3.6** Initial Consolidation Phase - Loading

Phase	Frequency (Hz)	Cycles(No.)	Max Load (kN)
1	5	3000	100
2	5	2500	260
3	10	200	240
4	10	2000	240
5	10	50000	240

Following the end of this initial phase of testing, the long term (consolidation) phase of the test was started.

### 3.8.2 Testing Overview

A total of five cyclic loading box tests were conducted, each lasting approximately 140 hours. Test 1 was conducted on reinforced ballast at a test frequency of 15 Hz. During the consolidation phase the loading and test frequency was varied significantly to evaluate the capabilities of the hydraulic load frame. The test frequency varied between 5 Hz and 30 Hz. Following this investigation (first 50 000 cycles) a test frequency of 15 Hz was chosen.

Test 1 was interrupted several times due to electricity supply problems affecting the entire suburb around the University. Test 2 was conducted with rigid polyurethane foam reinforced ballast for

the entire ballast depth. The ballast was unrestrained during the pouring/curing phases of the foam reinforcement and thus some separation and lifting of the ballast particles occurred as a result of the expansive forces that were generated during the expansion of the foam into the voids. After the pouring of the foam had been completed, a thin layer of ballast was placed over the foam layer which allowed the ballast and sleeper to bed into the reinforced foam layer. Test 2 was conducted at a frequency of 10 Hz.

Test 3 was also conducted with ballast reinforced with the rigid polyurethane foam for the entire ballast depth. However, a PY sleeper was placed on top of the ballast to prevent the ballast uplift during the foam application. Test 3 was conducted at a frequency of 10 Hz.

Test 4 was conducted on clean ballast with no reinforcement, also at a frequency of 10 Hz.

Test 5 was conducted with 50 % reinforcement. It consisted of a 150 mm ballast layer reinforced with rigid polyurethane foam overlain with a 150 mm layer of clean ballast. The reinforced ballast layer was prepared first with the sleeper being placed on the layer during curing to limit expansion. Once the foam reinforcement had cured the sleeper was removed, the second clean 150 mm ballast layer was placed and the test was conducted. This final test was also conducted at a frequency of 10 Hz. The various test configurations are shown in Figure 3.26. The tests are summarised in the test record shown in Table 3.7.

**Table 3.7** Cyclic ballast box test record summary

No.	Test	Comment	Test Frequency (Hz)	Total Cycles
1	Unreinforced Ballast	-	15	4,977,577
2	Reinforced Ballast	Free expansion	10	5,058,308
3	Reinforced Ballast	Expansion limited	10	5,040,036
4	Unreinforced Ballast	-	10	4,787,750
5	Reinforced Ballast (50%)	Expansion limited	10	4,967,957

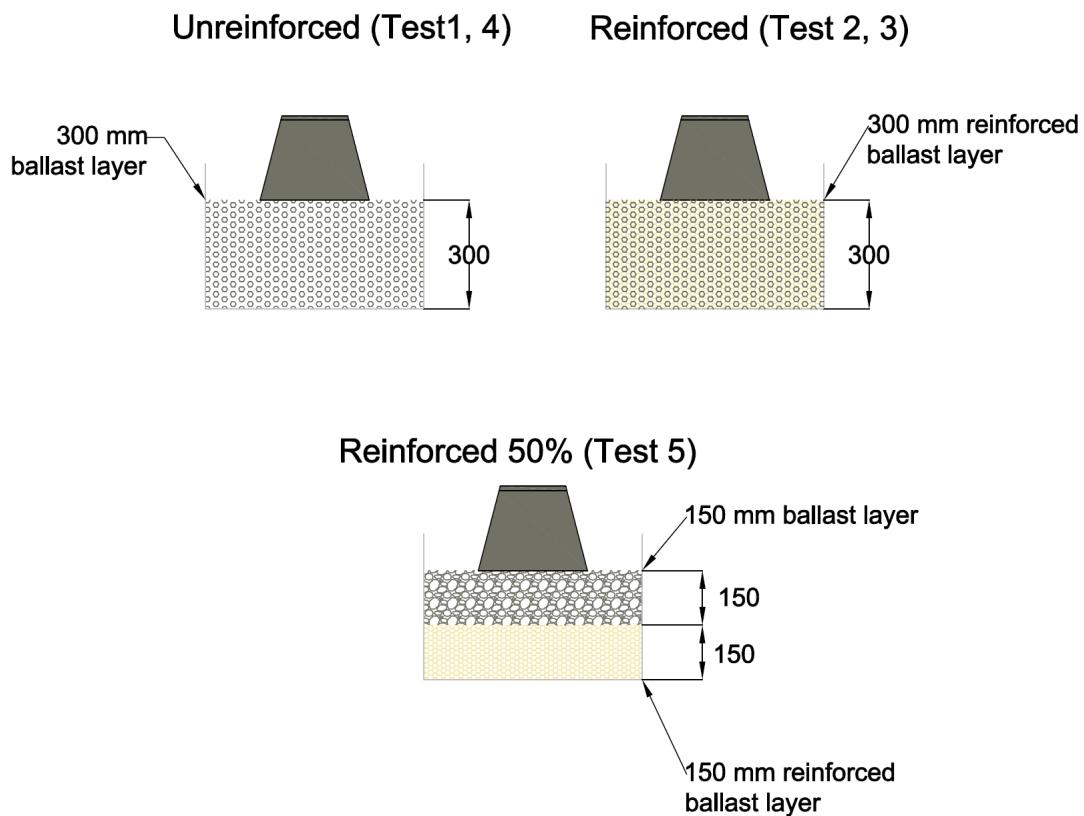


**Figure 3.26** Ballast and polyurethane reinforcement configurations tested

During the initial consolidation phase of the ballast, the initial loading that was performed during Test 1 was repeated. However due to the large initial displacements and significantly more elastic reinforced ballast properties, the actuator was not able to meet the required load at frequencies greater than 10 Hz. Thus, Test 2 and all subsequent tests were conducted at a frequency of 10 Hz. The consolidation phase loading regime that was used during Test 2 was also used for all subsequent tests. Load shedding was not a problem for Test 2 to Test 5, and as a result the main portion of each test was able to be executed in an uninterrupted manner for the entire duration of each test. Following the initial consolidation phase each test was then run until a total of at least 5,000,000 cycles had been reached. Loading was applied using a sine wave function with the hydraulic load frame in force controlled mode. The command vs actual load behaviour is shown in Figure 3.27.

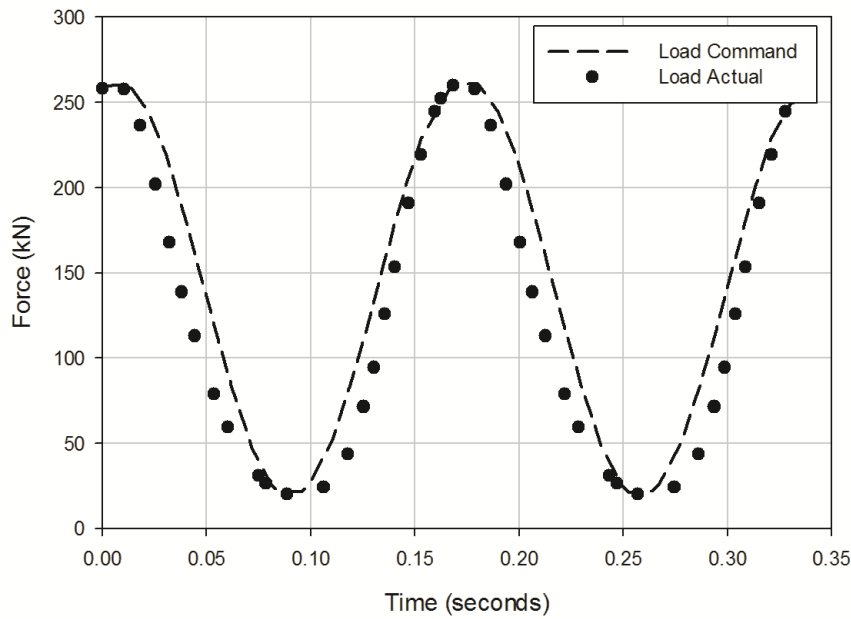


**Figure 3.27** Loading command and actual force output

### 3.8.3 Cyclic Testing

Determination of the axle load for the applied forces was done using Eisenmann's approach (Eisenmann, 1975). This is the approach adopted by Transnet Freight Rail to determine dynamic wheel loads. Determination of the impact factor is given by Equation 3.1.

$$\varphi = 1 + \delta \eta t \quad (3.1)$$

Where  $\delta$  is the factor for track quality (0.1 for very good condition to 0.3 for track quality in poor condition),  $\eta$  is determined by the speed of the vehicle and  $t$  represents the chosen upper confidence limits.

A heavy haul axle loading of 30 tons was taken as the starting point for the load determination.

The following values were chosen for  $\delta$ ,  $\eta$  and  $t$ . The value for  $\delta = 0.2$  (track in good condition). The value for  $\eta = 1.143$ , which corresponds to a speed of 80 km/h - a typical operating speed on heavy haul lines. The Upper confidence limit was chosen as 97.7 % giving a  $t$  value of 2.

$$\phi = 0.2 \times 1.143 \times 2 = 1.457$$

The final dynamic impact factor (DIF) or  $\phi$  is calculated as 1.457.

The AREMA standard specifies a maximum rail seat load  $q_r$  (kN) as  $0.60p$  where  $p$  is the wheel load for pre-stressed concrete sleepers at 760 mm.

Therefore, the axle load ( $P_{axle}$ ) in kN that was used for testing was calculated as follows:

$$P_{wheel} = 0.6 \times 15 \times 1.457 = 13.11 \text{ tons}$$

$$P_{axle} = 2 \times 13.11 \times 9.81 = 257.3 \text{ kN}$$

Thus a test axle load of 260 kN was chosen. The load was applied in a sinusoidal manner. The same test frequency was maintained throughout the entire duration of each test.

Each test was conducted to 5,000,000 cycles. Figure 3.28 shows the screen of the controller computer while a test was being conducted. Table 3.8 gives a summary of the main tests.

**Table 3.8** Settlement Test Summary

No.	Type	Frequency (Hz)	Cycles(No.)	Max Load (kN)
1	Unreinforced ballast	15	4,977,577	260
2	Reinforced ballast	10	5,058,308	260
3	Reinforced ballast	10	5,040,036	260
4	Unreinforced ballast	10	4,787,750	260
5	Partially Reinforced ballast(50 %)	10	4,967,957	260

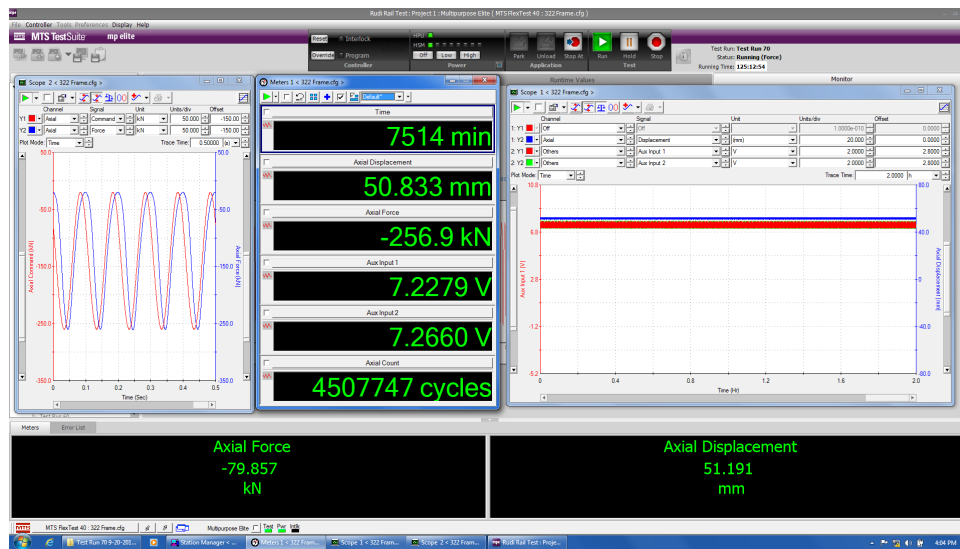


Figure 3.28 Controller computer monitoring screen

### 3.9 DATA ANALYSIS

Due to the large size of the data files, MATLAB code was written in order to process the data into a format that was suitable for use in a spreadsheet. Sigmaplot software was used to plot graphs and other figures that were required. An example of the raw data is shown in Appendix A.

An example of the raw actuator displacement data was plotted and this is shown in Figure 3.29. Raw actuator force data is plotted in Figure 3.30 and an example of the raw LVDT output data is plotted in Figure 3.31. Figure 3.32 shows the actuator displacement vs cycle count for a frequency sweep test that was conducted.

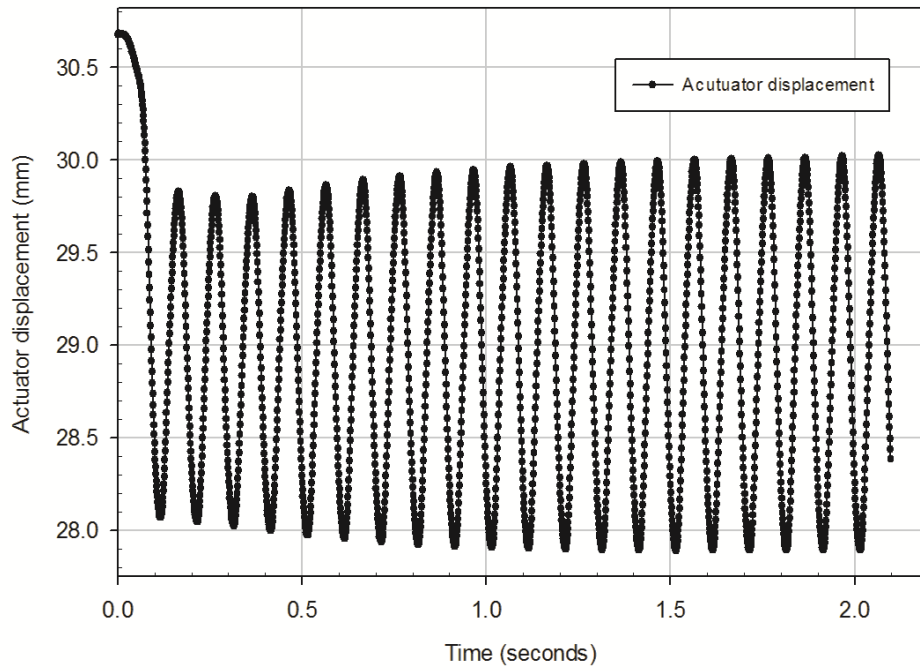


Figure 3.29 Typical raw data output, actuator displacement vs time

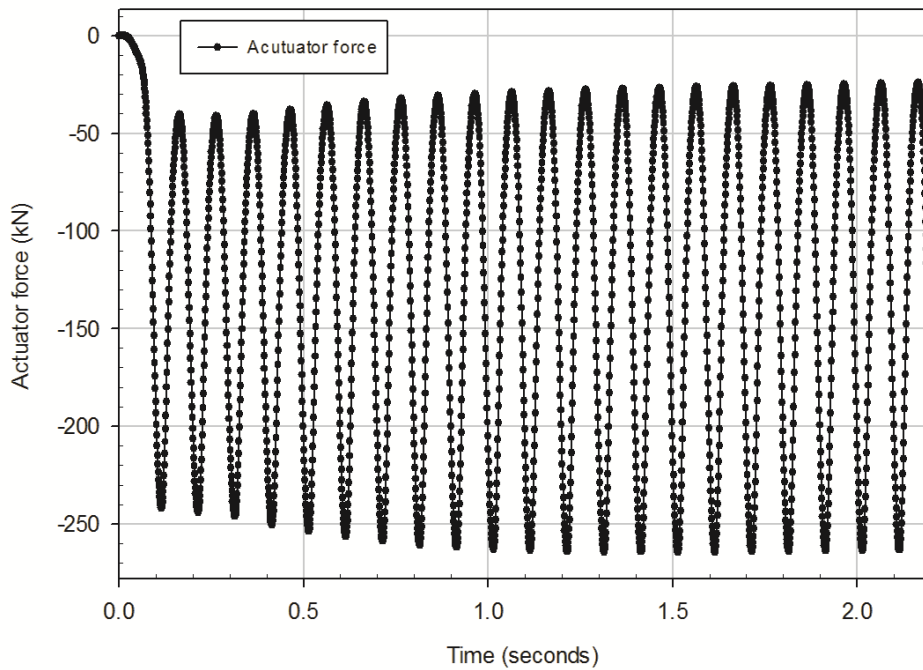
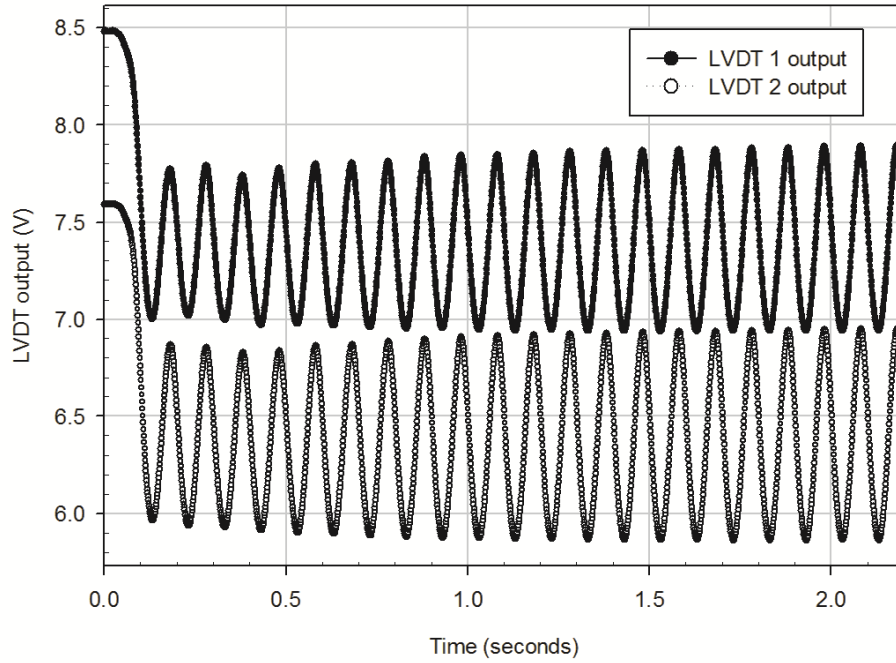
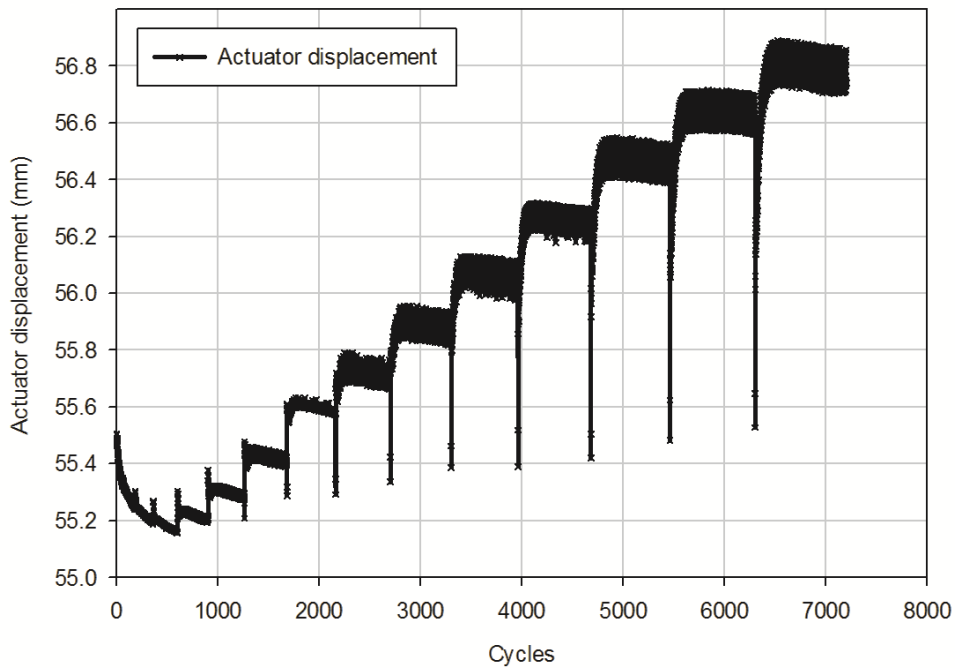


Figure 3.30 Typical raw data output, actuator force vs time



**Figure 3.31** Typical raw data output, LVDT output voltage vs time



**Figure 3.32** Typical raw data output, actuator displacement output vs cycles for a frequency sweep test

## **CHAPTER 4**

# **RESULTS AND DISCUSSION**

### **4.1 INTRODUCTION**

This chapter presents and discusses the results of the testing that was described in Chapter 3. Material testing was conducted on cylindrical samples of the rigid polyurethane foam that was used to reinforce the ballast. Cylindrical samples of ballast reinforced with the rigid polyurethane foam were also tested. The results from the five cyclic loading tests that were conducted on unreinforced, reinforced and partially reinforced ballast are also presented in this chapter. Grading analyses were performed on the unreinforced and partially reinforced ballast samples.

### **4.2 MATERIAL TESTING**

The first set of tests that were conducted were compression tests in order to determine the load versus deflection behaviour of the rigid polyurethane foam and rigid polyurethane foam reinforced ballast. The sample cylinders were compressed and the load deflection behaviour was recorded. The stress/strain behaviour of the material was determined from this load deflection behaviour. The stress vs strain plots of the rigid polyurethane foam samples are shown in Figure 4.1 and the stress vs strain plots of the reinforced ballast samples are shown in Figure 4.2.

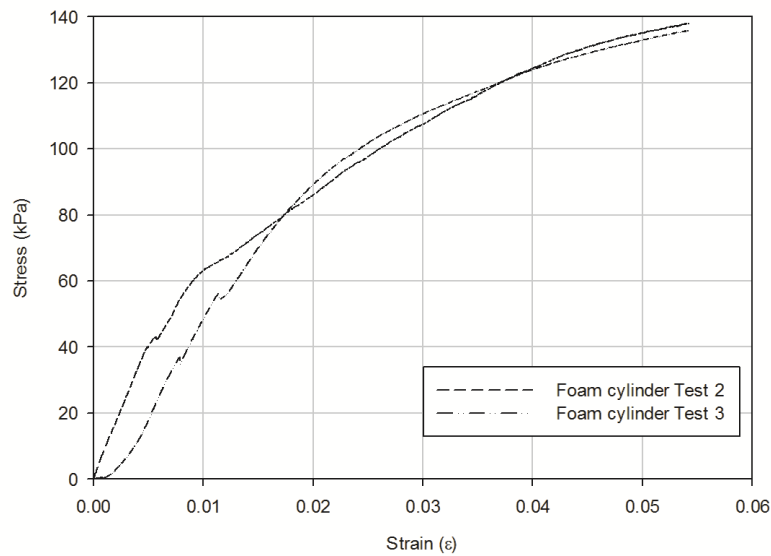


**Figure 4.1** Stress vs. strain plot of rigid polyurethane foam sample cylinders

The foam sample had a large elastic range however the E-value that is calculated is largely dependent on the strain level at which it is calculated. The E-value was calculated using the secant modulus between points. The average E-value for strain levels below 0.01 was approximately 7.2 MPa. For strain levels between 0.01 and 0.03 the E-value reduced to 2.25 MPa. For strain levels between 0.03 and 0.05 the E-value reduced to approximately 1.4 MPa.

The rigid polyurethane foam reinforced ballast samples were tested to much greater strain levels than the rigid foam only samples, as the behaviour of the composite material is of interest.

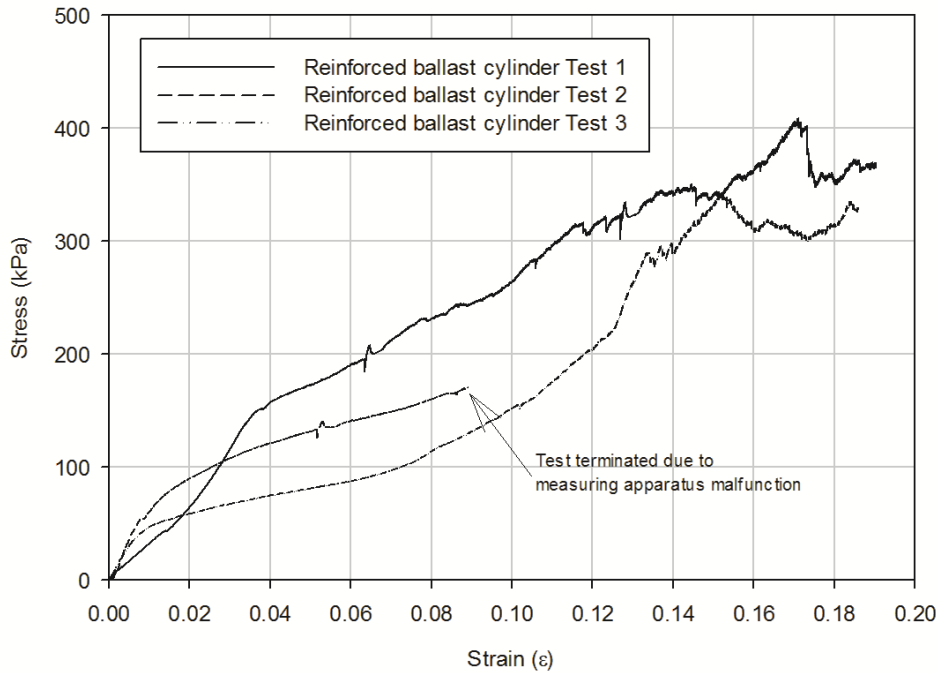


**Figure 4.2** Stress vs strain plot of reinforced ballast sample cylinders

At low strain levels the reinforced ballast samples exhibited similar strength and behaviour to the foam only samples, most probably as a result of the ballast stone being supported in a matrix of the reinforcement foam with minimal inter-particle contact. However as the level of compression and hence the strain level was increased, a constant increase in stress was observed. Sudden increases and decreases and other discontinuities in the stress/strain curve are as a result of particle rearrangement taking place. Once the foam between two adjacent ballast stones was sufficiently compressed the ballast made contact and the strength increased. This process was audible during testing, and the ballast stone contact on contact could be heard as the amount of compression was increased. Differences in slope and stress/strain curves as well as point of failure between the samples could be as a result of some samples having a more optimal particle arrangement in the reinforcement foam matrix. One test was stopped early due to a problem with the measuring apparatus. The two tests that were run to completion show that failure occurred at strain levels of 0.145 (corresponding compressive stress of 340 kPa) and 0.17 (corresponding compressive stress of 405 kPa) respectively.

The E-value that was calculated for strain level 0 to 0.01 was 6.89 MPa. For strain level 0.04 to 0.08 the reinforced foam ballast samples had an E-value of 4.45 MPa. The addition of ballast to the rigid polyurethane foam did result in an increase in E-value. Figure 4.3 shows a foam ballast cylinder

sample after testing. In the photograph a number of cracks can be seen.



**Figure 4.3** Reinforced ballast cylinder after testing

The densities of the samples were measured before and after testing and these results are shown in Table 4.1 and Table 4.2. The mass of each sample was measured before the volume determination was conducted. The volume of each sample was determined by filling a bucket of a known volume completely with the water and placing the sample in the bucket until the top was just submerged. The volume of water that was displaced was recorded. Gunter (1985) presented a range of rigid polyurethane foam compressive strengths as a function of density as shown in Chapter 2. The compressive strength of the foam cylinders from Tests 2 and 3 plotted within this range is shown in Figure 4.4.

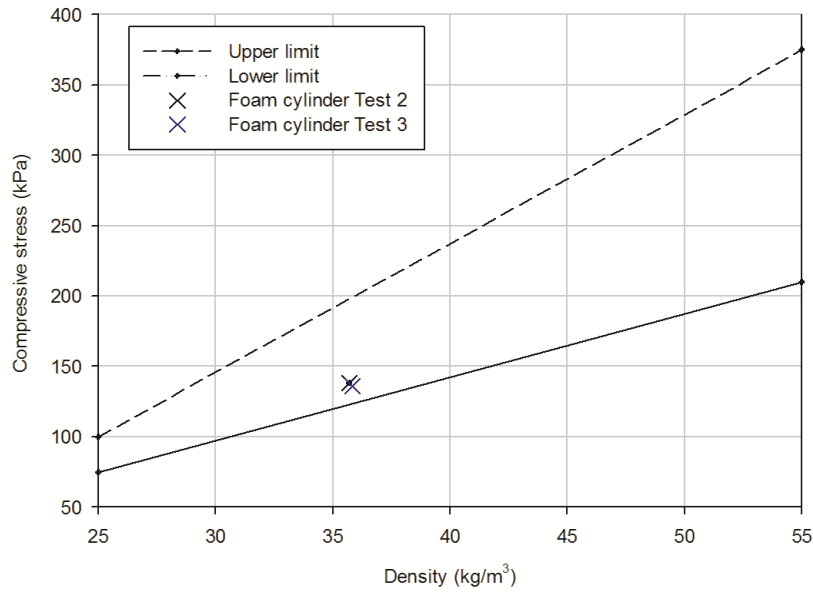


**Figure 4.4** Rigid polyurethane foam cylinder compressive strength test results (Adapted from (Gunter, 1985))

**Table 4.1** Polyurethane foam (PF) cylinder densities (kg/m<sup>3</sup>) before and after testing

Sample No.	Density Before	After
PF1	40.8	41.4
PF2	34.9	35.7
PF3	34.9	35.8
Average	36.9	37.7

**Table 4.2** Polyurethane reinforced ballast (PRB) composite cylinder densities (kg/m<sup>3</sup>) before and after testing

Sample No.	Before	After
PRB1	1182.5	1397.8
PRB2	1045.5	1257.0
PRB3	1178.5	1382.8
Average	1135.5	1345.9

The average sample density of the foam cylinders before testing was  $36.9 \text{ kg/m}^3$  and after testing it was  $37.65 \text{ kg/m}^3$  which represents a 1.4 % increase. The extent of permanent deformation was therefore minimal. Average density before testing of the reinforced ballast samples was  $1135.5 \text{ kg/m}^3$  and  $1345.9 \text{ kg/m}^3$  after testing which is a 18.5 % increase in density. The density before and after testing is lower than the loose bulk density of the ballast material. This is as a result of the uncompacted ballast experiencing uplift during the foam curing process resulting in lower densities due to the larger volume. Table 4.3 shows the permanent deformation of each sample after testing.

**Table 4.3** Polyurethane foam (PF) and PRB composite cylinder permanent deformation

Sample	Permanent Deformation (mm)
PF1	4.01
PF2	6.33
PF3	7.33
PRB1	44.67
PRB2	53.00
PRB3	47.67

The permanent deformation that was measured for the samples after testing and after the load was removed showed that on average the permanent deformation between the samples in the axial direction was 5.9 mm or 2.0 % of the original 300 mm length for a sample that was compressed 15 mm. The permanent deformation was about 45.5 % of the applied total deformation of the sample.

The foam reinforced ballast samples were compressed 60 mm and as a result their permanent deformation values were higher than those of the foam only samples. The average permanent deformation was 48.5 mm in the axial direction. The foam reinforced ballast samples retained 80.8 % of the total applied deformation. The two different sample sets behaved similarly at low strain levels and as a result, for lower strain levels the reinforced ballast sample would retain a lower amount of the applied compressive deformation. Compressing the foam reinforced ballast samples did result in cracking of the specimens because of the fact that at large deformation values/larger stresses the foam was not able to contain the ballast stone.

The rigid polyurethane exhibits behaviour that is significantly more elastic than just the ballast on its own. Combining the rigid polyurethane foam and the railway ballast produced a composite material

that had significantly more elasticity and a lower potential for permanent strain deformation than unreinforced ballast on its own. The composite material had greater E-value at all strain levels above 0.01.

Figure 4.5 shows the strength of the foam. As a result of the sleeper being placed on top of the foam during the pouring to limit expansion, it became "glued" to the entire reinforced ballast structure and this structure was able to support the entire mass of the test setup.



**Figure 4.5** Foam gluing reinforced ballast layer and sleeper to one another

### 4.3 SETTLEMENT BEHAVIOUR

In this section the settlement behaviour of the reinforced ballast (RB) tests that were performed are presented and discussed. The settlement behaviour is divided into two primary phases. The first phase is the "initial" phase where a large portion of the ballast settlement occurs as a result of the ballast layer being uncompacted at the start of each test. The second phase of the settlement behaviour is the "consolidation" phase. In this phase the ballast settlement rate is significantly lower. This concept is illustrated in Figure 4.6.

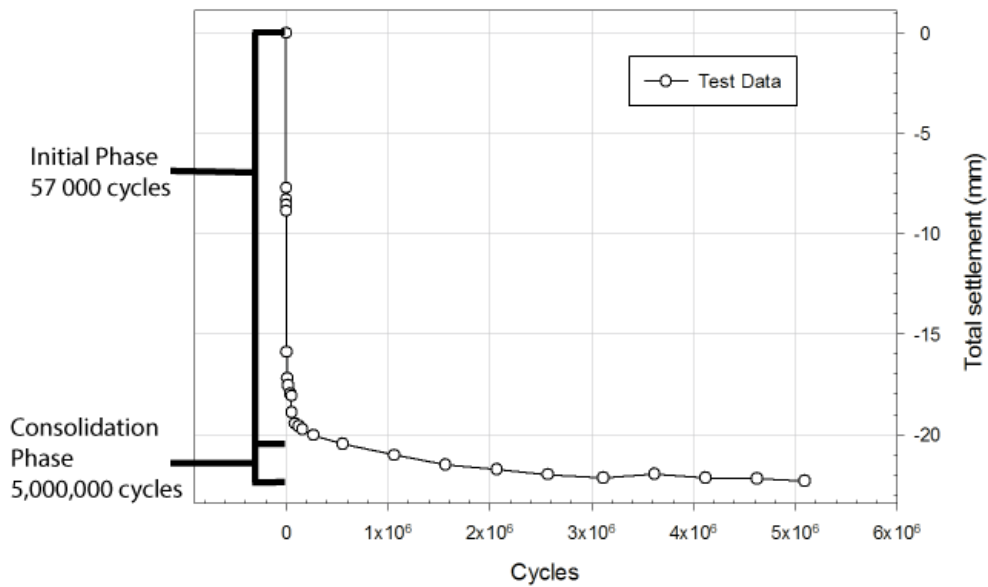


**Figure 4.6** Settlement behaviour breakdown

#### 4.3.1 Initial Phase

Due to the fact that the ballast was uncompacted, the initial phase of each test produced a significant amount of settlement. The results of the initial phase settlement are shown in Figure 4.7. The initial phase of each test was approximately 57 000 cycles as described in Chapter 3. The settlement results are summarised in Table 4.4.

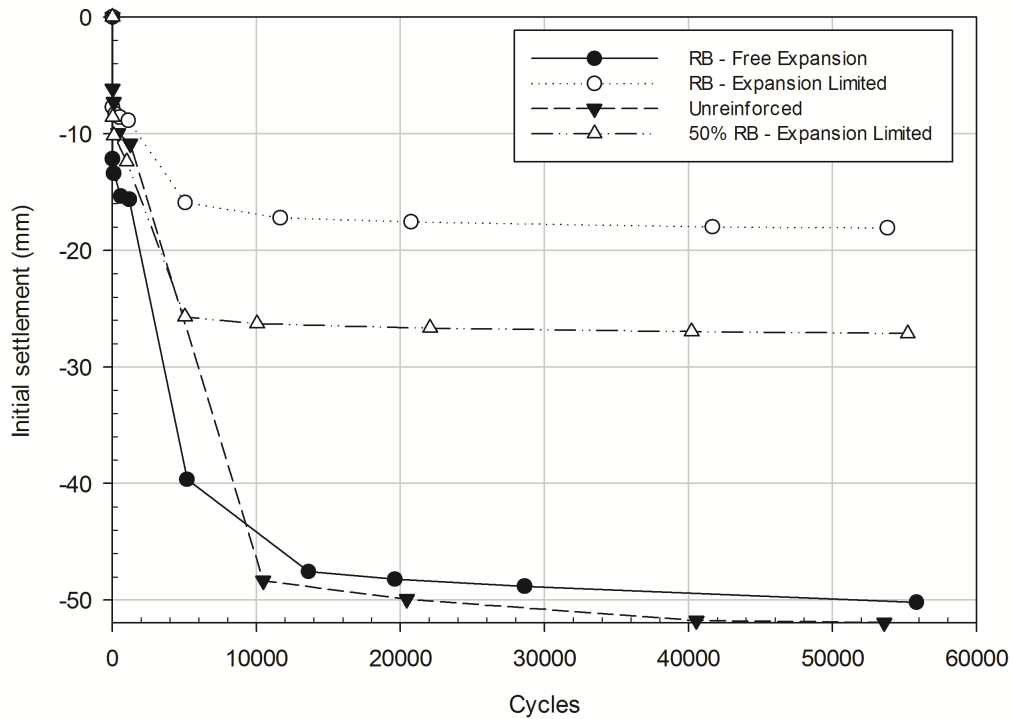


**Figure 4.7** Initial phase settlement

**Table 4.4** Initial phase settlement values

Test	Description	Initial phase settlement (mm)
2	Reinforced Ballast - Free Expansion	50.18
3	Reinforced Ballast - Expansion Limited	18.08
4	Unreinforced Ballast	51.91
5	50 % Reinforced Ballast	27.12

From Figure 4.7 it can be observed that the unreinforced ballast had the greatest amount of initial settlement. This is expected as the ballast was uncompacted before testing and thus loading would cause it to settle and the particles to reorientate. The ballast test where the polyurethane foam was allowed to expand freely also showed similar values of initial settlement, only exhibiting 3.5 % less settlement than unreinforced ballast during the initial phase of testing.

The test with 50 % reinforcement showed a significant reduction in initial settlement behaviour. The reinforcement of half of the ballast layer resulted in a reduction in initial settlement of 54 %. The test that showed the least amount of initial settlement was the test where the polyurethane foam was not able to expand freely. This was as a result of the sleeper being placed on the ballast during the process of foam injection. This test yielded a reduction in initial settlement of 33.84 mm which corresponds to a consolidation settlement of only 34 % of that of conventional unreinforced ballast under the same loading conditions.

The settlement results were plotted against a logarithmic scale as shown in Figure 4.8. Large increases in settlement values, especially in the case of the unreinforced ballast are as a result of increased loading of around 100 kN to 260 kN at  $10^3$  load cycles. It would appear that samples with reinforcement are less susceptible to increases in load resulting in reduced increases in settlement.

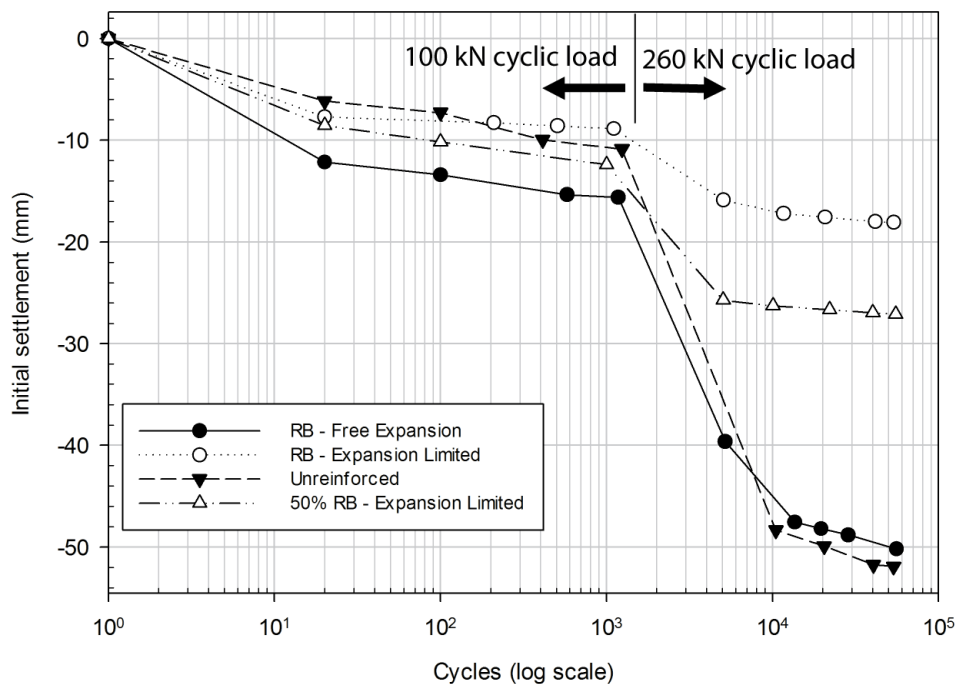


**Figure 4.8** Initial phase settlement plotted on a logarithmic scale

### 4.3.2 Consolidation Test Phase

Following the initial phase of testing where the ballast was allowed to compact and settle, the main (consolidation) test phase was started. This stage of the test consisted of the full axle loading being

applied for a total of 5 million load applications at the specified frequency (10Hz). At a test frequency of 10 Hz the main deformation mechanism in response to cyclic loads is the inception of plastic shakedown, as discussed in Chapter 2. The settlement plots for the tests are shown in Figure 4.9. Table 4.5 gives a summary of the final consolidation test settlement values.

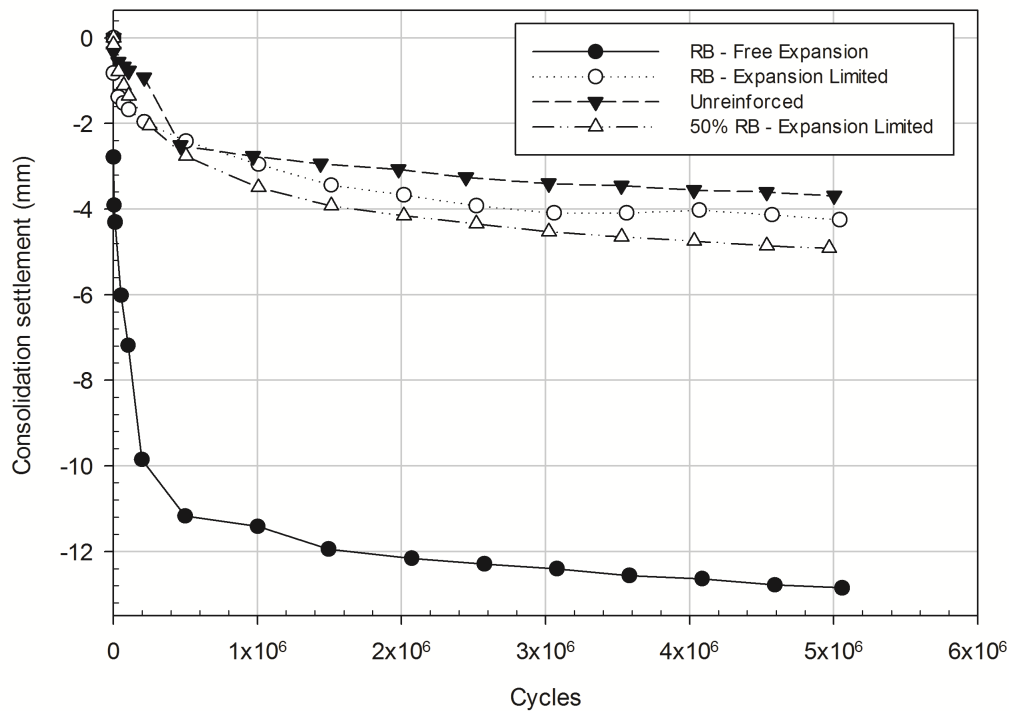


**Figure 4.9** Consolidation test phase settlement

**Table 4.5** Consolidation test phase settlement values

Test	Description	Consolidation phase settlement (mm)
2	Reinforced Ballast - Free Expansion	12.85
3	Reinforced Ballast - Expansion Limited	4.25
4	Unreinforced Ballast	3.69
5	50 % Reinforced Ballast	4.92

During the initial phase of the testing, the unreinforced ballast produced the most settlement. However during the consolidation phase of testing the unreinforced ballast settled the least (3.69 mm). Reinforced ballast with foam that was allowed to expand freely settled rapidly during the first 500 000

cycles of the test and then the settlement rate began to decrease. Nevertheless the reinforced ballast with free expansion settled 12.85 mm during the course of the main test which was significantly more than any of the other tests. This is most probably as a result of the lack of inter-particle contact between the ballast stones.

During the free expansion of the foam, expansive forces are generated and these forces are significant enough to lift the ballast stone. This results in the ballast particles losing contact with one another. Only once the foam-filled voids between the ballast are sufficiently compressed will the ballast particles begin to touch and the rate of settlement be reduced.

The complete ballast layer with full reinforcement settled 4.25 mm which is more than the unreinforced ballast. The ballast layer that was only 50% reinforced demonstrated a settlement of 4.92 mm. These three tests all produced settlement values within 1.23 mm of each other.

The results of the consolidation tests were also plotted on a logarithmic scale as shown in Figure 4.10.

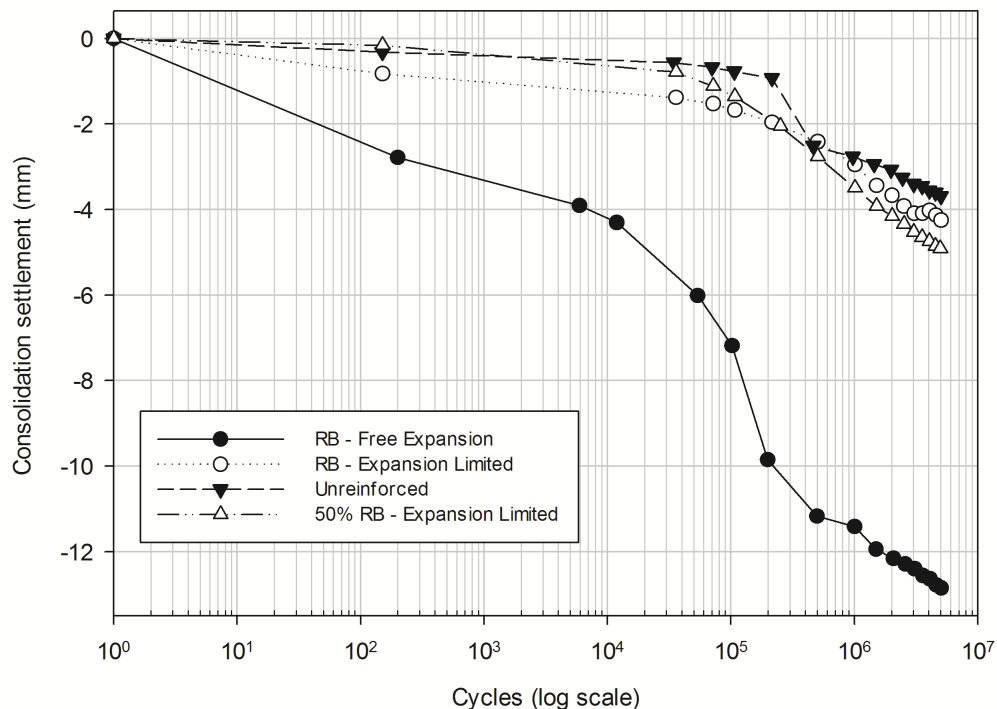


**Figure 4.10** Consolidation test phase settlement results plotted on a logarithmic scale

### 4.3.3 Consolidation Settlement Prediction Functions

Previous research on ballast box tests by Selig and Waters (1994) found that the power relationship defined by Equation 4.1 provides the best results for describing ballast settlement behaviour.

$$S_N = s_1 N^b \quad (4.1)$$

Where:

$s_1$  = settlement in the first cycle

$N$  = number of cycles

$b$  = empirical constant

Selig and Waters (1994) also used the logarithmic function defined by Equation 4.2 for describing ballast settlement.

$$S_N = s_1 (a \log N + 1) \quad (4.2)$$

Where:

$s_1$  = settlement in the first cycle

$N$  = number of cycles

$a$  = empirical constant

The two functions were plotted with the actual settlement results in order to examine their suitability for describing ballast settlement and reinforced ballast settlement behaviour. The models are not accurate at low cycle counts, but become more accurate with an increase in cycle count.

The settlement of the consolidation phase of Test 2 was plotted with the power and logarithmic settlement prediction functions as mentioned above. With  $s_1 = 3.5189$ , the values for  $a$  and  $b$  were determined using regression. Comparing the actual test settlement with these models gave good accuracy. The function in each case was determined in such a way that the final settlement value would be equivalent to the final actual recorded test settlement value. As seen in Figure 4.11a the two models

gave reasonably accurate results. The logarithmic function typically overestimated settlements and the power function typically underestimated settlement values.

The same procedure was followed for all the remaining tests and the results are plotted for Test 3 in Figure 4.11b, Test 4 in Figure 4.11c and Test 5 in Figure 4.11d.

Comparing the settlement prediction functions for Test 3 (reinforced ballast - limited foam expansion) it can be observed that the power and logarithmic prediction functions both greatly overestimated the amount of settlement that would take place at lower cycle counts.

The results of Test 4 are shown in Figure 4.11c. The power function seemed to accurately predict settlement values especially from 500,000 cycles onwards. The logarithmic function tended to greatly overestimate settlement values for all stages of the test.

The results of Test 5 is shown in Figure 4.11d. The power function tended to slightly underestimate settlement values while the logarithmic function overestimated the settlement that would occur.

A summary of the  $s_1$ ,  $a$  and  $b$  values as well as the coefficient of correlation ( $R^2$ ) values for the power and logarithmic prediction functions are given in Table 4.6.

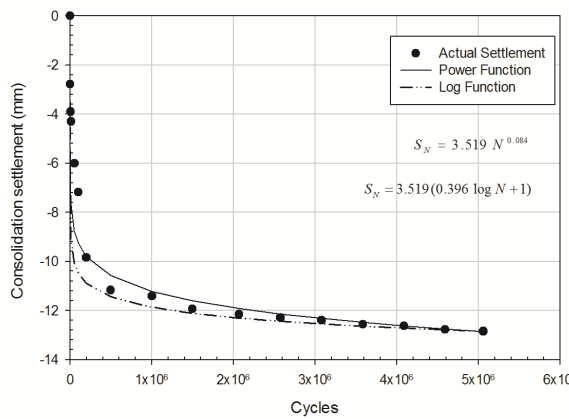
**Table 4.6** Consolidation phase settlement prediction equation constants and correlation coefficients

Test	Description	$s_1$	$a$	$b$	$R^2$ Power	$R^2$ Log
2	100 % Reinforced Ballast - Free Expansion	3.5189	0.3956	0.0839	0.81	0.63
3	100 % Reinforced Ballast - Expansion Limited	0.7414	0.7054	0.1131	0.77	0.43
4	Unreinforced Ballast	0.3357	1.4915	0.1554	0.78	0.31
5	50% Reinforced Ballast - Expansion Limited	0.0963	7.4749	0.2551	0.97	0.42

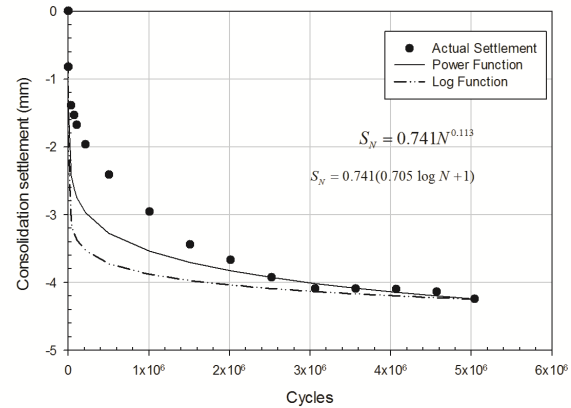
#### 4.3.4 Combined Settlement

Finally, the two phases of the testing were combined and compared. This represents all the cycles that were applied to each sample. These results are shown in Figure 4.12. The same results plotted on a logarithmic scale are shown in Figure 4.13.

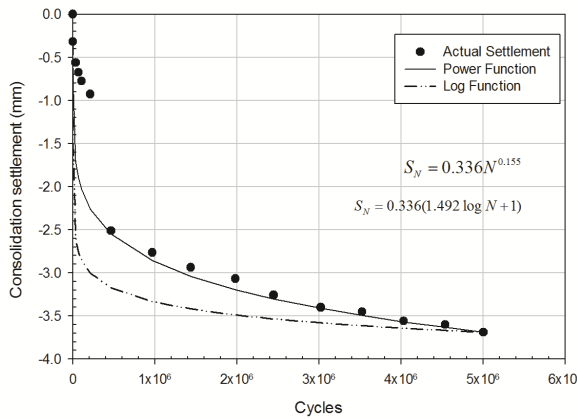
The test with the largest amount of combined settlement was the test with the reinforced ballast with



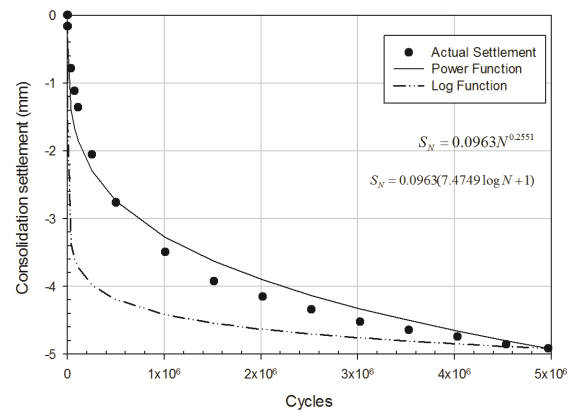
(a) Test 2: Reinforced ballast - free expansion



(b) Test 3: Reinforced Ballast - Expansion limited



(c) Test 4: Unreinforced ballast



(d) Test 5: 50% reinforced ballast

**Figure 4.11** Consolidation phase test settlement results plotted against power and logarithmic settlement prediction functions

free expansion, exhibiting a total settlement of 63.03 mm. This was significantly more than the other two reinforced ballast tests. The unreinforced ballast had the second largest total settlement at 55.60 mm but this was almost entirely due to the settlement in the initial phase, as the settlement during the consolidation phase of the test only accounted for 7.1 % of the total settlement. The summarised combined settlement results are shown in Table 4.7.

The "semi-reinforced" ballast test (50 % of ballast layer depth reinforced) showed the second least amount of settlement with a total settlement of 32.03 mm. The reinforced ballast sample that limited foam expansion had the least total settlement of 22.32 mm.

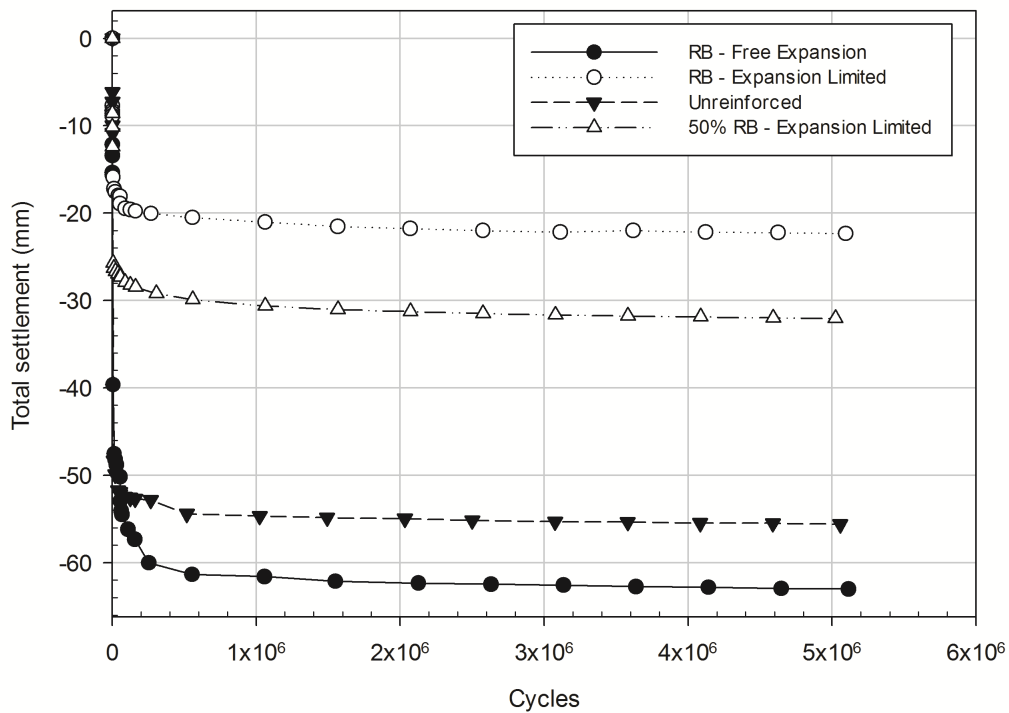


**Figure 4.12** Total test settlement values

**Table 4.7** Total test phase settlement values

Test	Description	Total settlement (mm)
2	Reinforced Ballast - Free Expansion	63.03
3	Reinforced Ballast - Expansion Limited	22.32
4	Unreinforced Ballast	55.60
5	50 % Reinforced Ballast - Expansion Limited	32.03

The use of rigid polyurethane foam as a means of reducing ballast settlement is a possibility provided that the expansion of the foam into the ballast voids does not lift the ballast significantly and remove inter-particle contact between the ballast stones. By reinforcing 50 % of a ballast layer the total settlement experienced by the layer can be reduced by 58 % compared to unreinforced ballast. Comparing the completely reinforced ballast layer (expansion limited) with the 50 % reinforced layer, the former produced a 45 % reduction in total settlement.

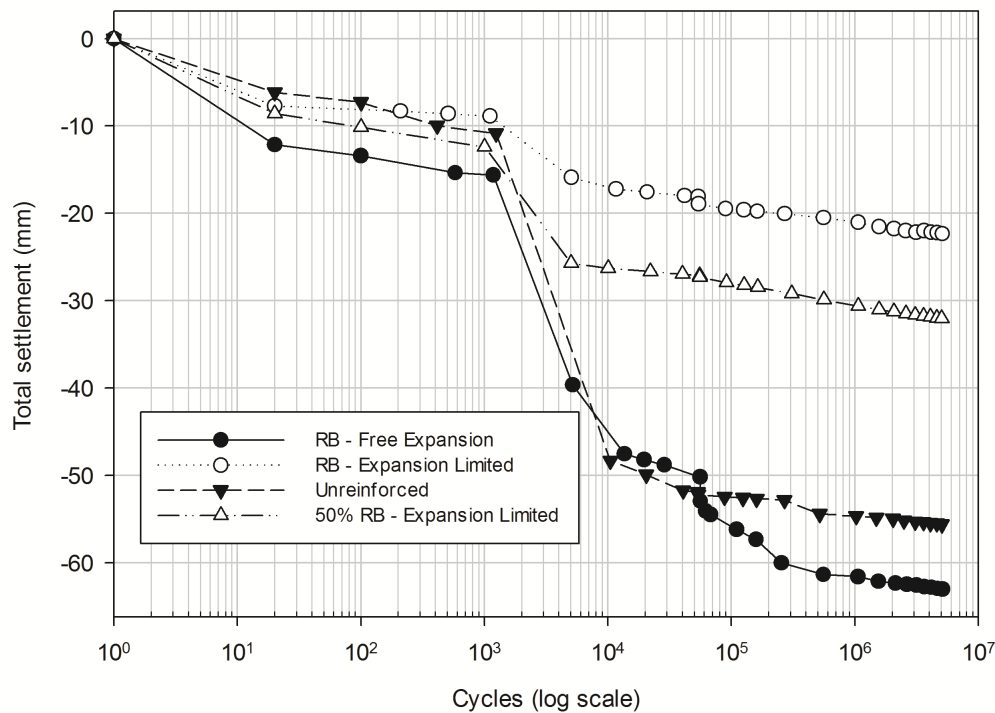


**Figure 4.13** Total test settlement values plotted on a logarithmic scale

The overall total settlement of the reinforced ballast (expansion limited) and 50 % reinforced ballast yielded settlements that were respectively 59.6 % less and 42.4 % less than conventional unreinforced ballast.

Although some of the reinforced tests showed more settlement during the main phase of the test, the large reduction in initial consolidation settlement should also be noted as a primary contributor to the reduced total settlement. Allowing the free expansion of the polyurethane foam reinforcement should be limited as increased settlement in all phases of testing was observed, and was even outperformed by unreinforced ballast. For use in the field, the foam should be poured/injected into an already existing track structure in order to prevent this ballast uplift from the foam expansion from occurring. When this ballast uplift/foam expansion is limited (as in Test 3 and Test 5) the ballast performs significantly better.

Reinforced ballast exhibits lower settlement values and as a result the ability for track to maintain good geometry in the field could be expected. The result of which could be longer maintenance intervals and lower dynamic forces at track transitions as a result of the reduction in differential

settlement.

The ballast strain results as shown in Figure 4.14 show similar trends to that of the settlement behaviour. The ballast strains shown have the same shape as the settlement graphs as it is defined as the ballast layer settlement divided by the ballast layer thickness.

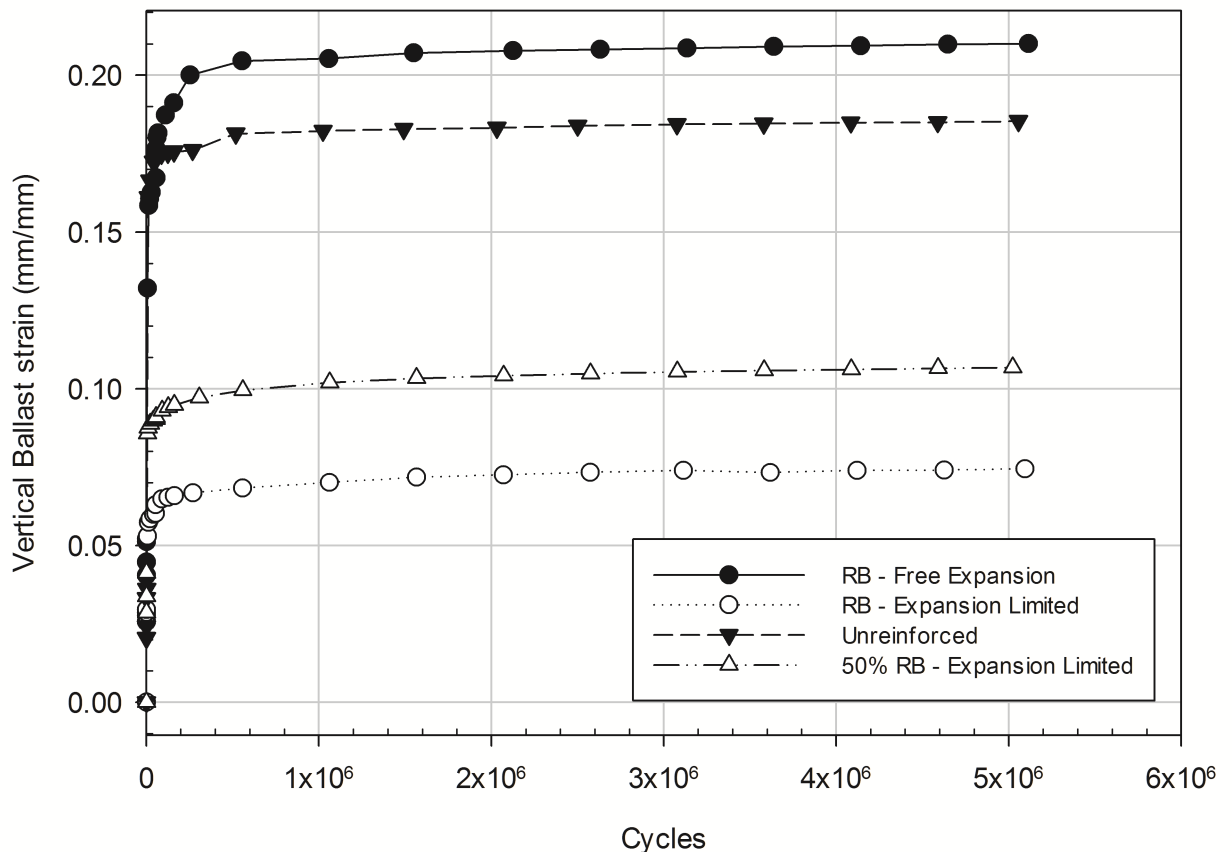


**Figure 4.14** Ballast strain comparison (Vertical (or axial) strain)

In the cyclic triaxial compression tests conducted by Keene, Edil, Tinjum and Brown (2012a) described in Chapter 2 the elastic strain between clean ballast and rigid polyurethane foam (RPF) reinforced ballast was compared with the RPF reinforced ballast samples up until 250 000 cycles with the rate of elastic strain accumulation remaining more or less constant over a long duration. Testing the samples to 5 million load cycles (10X longer) in the ballast box tests confirmed this trend continued over the long term.

The compression of the ballast layer after testing was visible in a distinct region directly under the sleeper and this is shown in Figure 4.15 which was taken after the completion of Test 2 (reinforced

ballast with free expansion of polyurethane foam). This is as a result of the limited horizontal and lateral movement of the sleeper.



**Figure 4.15** Compression and settlement of the ballast due to sleeper contact stress

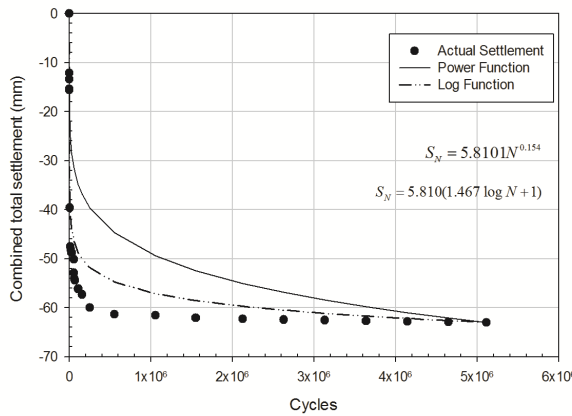
#### 4.3.5 Combined Settlement Prediction Functions

The results of the combined settlement were again plotted with predicted settlement power and logarithmic functions. The combined settlement results of Test 2 along with the power and logarithmic settlement prediction functions are shown in Figure 4.16a. In this case it was the logarithmic function that provided the closest settlement estimate, however both the power and logarithmic prediction functions underestimated the amount of settlement.

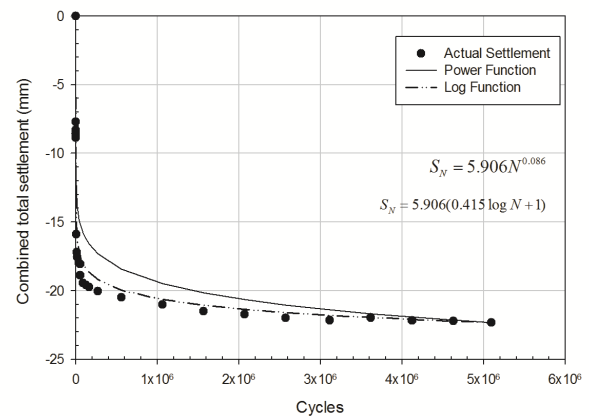
The results of Test 3 are shown in Figure 4.16b. Settlement values were underestimated by both the power and logarithmic prediction functions, but the logarithmic function did provide the nearest estimation.

Power and logarithmic settlement prediction functions plotted against actual total settlement for Test 4 are shown in Figure 4.16c. The same trend as in Test 2 and Test 3 was observed with both forms of prediction functions underestimating the settlement, but the logarithmic function was closer to the true values than the power function. The same trend was observed for Test 5 as shown in Figure

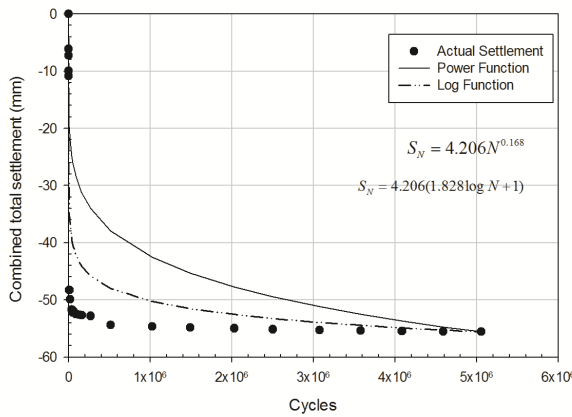
4.16d. A summary of the various constants is shown in Table 4.8.



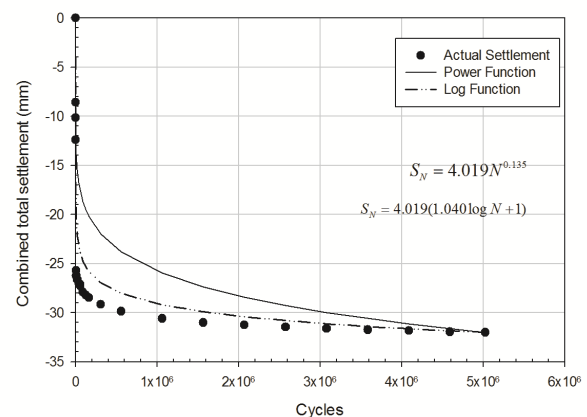
(a) Test 2: Reinforced ballast - free expansion



(b) Test 3: Reinforced ballast - expansion limited



(c) Test 4: Unreinforced ballast



(d) Test 5: 50% reinforced ballast

**Figure 4.16** Combined test phases settlement results plotted against power and logarithmic settlement prediction functions

**Table 4.8** Combined settlement prediction equation constants and coefficient of correlation ( $R^2$ ) values

Test	Description	$s_1$	$a$	$b$	$R^2$ Power	$R^2$ Log
2	100 % Reinforced Ballast - Free Expansion	5.8101	1.4672	0.1543	0.38	0.88
3	100 % Reinforced Ballast - Expansion Limited	5.9059	0.4145	0.0861	0.64	0.96
4	Unreinforced Ballast	4.2064	1.8279	0.1677	0.22	0.77
5	50 % Reinforced Ballast - Expansion Limited	4.0191	1.0400	0.1345	0.29	0.88

The coefficient of correlation values ( $R^2$ ) for the power functions used to theoretically predict the settlement of the consolidation phase of each test were significantly higher than the  $R^2$  values for the logarithmic prediction functions. The lowest power  $R^2$  value being 0.77 compared to 0.43 for the logarithmic prediction function of the same test. The best  $R^2$  value obtained for any function for the consolidation phase of the testing was 0.97 for the power function.

The coefficient of correlation values ( $R^2$ ) for the power functions used to theoretically predict the total settlement of each test were significantly lower than the  $R^2$  values for the logarithmic prediction functions. For the total settlement  $R^2$  values, the power functions were not adequate and the logarithmic prediction function gave better correlation. The lowest  $R^2$  value for the total settlement logarithmic prediction functions was 0.77 and for the same test the  $R^2$  value for the power function was 0.22. A summary of these results is provided in Table 4.9.

**Table 4.9** Comparison of  $R^2$  values for different test phases (consolidation phase and combined phase)

Test	Initial phase		Initial and consolidation phase	
	Power	Logarithmic	Power	Logarithmic
2	0.81	0.63	0.38	0.88
3	0.77	0.43	0.64	0.96
4	0.78	0.31	0.22	0.77
5	0.97	0.42	0.29	0.88

From these results, and from those in the previous section it would appear that when there is significant initial settlement in early load cycles (such as in uncompacted ballast), the logarithmic prediction function would be the ideal form to use, as it provides the closest estimate in these cases. For test samples where initial settlement is not that significant, the power function tended to provide superior results. For this reason the prediction function chosen should be selected based on the present testing conditions.

#### 4.4 BALLAST LAYER MODULUS

The resilient sleeper deflection was firstly plotted for different tests as shown in Figure 4.17. All the reinforced ballast tests show a decrease in resilient sleeper deflection from the start to cycle

1,000,000. After cycle 1,000,000, the resilient sleeper deflection remains between 0.75 mm/cycle to 1.0 mm/cycle with a gradual decrease as the number of load cycles increases. Even the 50 % reinforced ballast layer exhibited these properties despite the presence of a conventional 150 mm ballast layer.

The unreinforced ballast sample initially had lower resilient sleeper deflection but after 500,000 load cycle applications this resilient sleeper deflection began to increase. This could be attributed to the fact that ballast breakage was taking place and thus the ballast became fouled leading to a loss of strength, which would increase the resilient sleeper deflection. Typically in practice a sleeper deflection of approximately 0.3 mm to 0.6 mm can be expected. Significantly higher sleeper deflections were observed during this test and this could be attributed to the fact that the entire test system is very stiff and only a ballast layer was tested with no subgrade, pads, or rails. In practice these components would all contribute to reduce the sleeper deflection.

The samples that were fully reinforced experienced higher resilient sleeper deflections than the unreinforced and 50 % reinforced samples. This could be explained by the fact that the polyurethane foam reinforcement made the ballast layer far more elastic resulting in more deflection in each load application. The 50 % reinforced sample showed a steady decrease in resilient sleeper deflection, as observed with the other reinforced ballast samples.

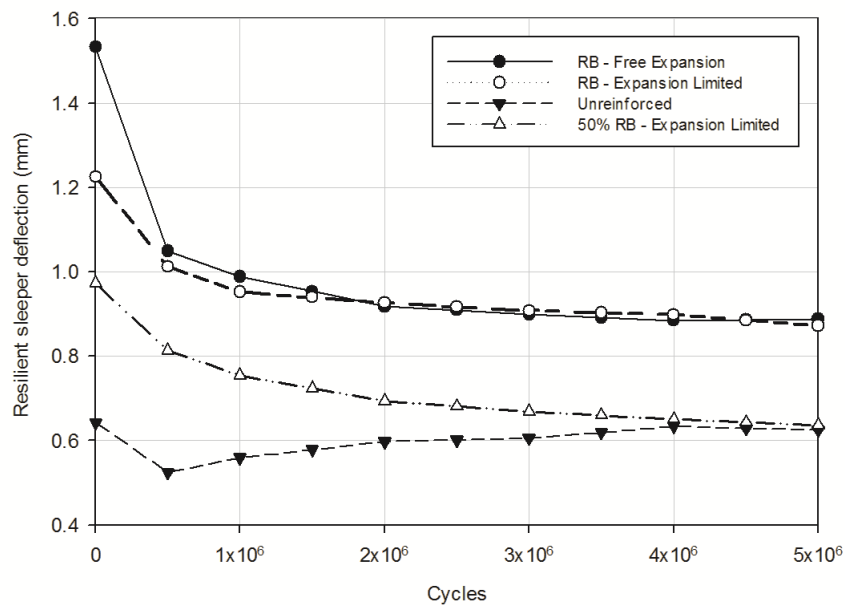


**Figure 4.17** Resilient sleeper deflection with increasing cycles

Ballast layer modulus was calculated by dividing the stress applied by the ballast layer strain for that cycle. The stress applied for each cycle was the same (constant load and no significant change in sleeper area).

The stress directly below the sleeper is approximately 390 kPa, assuming a sleeper area of 2200 mm x 300 mm and a load of 260 kN.

Using the relationship between stress (force over an applied area) and strain, Equation 4.3 was used to calculate the ballast layer modulus.

$$E = \frac{\sigma}{\epsilon} \tag{4.3}$$

with:

$$\sigma = 393 \text{ kPa}$$

$\epsilon$  = ballast layer strain for the cycle

The ballast layer modulus for a number of cycles were calculated and plotted below as shown in Figure 4.18.

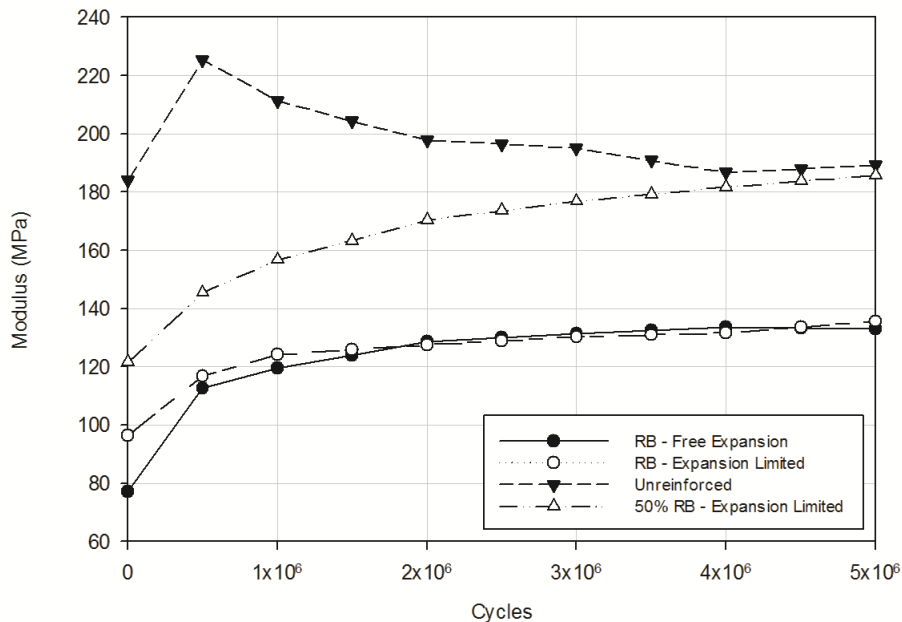


**Figure 4.18** Ballast layer modulus with increasing cycles

The unreinforced ballast layer had the highest initial modulus, with a modulus of 184 MPa. The modulus of the unreinforced ballast layer increased up until 500,000 cycles, after which a gradual decrease in stiffness can be observed, most likely as a result of ballast breakdown, causing the ballast layer to become fouled and leading to a loss in strength.

The "semi-reinforced" ballast layer (50 % reinforcement) showed an increase in stiffness throughout the duration of the test. The other two fully reinforced ballast tests showed lower initial moduli than the "semi-reinforced" and unreinforced ballast tests. The 50% reinforced ballast started with an initial modulus of 121.48 MPa and this increased to 185.82 MPa over the course of the test. At the end of the test the 50 % reinforced ballast sample had stiffness that was approximately equal to that of the unreinforced ballast sample (186 MPa vs 189 MPa respectively)

The completely reinforced ballast sample that had the polyurethane foam expansion limited achieved a 40.5% increase in modulus over the course of the test. Even the test where the polyurethane foam reinforcement was allowed to freely expand (which performed very poorly with regard to settlement) achieved a 72 % increase in modulus over the course of the test.

In the case of the fully reinforced ballast, the modulus of the layer gradually increased with the increase in load cycles. This increase in modulus could be as a result of the small foam filled gaps between the ballast stones becoming fully compressed allowing the ballast stones to regain contact with one another (see in Figure 4.19). The final stiffness values for the fully reinforced ballast layers was found to be significantly lower than those of the unreinforced and 50 % reinforced ballast layers. Interestingly the unreinforced ballast layer stiffness between the first cycles and the end showed only a 2.8 % difference, whereas all the reinforced ballast samples showed significant stiffness gains of at least 40% (fully reinforced expansion) to 72 % as in the case of the fully reinforced ballast layer with unlimited foam expansion.

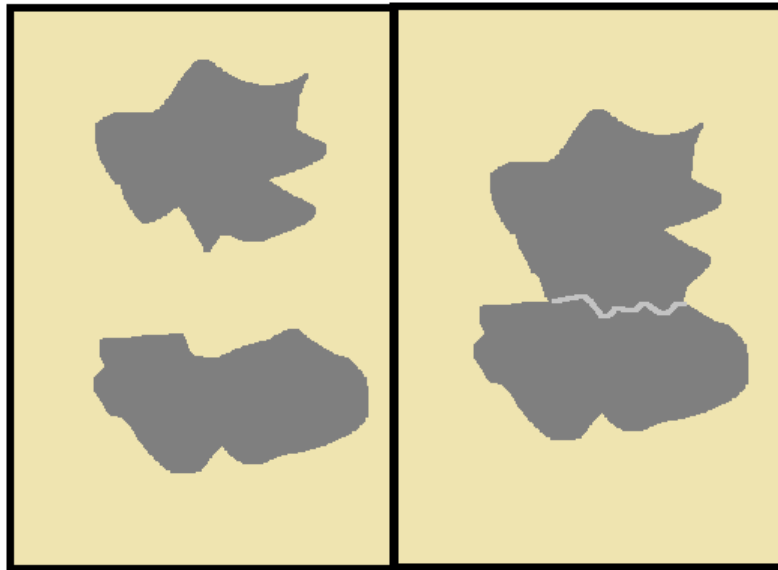


**Figure 4.19** Foam filled void between ballast stone (left), foam sufficiently compressed allowing ballast contact to occur (right)

Comparing the E-value results between Figure 4.1, Figure 4.2 and Figure 4.18 the addition of ballast stone to the polyurethane foam results in an increase in E-value. The greater the proportion of ballast, the greater the E-value is likely to be. The polyurethane foam reinforcement on its own is more elastic than ballast stone and is able to deform significantly. When adding ballast stone to the cylindrical samples the amount of strain the cylindrical sample undergoes is reduced resulting in higher E-values for the composite materials at the same stress level. The reduction in the amount of rigid polyurethane foam reinforcement in a ballast sample leads to an increase in E-value.

These results conclude with those of Keene, Edil, Tinjum and Brown (2012b) who found that the elastic moduli of the reinforced ballast samples is less than that of unreinforced ballast.

One additional point of interest is the fact that during the cyclic loading box tests the E-value or modulus value increased during the test, while in the case of the cylindrical samples the E-value decreased as the test progressed. A possible explanation for this behaviour could be the difference between the static (cylindrical tests) vs. cyclic loading nature of the box tests. In the case of the static test the load is applied slowly and at a constant rate. The cyclic loading nature of the box tests and the modulus value that is derived from the test could be as a result of the resilient modulus due to the cyclic loading behaviour of the test which is not present in the static test of the cylindrical foam samples.

#### 4.5 LOAD VS DEFLECTION BEHAVIOUR

The load-deflection behaviour of the different tests were compared. The load-deflection behaviour of the actuator itself was compared to that of the actual sleeper. The typical load-deflection curve for the actuator during a full cycle is shown in Figure 4.21.

It should be observed that during unloading the deflection behaviour does not plot exactly on the loading section of the curve. Comparing the actuator load vs displacement behaviour with that of the sleeper is shown in Figure 4.20.

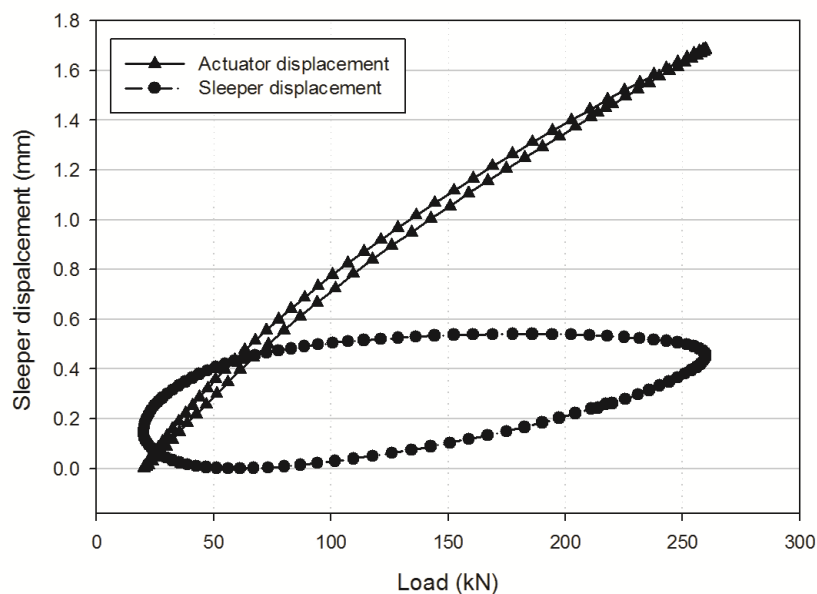


**Figure 4.20** Typical load-deflection behaviour of the hydraulic load frame actuator and sleeper during a cycle

From Figure 4.21 it can be seen that there is a significant difference in the behaviour between the actuator and the sleeper during the same load cycle. The loading and unloading behaviour between the two is completely different and while the actuator reaches its maximum deflection at the maximum load (260 kN) the sleeper reaches its maximum deflection at approximately 150 kN. One possible reason for this behaviour is the slight bending of the beam that is used to apply the loading to the sleeper. The beam bending is approximately 1.2 mm at the maximum applied load of 260 kN. The beam may also apply some damping to the loading and unloading behaviour of the sleeper resulting in response that is different from the actuator load deflection behaviour. The discrepancy between

the maximum deflection and maximum load could also be explained due to inertial effects causing a delayed response to loading. The sleeper load-deflection behaviour for each test midway (cycle 2,500 000) through the consolidation phase was plotted as shown in Figure 4.21. In order to calculate the ballast layer modulus, the maximum deflection and maximum load were used as shown in Figure 4.21.

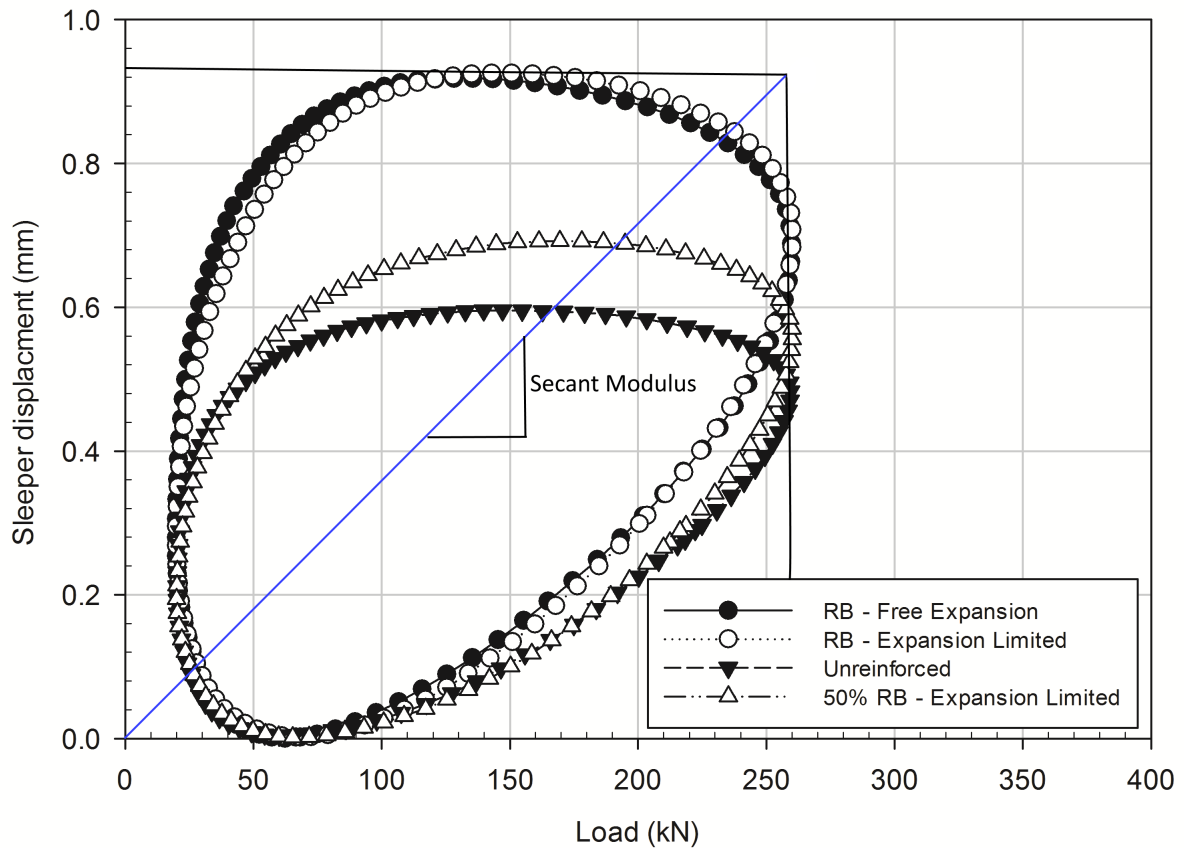


**Figure 4.21** Ballast layer modulus calculation definition

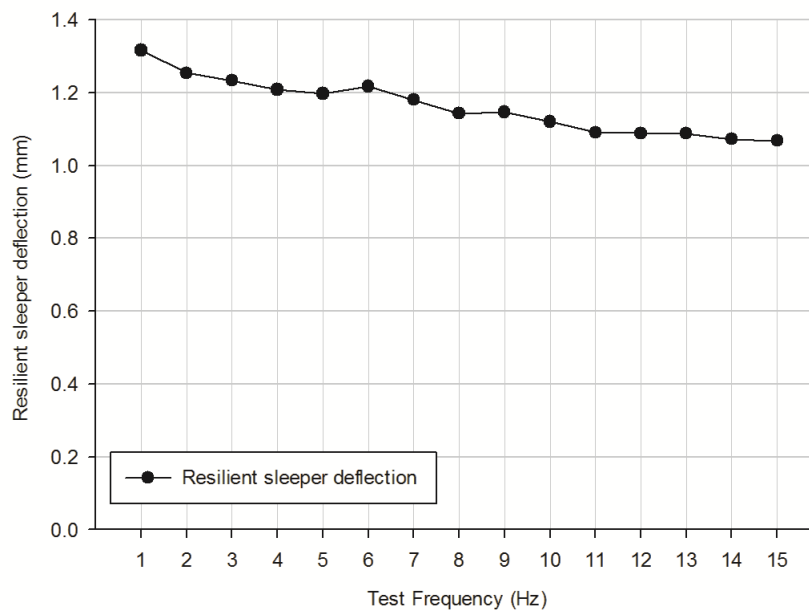
It is clear from the data plotted in Figure 4.21 that the fully reinforced ballast layer tests experienced a larger range of deflection during a cycle than that of the unreinforced ballast. Sleeper deflection for the fully reinforced ballast layers is approximately 0.3 mm greater than that of the unreinforced ballast. The 50 % reinforced ballast layer had a lower deflection in a cycle than the fully reinforced ballast layers. However, the deflection of this 50 % reinforced ballast layer was still greater than that of the unreinforced ballast layer by about 0.1 mm. The loading/unloading behaviour difference between the actuator deflection and the sleeper deflection is prevalent in all the sleeper deflection plots.

## 4.6 EFFECT OF TEST LOAD FREQUENCY

### 4.6.1 Frequency Sweep

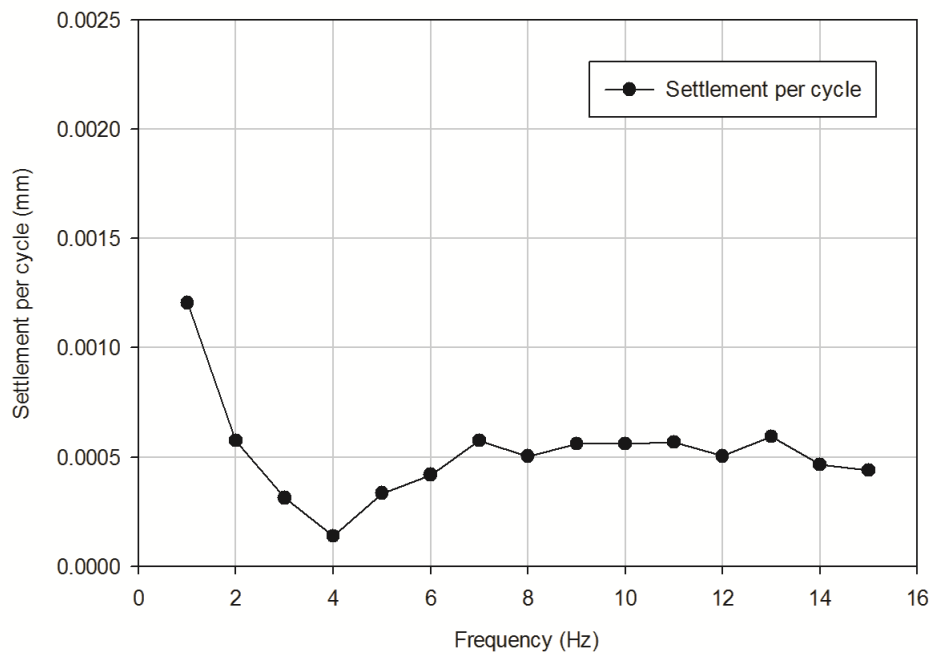
A test was conducted in which the 260 kN cyclic load was applied across a range of frequencies from 1 Hz to 15 Hz at 1 Hz increments. At each frequency, a constant testing time was applied, resulting in a variation in the number of cycles from 60 to 900 for the 1 Hz to 15 Hz frequency range. The effect of the change in frequency was examined by comparing the sleeper deflection and settlement per cycle.

Figure 4.22 shows the sleeper deflection that was measured over the range of test frequencies.



**Figure 4.22** Effect of loading frequency on sleeper deflection

The resilient sleeper deflection decreases as the frequency increases and at higher frequencies the resilient sleeper deflection does not change significantly at all, specifically in the 10 Hz to 15 Hz range. Figure 4.23 shows the effect of loading frequency on the settlement per load cycle.



**Figure 4.23** Effect of loading frequency on settlement per cycle

The settlement per cycle remains fairly constant between the different frequencies from 6 Hz onwards. Small differences in settlement per cycle could be explained by the response of the loading beam and/or hydraulic load frame. Between 8 Hz and 15 Hz there is no significant difference between the settlement per cycle values.

#### 4.7 BALLAST BREAKDOWN

Tests 1 and 4 were conducted on unreinforced ballast. After each test was conducted the sleeper was removed, the ballast was inspected, and a grading analysis was conducted. The grading analysis was done by taking a sample of ballast from each end of the box at the position corresponding to the sleeper rail seat where the loading was applied in addition to the centre of the box corresponding to the position of the center of the sleeper. This is shown in Figure 4.24.

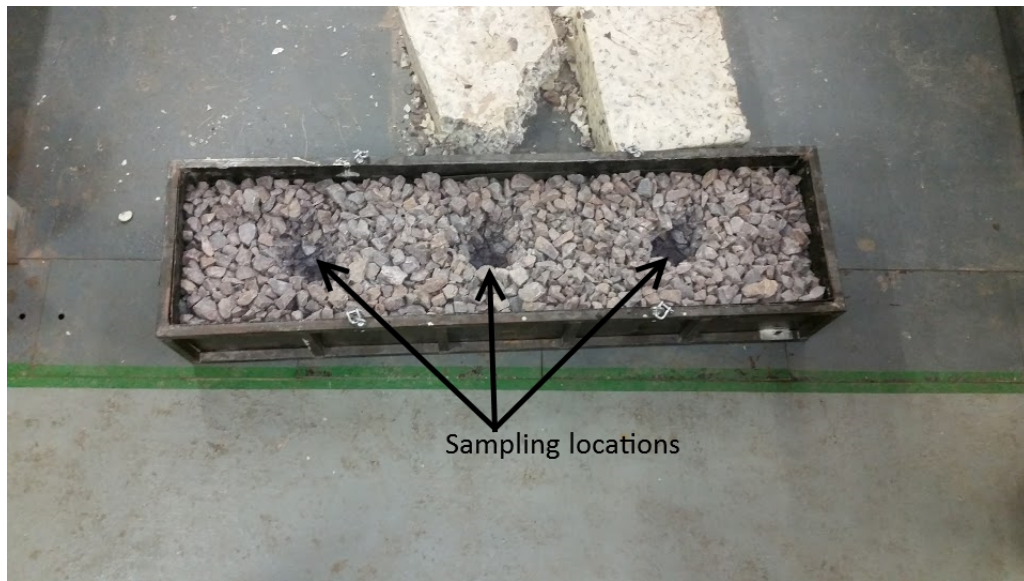


**Figure 4.24** Positions of ballast removed for grading through the entire ballast layer depth

Particle breakage was visible in the ballast and the fines that were generated were also visible. Figure 4.25 shows the ballast after testing with visible fines. The breakage and fracturing of the ballast was also visible and this is shown in Figure 4.26. The corner breakage and attrition of asperities is visible which is indicative of deformation mechanism of Range I ( $< 20$  Hz). Also visible in Figure 4.26 are Type I and Type II particle splitting as illustrated by Sun et al. (2014) in Chapter 2. These particle splits are indicative of deformation mechanisms of Range II and Range III (i.e. frequencies  $> 20$  Hz). However the particle splits achieved by Sun et al. (2014) were done in a triaxial apparatus and in this case the particle breakage most likely occurred as a result of sleeper contact as the test frequency did not exceed 10 Hz.



**Figure 4.25** Fines generated during the test as a result of ballast breakdown



**Figure 4.26** Breakage of ballast

The results of the grading analysis for Test 1 is shown in Figure 4.27 while the results for the grading analysis that was conducted on Test 4 is shown in Figure 4.28. The unreinforced ballast from Test 5 ("semi-reinforced ballast") was graded as well as shown in Figure 4.29. The results from these grading analyses clearly show the breakdown of the ballast during loading.

The breakage index could be quantified by comparing the plots of the particle size distributions. As

the amount of breakage increases the particle size distribution shifts to the left and the area between this new line and the original particle size distribution is considered as the breakage zone (Christie et al., 2007). Christie et al. (2007) states that the breakage potential is considered to be the area between the original particle size distribution and an arbitrary reference line (Maximum breakage line) connecting the point between the intersection of  $d_{95}$  of the largest sieve size and the minimum particle size of 2.36 mm.

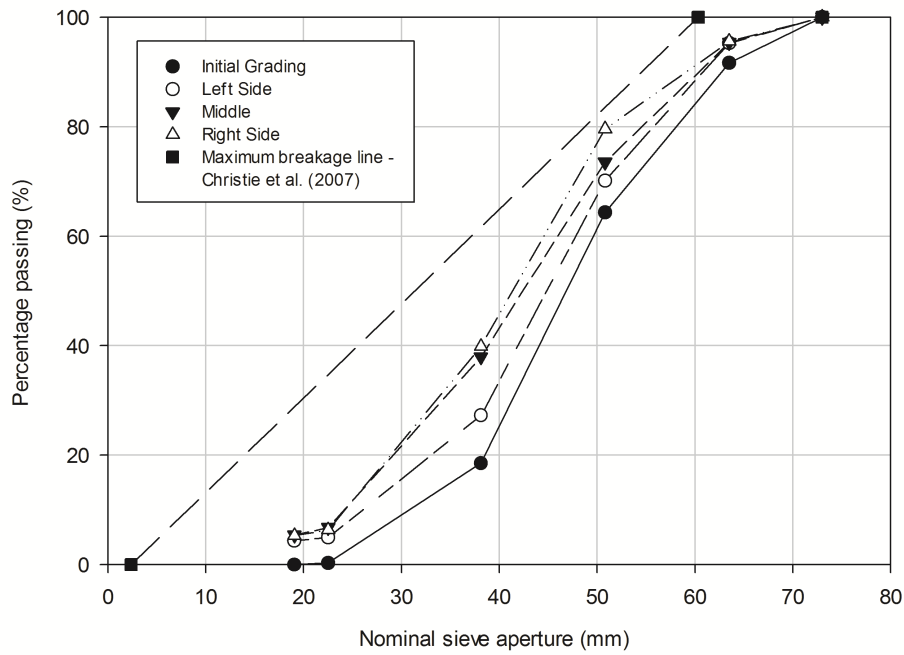


**Figure 4.27** Grading analysis after Test 1 on unreinforced ballast

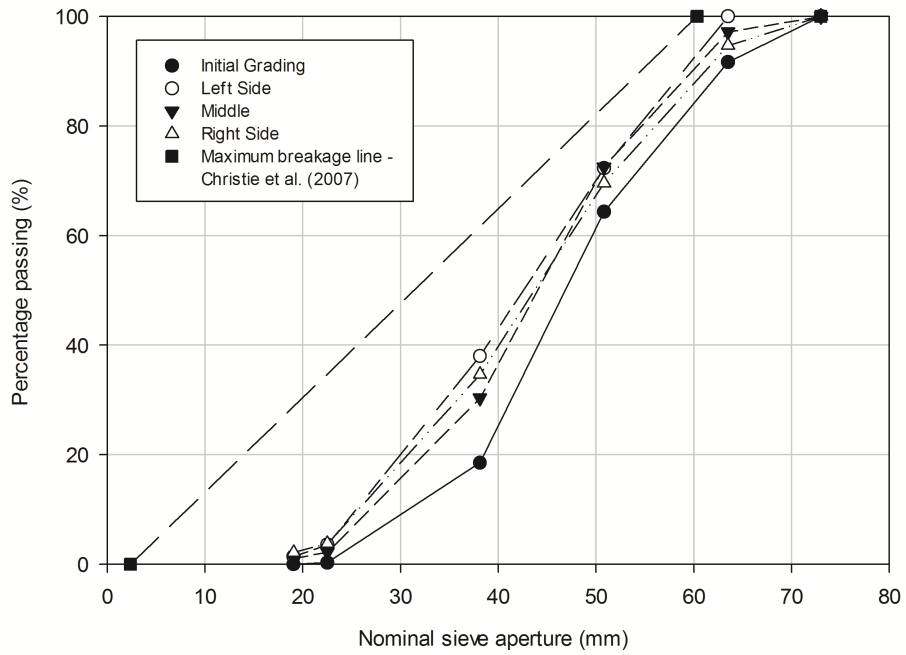


**Figure 4.28** Grading analysis after Test 4 on unreinforced ballast

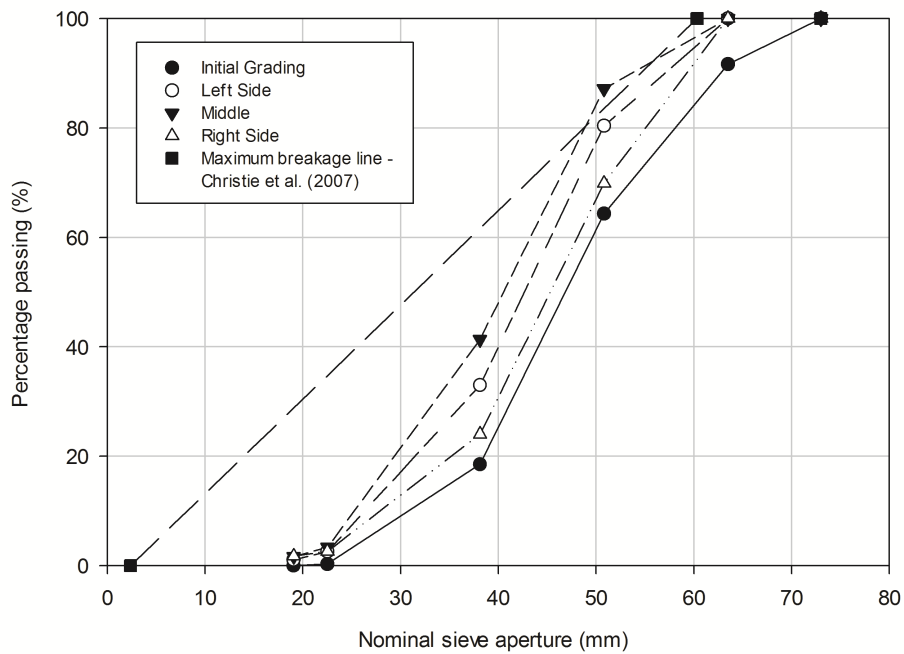


**Figure 4.29** Grading analysis after Test 5 on "semi-reinforced" ballast

The ballast breakage index (BBI) was calculated for each of the tests and the results are shown in Table 4.10. Test 1 was conducted at a loading frequency of 15 Hz while all the other tests were conducted at a loading frequency of 10 Hz. The increased loading frequency produced 0.5 % more ballast breakage than the other reinforced ballast tests. The BBI value of 3.81 was equal to that of the semi-reinforced ballast test. Discrepancies in the BBI values between the various locations in the box could be as a result of a number of factors:

- Uncompacted ballast at the start of the test compacting and causing differential settlement which would lead to sections experiencing more stress than others.
- During the initial phase and consolidation phase of the testing process some sections of ballast may have found a more optimal packing arrangement leading to lower ballast degradation.

**Table 4.10** Ballast Breakage Index (BBI) results in % of total maximum breakage

Ballast Breakage Summary (BBI %)					
Test	Description	Left	Middle	Right	Average
1	15 Hz Unreinforced	2.51	4.10	4.81	3.81
4	10 Hz Unreinforced	4.19	2.85	2.88	3.31
5	10 Hz 50% Reinforced	3.67	5.24	2.52	3.81

In Figure 4.29 it can be seen that the grading of the ballast falls outside of the theoretical maximum ballast breakage line. This could be as a result of the significantly smaller ballast layer, which only had a depth of 150 mm. The fact that the ballast below this thin layer was reinforced with a rigid polyurethane foam could also play a role in the ballast breakage behaviour. Nevertheless, the average ballast breakage for Test 5 ("semi-reinforced ballast") shows that the ballast breakage was the same as for unreinforced ballast loaded at 15 Hz and only marginally less (0.5 %) than for unreinforced ballast at 10 Hz.

Figure 4.30 shows the reinforced ballast layer upside down after removal from the box following the completion of the test. From Figure 4.30 and Figure 4.31 it is clear that all voids were filled and full ballast layer penetration was achieved.



**Figure 4.30** Reinforced ballast layer after removal from box after testing (upside down)



**Figure 4.31** Close-up of a cross section of reinforced foam ballast layer - note full foam penetration and void filling

#### 4.7.1 Equivalent Tonnage

Selig and Waters (1994) presents the equation for converting load cycles to gross tonnage as shown in Equation 4.4.

$$C_m = \frac{10^6}{A_t N_a} \quad (4.4)$$

Where:

$C_m$  = number of load cycles/MGT

$A_t$  = axle loads in tons, and

$N_a$  = number of axles/load cycle

Therefore:

$$C_m = \frac{10^6}{30 \times 4} = 8333.33$$

Therefore 5,000,000 load cycles at an equivalent axle loading of 30 tons represents 600 MGT. Comparing this gross tonnage to the Ermelo - Richards Bay Coal Line in South Africa where approximately 75 MGT of coal are exported a year and taking the mass of the wagons and locomotives into account, this corresponds to approximately 5 years of traffic on the line.

#### 4.8 SUMMARY OF RESULTS AND DISCUSSION

The lowest amount of settlement (18.08 mm) after 5 million load cycles, was observed for the fully reinforced ballast layer with expansion limited. The greatest amount of initial settlement (62.61 mm) was observed after 5 million load cycles during the unreinforced ballast test that was conducted at a load frequency of 15 Hz. As discussed previously, this initial phase of testing was conducted at frequencies of greater than 15 Hz while the capabilities of the load frame were tested. Excluding the large 15 Hz test settlement value, the largest initial settlement was observed in the unreinforced ballast test at 10 Hz. The fully reinforced ballast layer with free expansion exhibited marginally less initial settlement than that of the unreinforced ballast layer (50.17 mm and 51.91 mm respectively). Comparing the initial settlement values of the 50 % reinforced ballast layer with the other tests it can be observed that the initial settlement was approximately half that of the unreinforced ballast and approximately twice that of the fully reinforced ballast layer with expansion limited.

Comparing the settlement during the consolidation phase of the test, the least amount of settlement was observed in the unreinforced ballast test at 10 Hz (3.69 mm). The reinforced ballast layer with free expansion exhibited the most settlement during the consolidation phase. The reinforced ballast test with expansion limited (4.25 mm) and 50 % reinforcement (4.92 mm) did settle more than the unreinforced ballast test, but significantly less than the reinforced ballast test with free expansion (12.85 mm).

The final settlement values for the initial and consolidation test phases as well as the total settlement are shown in Figure 4.32.

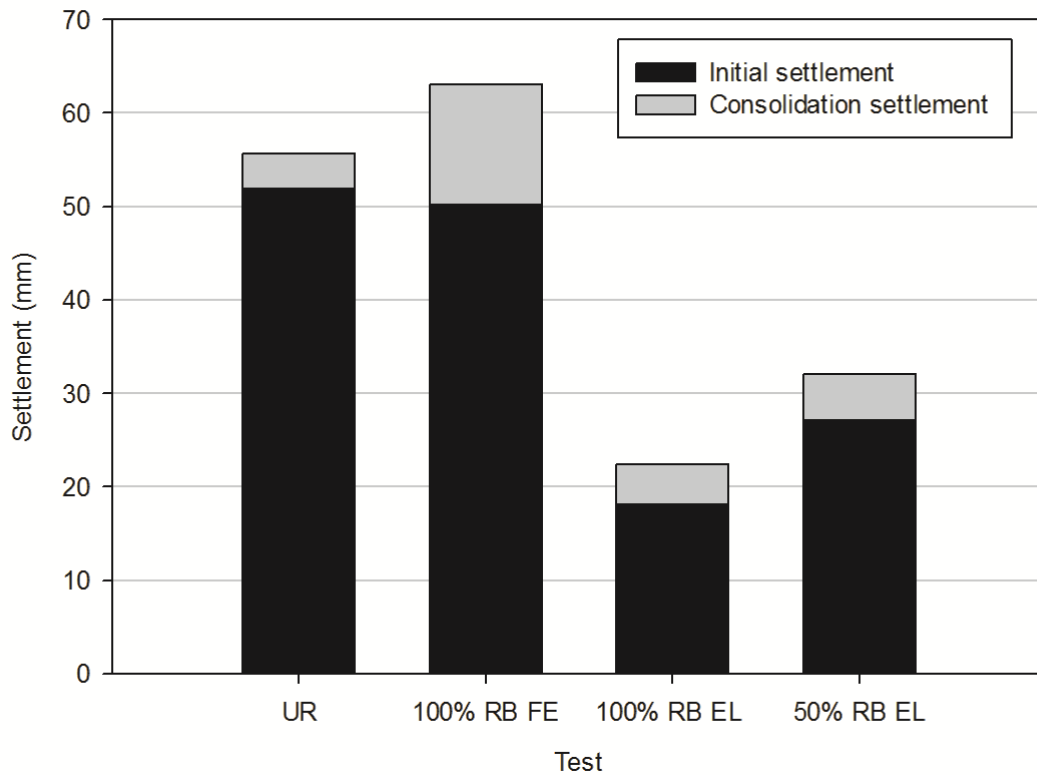


**Figure 4.32** Comparison of initial, consolidation and final total settlement results

Comparing the final total settlement values of the various tests, it can be observed that the best performing test was the reinforced ballast with expansion limited (22.32 mm). The next best performing test was the 50 % reinforced ballast layer with expansion limited (32.03 mm). In terms of reducing total settlement, reinforcing ballast with rigid polyurethane has a clear benefit provided the foam is not allowed to freely expand during pouring.

The final resilient sleeper deflections are shown in Figure 4.32. Rigid polyurethane foam reinforced ballast layers exhibit greater resilient sleeper deflections than that of unreinforced ballast. The values plotted in Figure 4.32 are from the end of each test after 5,000,000 cycles. It should be observed that the trend during the test shows that for the unreinforced ballast tests the resilient sleeper deflection increases with increasing load applications and the reverse is true for the reinforced ballast layers. Comparing the 50% reinforced ballast layer resilient sleeper deflection with that of the unreinforced ballast layer test conducted at the same frequency the difference in resilient sleeper deflection is negligible with a difference of 0.02 mm between the two.

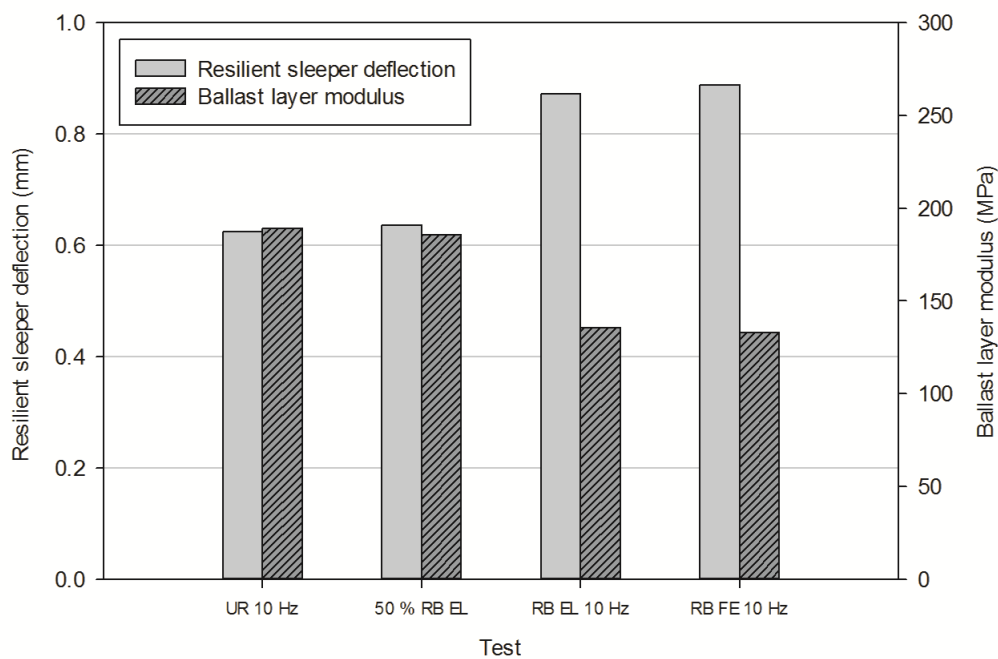


**Figure 4.33** Comparison of final resilient sleeper deflection and ballast layer modulus results

Comparing the layer modulus values of the different tests, the trends that can be observed between the resilient sleeper deflection values and the stiffness values are similar (as the layer modulus is derived from the resilient sleeper deflection values). Unreinforced ballast tests showed greater modulus values (due to lower resilient sleeper deflection values). Reinforced ballast tests showed lower modulus values that increased with the amount of load applications while the unreinforced ballast test showed a decrease in modulus as the amount of load cycles were increased, most likely due to an increase in ballast breakage and fouling resulting in a loss of strength.

## CHAPTER 5

# CONCLUSION AND RECOMMENDATIONS

This chapter provides a brief summary of the findings from Chapter 4, and an outcome with relation to the objectives outlined in Chapter 1 are also presented.

### 5.1 CONCLUSION

The conclusions from this research, based on the results from Chapter 4 are listed.

#### 5.1.1 Material Testing

- The rigid polyurethane exhibits behaviour that is significantly more elastic than just the ballast on its own. Combining the rigid polyurethane foam and the railway ballast produces a composite material that has significantly more elasticity and a lower potential for permanent strain deformation than unreinforced ballast on its own.
- Values of Young's modulus for the polyurethane foam reduced from approximately 7.2 MPa to approximately 1.5 MPa at 5% strain.
- Values of Young's modulus for the combined polyurethane foam and ballast at below 1% strain was 6.9 MPa indicating that at low strain levels the composite material behaves just as the foam would, most likely as a result of the foam filled voids between the ballast stone.
- For the polyurethane foam/ballast composite material at increased strain levels the Young's modulus was approximately four times greater than that of the foam only (1.5 MPa vs 4.5 MPa).
- When large strains are experienced by the polyurethane foam/ballast composite material (i.e 60 mm deformation on a 300 mm sample) the composite material retained 80 % of the deformation

as permanent deformation.

### 5.1.2 Ballast Breakage

- Visual inspection of the foam reinforced samples showed no ballast breakage or fines generation in the areas covered by foam.
- Testing at a higher frequency seemed to produce slightly more ballast breakage.
- In the case of the reinforced ballast test with 50 % reinforcement the ballast grading curve plotted above the maximum theoretical ballast breakage line. This could be attributed to the fact that the maximum ballast breakage line was developed for use with ballast only layers.
- The shallow ballast only layer depth (150 mm) underlain with a 150 mm polyurethane foam reinforced ballast layer did result in more particle breakage despite the decrease in stiffness as a result of the polyurethane foam reinforcement.
- The unreinforced and 50 % reinforced ballast tests produced more or less the same ballast breakage (i.e. BBI = 3.3 to 3.8 %)

### 5.1.3 Settlement Behaviour

- The reinforcement of ballast using rigid polyurethane foam is suitable for reducing settlement in track structures.
- Rigid polyurethane foam may settle more in the long term. The reduction in initial settlement leads to significantly less settlement overall, despite settlement in the consolidation phase of the test being greater.
- Rigid polyurethane foam reinforced ballast settled 60 % less than conventional unreinforced ballast, and reinforcing only 50 % of a ballast layer lead to a reduction in settlement of 42 % compared to that of conventional unreinforced ballast.
- In the case of rigid polyurethane foam reinforced ballast, the modulus increased as the number of cycles increased (25 % increase in stiffness for the 50% reinforced ballast layer) and 20 % increase for the layer that was fully reinforced with foam expansion limited. This increase in layer stiffness with time could be used to aid engineers in the design of track transitions or as a solution to problem track transition sections.
- The significant reduction in total settlement of ballast layers reinforced with rigid polyurethane

foam could result in better long term track geometry stability. As a result, longer track lifecycle can be expected when using rigid polyurethane foam as ballast reinforcement.

- The power and logarithmic function settlement prediction equations can be used for predicting the settlement of reinforced ballast samples. Theoretical logarithmic prediction functions are more suitable for predicting settlements on tests with large initial settlement. Similarly for tests with small initial settlement values, power functions provide a more suitable method for predicting settlement.

#### 5.1.4 Load vs Deflection Behaviour

- Actuator and sleeper load deflection behaviour were found to be significantly different from one another.
- The load-deflection behaviour of the sleeper was found to have a wider response to changes in load than the actuator.
- Maximum sleeper deflection did not occur at the maximum load measured by the actuator load cell. This is most likely as a result of the bending of the beam used to apply the loading to the sleeper which provided some aspect of damping to the system.
- The importance of load local load deflection measurement is therefore highlighted by these observations.

#### 5.1.5 Effect of Test Frequency

- The effect of different frequencies on the behaviour of the ballast with regard to sleeper deflection and settlement per cycle are not significant.
- The amount of sleeper deflection and settlement per cycle does not vary significantly between 8 Hz to 15 Hz.

In conclusion, the use of rigid polyurethane foam as a means of reinforcing railway ballast has numerous benefits. A reduction in total settlement was achieved. The composite rigid polyurethane foam and ballast material produced a layer that resulted in a structure that decreased resilient sleeper deflection and increased layer modulus values with an increase in load applications. The behaviour of the foam and foam/ballast composite material were quantified and the settlement and load deflection behaviour of unreinforced and reinforced ballast was characterised.

## 5.2 RECOMMENDATIONS

Recommendations for future work are now listed.

### 5.2.1 The future use of rigid polyurethane foam in ballast reinforcement

- Further investigation into different levels of ballast reinforcement i.e. 50 %, 75 % and the effect this would have on settlement and track stiffness parameters.
- Further investigation into the level of ballast uplift as a result of foam expansion and the effect thereof.

### 5.2.2 Recommendations for further study

- Further investigation into the long term life cycle of the rigid polyurethane foam whose properties continued to improve even at 5,000,000 load cycles. It is unclear whether this would continue in the field (UV rays, rain, etc.).
- For use in the field, the expansion of the foam should be limited by pouring the foam into a track structure that has already been completed. Pouring/injecting the foam into a track structure and allowing the foam to rise freely and then placing a sleeper (as with Test 2) leads to significantly reduced track performance.
- Investigation into the load-deflection behaviour of the actuator compared to that of the sleeper if the loading beam element of the system was removed.
- More study into the effect of test frequency on the settlement and ballast breakage behaviour of various unreinforced and reinforced ballast samples.
- Measurement of difference in horizontal ballast pressure in ballast layer between unreinforced and polyurethane foam reinforced ballast materials in a box test could be of future interest.

## REFERENCES

- Al-Saoudi, N. K. and Hassan, K. H. (2014), 'Behaviour of track ballast under repeated loading', *Geotechnical and Geological Engineering* **32**(1), 167–178.
- Ame (1993), *Track Transition Problems and Remedies*.
- Aursudkij, B. (2007), 'A laboratory study of railway ballast behaviour under traffic loading and tamping maintenance', (September).  
**URL:** <http://theses.nottingham.ac.uk/321/>
- Bilow, D. N. and Randitch, P. (2000), Slab Track for the Next 100 Years, *in* 'Rail Transit Conference'.
- Brown, J. (1983), Continuous Slab Track, *in* 'Track Course', London.
- Brown, S. and Hyde, A. (1975), 'Significance of cyclic confining stress in repeated-load triaxial testing of granular material', *Transportation Research Record* (537).
- Christie, D., Lackenby, J., Indraratna, B. and McDowell, G. (2007), 'Effect of confining pressure on ballast degradation and deformation under cyclic triaxial loading', *Géotechnique* **57**(6), 527–536.
- Collins, I. F. and Boulbibane, M. (2000), 'Geomechanical Analysis of Unbound Pavements Based on Shakedown Theory'.
- Craig, R. and Knappett, J. (2012), *Craig's Soil Mechanics*, 8th edition edn, Spon Press. Dundee.
- CSIR (1986), *TMH1: Standard Methods of Testing Road Construction Materials*, Center for Scientific and Industrial Research.
- Dawson, A. (1990), 'Introduction to soils and granular materials', *Lecture Notes from Residential*

## References

---

- Course, Bituminous Pavements-Materials, Design and Evaluation .*
- Eales, H. and Cawthorn, R. (1996), 'The bushveld complex', *Developments in Petrology* **15**, 181–229.
- Eisenmann, J. (1975), 'Dynamic wheel load fluctuations-road stress', *Strasse und Autobahn* **4**(2).
- Esveld, C. (2001), *Modern Railway Track*, Delft University of Technology.
- Google and AfriGIS (2015), *Google Maps*.
- Gunter, O. (1985), 'Polyurethane handbook', *Hanser: Munich .*
- Hardin, B. O. (1985), 'Crushing of Soil Particles'.
- HBM (2015), *HBM - Inductive Standard Displacement Transducers: Data Sheet*, HBM. B0553-9.0 en.
- Hicks, R. G. and Monismith, C. L. (1971), 'Factors influencing the resilient response of granular materials', *Highway research record* (345).
- Indraratna, B. (2000), 'State of the art large scale testing of ballast'.
- Indraratna, B., Ionescu, D., Christie, H. D. and Chowdhury, R. N. (1997), 'Compression and Degradation of Railway Ballast Under One-Dimensional Loading', *Australian Geomechanics* **32**(December), 48–61.
- Indraratna, B., Khabbaz, M. H., Salim, W., Lackenby, J. and Christie, D. (2004), 'Ballast characteristics and the effect of geosynthetics on rail track deformation', pp. 3–12.
- Indraratna, B. and Salim, W. (2003), 'Deformation and Degradation Mechanics of Recycled Ballast Stabilised With Geosynthetics', *Soils and Foundations* **43**(4), 35–46.
- Indraratna, B., Wijewardena, L. and Balasubramaniam, a. (1993), 'Large Scale Triaxial Testing of Greywacke Rockfill', *Geotechnique* **43**(September), 37–51.
- Keene, A., Edil, T., Fratta, D. and Tinjum, J. (2013), 'Modeling the effect of polyurethane stabilization on rail track response', *Geocongress 2013 .*

## References

---

- Keene, A., Edil, T., Tinjum, J. and Brown, R. (2012a), 'Characterization of polyurethane-stabilized ballast', *3rd International Conference on New Developments in Soil Mechanics and Geotechnical Engineering* (June), 28–30.  
**URL:** <http://zm2012.neu.edu.tr/ZM2012 DVD/New Methods in GE/099.pdf>
- Keene, A., Edil, T., Tinjum, J. and Brown, R. (2012b), 'Railway substructure stabilization with polyurethane injections', *Mid-Continent Research Forum 2012* .
- Keene, A., Tuncer, E. and Tinjum, J. (2012), Mitigating ballast fouling impact and enhancing rail freight capacity, Technical Report CFIRE 04-07, National Center for Freight Infrastructure Research and Education (CFIRE).
- Kennedy, J., Woodward, P., Medero, G. and Banimahd, M. (2013), 'Reducing railway track settlement using three-dimensional polyurethane polymer reinforcement of the ballast', *Construction and Building Materials* **44**, 615–625.
- Lade, P. V., Yamamuro, J. A. and Bopp, P. A. (1996), 'Significance of Particle Crushing in Granular Materials'.
- Lee, K. L. and Farhoomand, I. (1967), 'Compressibility and crushing of granular soil in anisotropic triaxial compression', *Canadian Geotechnical Journal* **4**(1), 68–86.
- Lei, X. and Zhang, B. (2010), 'Analyses of dynamic behavior of track transition with finite elements', *Journal of Vibration and Control* **17**(11), 1733–1747.  
**URL:** <http://jvc.sagepub.com/cgi/doi/10.1177/1077546310385035>
- Lekarp, F., Isacsson, U. and Dawson, A. (2000), 'State of the Art. I: Resilient Response of Unbound Aggregates', *Journal of Transportation Engineering* **3**(1), 3–46.
- Leslie, D. (1975), 'Shear strength of rockfill', *Physical Properties Engineering Study No 526*, 124.
- Li, D. and Davis, D. (2005), 'Transition of railroad bridge approaches', *Journal of Geotechnical and Geoenvironmental Engineering* **131**(11), 1392–1398.
- Li, D. and Selig, E. (1994), 'Track modulus its meaning and factors influencing it', *Transportation Research Record: Journal of the Transportation Research Board* **1470**, 47–54.

## References

---

- Li, D., Smith, L., Doe, B., Otter, D. and Uppal, S. (2003), 'Study of bridge approach and track transition degradation - factors and mitigation', *Federal Railroad Administration Contract DTFR53-01-H-00305*.
- Lim, W. (2004), 'Mechanics of railway ballast behaviour', (May).  
**URL:** <http://etheses.nottingham.ac.uk/archive/00000060/>
- Marsal, R. J. (1967), 'Large-scale testing of rockfill materials', *Journal of the Soil Mechanics and Foundations Division* **93**(2), 27–43.
- McDowell, G., Bolton, M. and Robertson, D. (1996), 'The fractal crushing of granular materials', *Journal of the Mechanics and Physics of Solids* **44**(12), 2079–2101.
- McNally, G. (2002), *Soil and Rock Construction Materials*, CRC Press.  
**URL:** <https://books.google.co.za/books?id=vB4LVNXyjLoC>
- Michas, G. (2012), Slab track systems for high-speed railways, Master's thesis, Royal Institute of Technology, Stockholm. Department of Transport Science.
- Nakata, A., Hyde, M., Hyodo, H. et al. (1999), 'A probabilistic approach to sand particle crushing in the triaxial test', *Geotechnique* **49**(5), 567–583.
- Neidhart, T. (2005), 'True-to-scale in situ tests determining dynamic performance of earthworks under high speed train loading'.
- Nicks, J. (2009), The Bump at the End of the Railway Bridge, PhD thesis, Texas AM University.
- Pretorius, F. (1993), *The state of the art of ballast fouling and screening maintenance system*, Johannesburg: Track Testing Centre, Report.
- Ramamurthy, T. (2001), 'Shear strength response of some geological materials in triaxial compression', *International Journal of Rock Mechanics and Mining Sciences* **38**(5), 683–697.
- Read, D. and Li, D. (2006), 'Research Results Digest 79-Design of Track Transitions', *Transportation Cooperative Research Program* (October), 1–36.
- Rose, J. (1998), Long-term performances tests, and evaluations of asphalt trackbeds, in '1998 Track

## References

---

- and Structures', AREMA, Chicago, IL.
- Rose, J., Walker, L. and Li, D. (2002), Heavy haul asphalt underlayment trackbeds: Pressure, deflection, materials, properties, measurements, *in* 'Proceedings, Railway Engineering 2002', Engineering Technics Press, Edinburgh.
- Rostler, F., White, K., Nair, K., Hicks, R. and Newton, J. (1966), Study of methods of stabilizing conventional ballast using polymers, Technical report, Materials and Research Development Inc., Oakland, CA.
- Rusnak, J. and Mark, C. (2000), Using the point load test to determine the uniaxial compressive strength of coal measure rock, *in* 'Proceedings of the 19th international conference on ground control in mining. Morgantown, WV: West Virginia University', pp. 362–371.
- Salim, W., Christie, D., Khabbaz, H. and Aratna, B. (2006), 'Geotechnical properties of ballast and the role of geosynthetics in rail track stabilisation', *Proceedings of the ICE - Ground Improvement* **10**(3), 91–101.
- Sasaoka, C. and Davis, D. (2005), 'Implementing track transition solutions for heavy axle load service', *In Proceedings, AREMA 2005 Annual Conference Chicago, IL.* .
- Selig, E. T. and Waters, J. M. (1994), *Track Geotechnology and Substructure Management*, Thomas Telford.
- Shahin, M. a., Indraratna, B. and Salim, W. (2007), 'Stabilisation of granular media and formation soil using geosynthetics with special reference to railway engineering', *Proceedings of the ICE - Ground Improvement* **11**(1), 27–43.
- Sharpe, P., Armitage, W., Heggie, W. and Rogers, A. (2002), Innovative design of transition zones, *in* 'Proceedings, Railway Engineering 2002', Engineering Technics Press, Edinburgh.
- Shenton, M. (1974), Deformation of railway ballast under repeated loading conditions, number 76-TR-1.
- Shukla, S. K. (2002), *Geosynthetics and Their Applications*, Thomas Telford.
- Spoornet (1998), S406 (1998) Specification for the supply of stone., Technical report, Spoornet.

## References

---

- Steidl, ed. (2009), *High Speed in Europe*, UIUC.
- Sun, Q., Indraratna, B. and Nimbalkar (2014), 'Effect of cyclic loading frequency on the permanent deformation and degradation of railway ballast', *Geotechnique* **64**(9), 746–751.
- Sussman, T. and Selig, E. (1998), *Track Component Contributions to Track Stiffness*, E.T. Selig, Inc.
- Szycher, M. (1999), *Szycher's handbook of polyurethanes*, CRC press.
- Warren, B. (2015), Field application of expanding rigid polyurethane stabilization of railway track substructure, Master's thesis, University of Wisconsin-Madison.
- Woodward, P. (2007), 'Geocomposite technology: reducing railway maintenance', *Proceedings of the ICE- ...* pp. 109–115.
- Woodward, P. K., Kennedy, J., Medero, G. M. and Banimahd, M. (2012), 'Application of in situ polyurethane geocomposite beams to improve the passive shoulder resistance of railway track', *Proceedings of the Institution of Mechanical Engineers, Part F: Journal of Rail and Rapid Transit* .
- Woodward, P., Kennedy, J. and Medero, G. (2009a), 'Three-dimensional track reinforcement using polymer geocomposites', *Proceedings of the American railway engineering and maintenance of way association* .
- Woodward, P., Kennedy, J. and Medero, G. (2009b), 'Three dimensional track reinforcement using polymer geocomposites', *Proceedings of the American Railway Engineering and Maintenance of Way Association* **44**.

## APPENDIX A

## APPENDIX A

### A.1 RAW DATA

File Path: C:\Users\Administrator\Desktop\RudiMTS\Test Run 33 8-12-2015 3 07 4

Test: Rudi Rail Test

Test Run: Test Run 33

Date: 8/11/2015 7:07:15 AM

Axial Count	Time	Axial Force	Axial Displacement	Aux Input 1	Aux Input 2
cycles	sec	kN	mm	V	V

0	18.332275390625	0.0207214622497559	45.0027398765087		
---	-----------------	--------------------	------------------	--	--

5.93058824539185	6.28186941146851				
------------------	------------------	--	--	--	--

0	18.333251953125	0.0415230178833008	45.0033470988274		
---	-----------------	--------------------	------------------	--	--

5.93006324768066	6.28201770782471				
------------------	------------------	--	--	--	--

0	18.334228515625	0.0365721054077148	45.002106577158		
---	-----------------	--------------------	-----------------	--	--

5.92962789535522	6.28221082687378				
------------------	------------------	--	--	--	--

0	18.335205078125	0.0180862846374512	45.0042337179184		
---	-----------------	--------------------	------------------	--	--

5.92944049835205	6.28237724304199				
------------------	------------------	--	--	--	--

....

### A.2 MATLAB CODE

The code used for the processing of the large data files is shown here.

```
clear all
```



```
Freq = load('TR58.txt');  
[n5,p5]=size(Freq);  
max = 0;  
minimum =0;  
max3 = 0;  
minimum3 =0;  
max2 = 0;  
minimum2 =0;  
  
for i=1:n5-1  
  
    cyclenumber = floor(Freq(i,1)+1) ;  
    cyclenumber2 = floor(Freq(i+1,1)+1);  
    check1 = Freq(i,4) ;  
    check2 = Freq(i+1,4) ;  
    check3 = Freq(i,6) ;  
    check4 = Freq(i+1,6) ;  
    check5 = Freq(i,5) ;  
    check6 = Freq(i+1,5) ;  
    checkfinal = Freq(n5,2) ;  
    checkfinal3 = Freq(n5,2) ;  
    checkfinal2 = Freq(n5,2) ;  
    cyclefinal = Freq(n5,1);  
  
    if check1 >= check2  
        checkresult = check1 ;  
    else  
        checkresult = check2 ;  
    end  
  
    if check1 <= check2  
        checkresult2 = check1 ;  
    else
```

```
        checkresult2 = check2 ;
    end

    if check3 >= check4
        checkresult3 = check3 ;
    else
        checkresult3 = check4 ;
    end

    if check3 <= check4
        checkresult4 = check3 ;
    else
        checkresult4 = check4 ;
    end

    if check5 >= check6
        checkresult5 = check5 ;
    else
        checkresult5 = check6 ;
    end

    if check5 <= check6
        checkresult6 = check5 ;
    else
        checkresult6 = check6 ;
    end

    if cyclenumber == cyclenumber2
        if checkresult > max ;
            max = checkresult ;
        end
        if checkresult2 < minimum ;
            minimum = checkresult2 ;
        end
    end
end
```

```
end

    if checkresult3 > max3 ;
        max3 = checkresult3 ;

    end

    if checkresult4 < minimum3 ;
        minimum3 = checkresult2 ;
    end

    if checkresult5 > max2 ;
        max2 = checkresult5 ;
    end

    if checkresult6 < minimum2 ;
        minimum2 = checkresult6 ;
    end

    FreqOut (cyclenumber,1) = cyclenumber ;
    FreqOut (cyclenumber,2) = checkresult;
    FreqOut (cyclenumber,3)= checkresult2;
    FreqOut (cyclenumber,6) = checkresult3;
    FreqOut (cyclenumber,7)= checkresult4;
    FreqOut (cyclenumber,4) = checkresult5;
    FreqOut (cyclenumber,5)= checkresult6;

end

max =0 ;
minimum =0;
max3 = 0;
minimum3 =0;
```



```
max2 = 0;
minimum2 =0;
FreqOut (cyclenumber,1) = cyclenumber ;
FreqOut (cyclenumber,2) = checkresult;
FreqOut (cyclenumber,3) = checkresult2;
FreqOut (cyclenumber,6) = checkresult3;
FreqOut (cyclenumber,7) = checkresult4;
FreqOut (cyclenumber,4) = checkresult5;
FreqOut (cyclenumber,5) = checkresult6;

    if i == n5-1
        FreqOut (cyclenumber2,2) = checkfinal ;
        FreqOut (cyclenumber,4) = checkfinal3 ;
        FreqOut (cyclenumber,6) = checkfinal2;
        FreqOut (cyclenumber,1) = cyclefinal;
    end

end

disp('Done the first part')
disp('Now going to remove zeros')
FreqOut (all (FreqOut==0,2),:)=[];
dlmwrite('TR58Output.csv', FreqOut, 'delimiter', ',', 'precision', 9);
FreqOut
```